CHARACTERISATION OF PREFERRED ORIENTATION IN CRYSTALLINE MATERIALS BY X-RAY POWDER DIFFRACTION

HUSINSYAH SITEPU

Thesis submitted in partial fulfilment of the requirements

for the degree of Master of Applied Science (Physics)

at the Curtin University of Technology,

Perth, Western Australia

March, 1991

ABSTRACT

Texture, *i.e.* preferred orientation, can cause large systematic errors in quantitative analysis of crystalline materials using x-ray powder diffraction (XRPD) data. Various mathematical forms have been proposed for the application of preferred orientation corrections. The most promising of these appears to be the single-parameter March (1932) model proposed by Dollase (1986).

Li and O'Connor (1989) applied the March model to determine the level of preferred orientation in various gibbsites using two procedures. The first involved the Rietveld (1969) least squares pattern-fitting method. Each pattern was Rietveld-analysed in two ways, initially assuming random orientation of the crystallites and subsequently with the March model. The second procedure for preferred orientation analysis, described here as the line ratio method, determines preferred orientation factors according to the intensity ratios of carefully selected line pairs.

In the thesis the procedures proposed by Li and O'Connor for texture analysis have been evaluated with XRPD data sets for molybdite, calcite and kaolinite. The results indicate that while the March formula improves agreement between the calculated and measured patterns in Rietveld analysis, other forms of systematic error in the intensity data appear to limit the effectiveness of the March formula in general. It has been found also that the line ratio method improves agreement between the data sets, but less effectively than the Rietveld method. It is proposed that extinction is likely to be the most influential source of systematic error competing with texture.

LIST OF ABBREVIATIONS

The following abbreviations are used extensively in the thesis :

XRD	:	x-ray diffraction
XRPD	:	x-ray powder diffraction
NPD	:	neutron powder diffraction
PSD	:	particle size distribution
PO	:	preferred orientation
ODF	:	orientation distribution function
FWHM	:	full-width at half maximum
RLV	:	reciprocal lattice vector
JCPDS	:	Joint Committee for Powder Diffraction Standards
I_{obs}	:	observed Bragg intensity
I_{corr}	:	corrected Bragg intensity

ASSUMED BACKGROUND FOR THESIS

It is assumed that the readers have a basic understanding of crystallography and diffraction principles at the level of the text *"Elements of X-ray Diffraction"*, authored by B.D. Cullity (1978), 2nd edition. Addison-Wesley.

ACKNOWLEDGMENTS

I wish to express gratitude to my supervisor, Professor Brian H. O'Connor, for his guidance and invaluable assistance through the course of this thesis study. Special thanks are also due to Professor Li Deyu for his expert advice on diffraction science.

I also thank my sponsor IDP (International Development Program of Australian Universities and Colleges), Canberra - in particular, Mrs Lyn Brooks, Mrs Nora Fleming and Mrs Calmar P. N. Annandale for administering the fellowship awarded to me for the thesis study.

Ms Jaine Steer of Curtin University is thanked for providing advice on XRPD data collection methods.

Mr Malcolm Pryce, Chemistry Centre, Western Australia is thanked for providing kaolinite specimens.

Assistance with collection of diffraction data was kindly given by Alcoa of Australia Ltd., Research and Development Department, Kwinana, Western Australia. The author thanks Dr Gerald Roach, Mr John Cornell and Mr Nick Pearson of Alcoa for these arrangements.

Dr Roderick J. Hill of CSIRO Division of Mineral Products, Victoria, Australia, and Dr Chris J. Howard of Australian Nuclear Science and Technology Organisation, Lucas Heights Research Laboratories, NSW, Australia, are gratefully acknowledged for their provision of Rietveld software.

Mr Terry Edmett of the School of Physical Sciences, Curtin University, is thanked for helping to transfer and re-format this document from Worstar 4 to the Microsoft Word version 5.

Ms Elaine Miller provided invaluable assistance with proof reading and with some word processing corrections.

Lastly, I would like to say thanks to my wife, Ella, for her encouragement and understanding especially during the last few months.

CHARACTERISATION OF PREFERRED ORIENTATION IN CRYSTALLINE MATERIALS BY X-RAY POWDER DIFFRACTION

TABLE OF CONTENTS

List of Figures

List of Tables

CHAPTER 1

INTRODUCTION

I.1 Background to Study

Texture Characterisation

The texture, *i.e.* preferred orientation (PO), of polycrystalline materials has been studied for many years, particularly in relation to metals, rocks and minerals. Metals have been the most intensively studied class of materials and have formed the basis of most of the theoretical work in the field. Rock and minerals, which have received less attention principally due to the greater complexity of their crystal structures, can now be studied more readily using the powerful computational procedures which have become available (Weiss and Wenk, 1985).

Wever (1924) described the first study of PO in a metal using a pole-figure obtained by the x-ray diffraction (XRD) Laue method. The phenomenon was described by Cullity (1978) using the example of a very coarse-grained sheet of a cubic metal containing 10 grains. Cullity plotted the positions of their {100} poles on a single stereographic projection with the projection plane parallel to the sheet surface. Since each grain has three {100} poles, there will be a total of 3 x 10 = 30 poles plotted on the projection. Figure 1.1 shows the grains with random orientation. It is seen that if the orientation is random, there will be equal numbers of poles in equal areas on the surface of a reference sphere centred on the specimen. However, if PO is present, the poles will cluster together into certain areas of the projection, leaving other areas virtually unoccupied as shown in Figure 1.2.

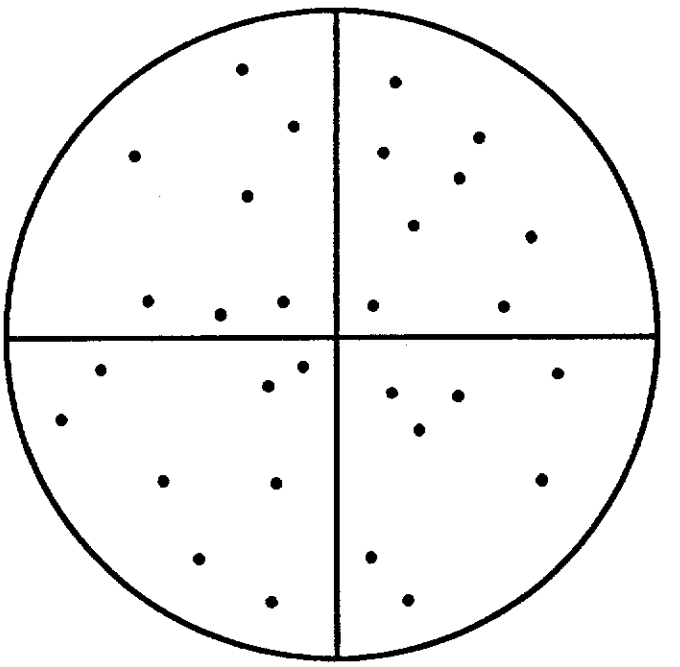

Fig. 1.1. A (100) pole figure for sheet material, illustrating random orientation. (Cullity, 1978).

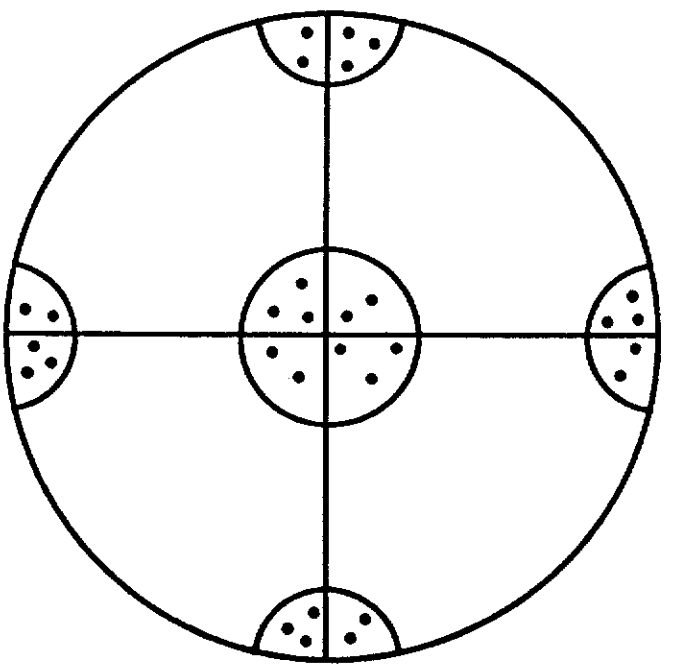

Fig. 1.2. A (100) pole figure for sheet material, illustrating PO. (Cullity, 1978).

The Wever method for describing pole figures, as illustrated in Figures 1.1 and 1.2, cannot be used when the grain size of the specimen is very small as the diffraction effects from the very large number of grains form an intensity continuum. The (hkl) pole-figure of a fine-grained material may be constructed by analysing the distribution of intensity around the circumference of the corresponding (hkl) ring of the Debye-Scherrer diffraction pattern. There are two methods available for this purpose - the photographic and the diffractometer methods (Cullity, 1978).

Methods for measurement of pole-figures have improved dramatically in recent years through the use of fully automated x-ray and neutron diffractometers with which data can be rapidly obtained. While x-ray and neutron methods provide pole-figures of high precision, attention must still be paid to estimation of measurement errors (Weiss and Wenk, 1985).

Bunge (1985) described in detail the orientation distribution function (ODF) formalism for modelling texture. The ODF was defined as the volume fraction of crystallites $(\delta V)/V$ with orientation angle g within the range $g + \delta g$. The ODF f(g) is thus defined by :

$$(\delta V)/V = f(g)\, \delta g \qquad \ldots \quad (1.1)$$

By an appropriate definition of the orientation element δg it is possible to normalise function f(g) in such a way that the function integral over all of angular space is

$$\int f(g)\, dg = 1 \qquad \ldots \quad (1.2)$$

Oertel (1985), in reviewing the March (1932) model of PO based on ODFs for rigid rod- or plate-shaped grains, established that the March model is acceptable for describing texture in such materials.

Complications Caused by Extinction when Characterising PO by XRD Methods

In characterising PO by XRD methods, the results may also be influenced by the extinction phenomenon which can cause reductions in XRD intensities. Zachariasen (1967) proposed a general theory of extinction, based on the coupling between incident and diffracted beams. In this theory, formulae were derived for the intensity diffracted by a finite perfect crystal and for the intensity diffracted by a finite mosaic crystal. Zachariasen (1968, 1969) carried out a comprehensive experimental study for which he obtained sound agreement between the experimental results and theoretical expressions for lithium fluoride, quartz, phenakite, hambergite and calcium fluoride.

Cooper *et al.* (1968) and Cooper and Rouse (1970) applied the Zachariasen theory to XRD and neutron powder diffraction (NPD) data for barium fluoride, strontium fluoride and calcium fluoride. The results obtained by NPD for these materials indicated that the theory of Zachariasen is not generally valid and that the discrepancies for XRD data are more substantial.

Sabine (1988) experimented with polycrystalline specimens of magnesium oxide (MgO) using NPD and verified that the results should be identical to the Zachariasen theory of extinction if the Lorentzian and Gaussian functions are used for primary and secondary extinction, respectively.

Assessment of PO Using Powder Diffraction Data

Rietveld's (1969) pattern-fitting method for crystal structure refinement (see Section 2.2) made provision for the correction of PO in NPD refinements according to,

$$I_{corr} = I_{obs} \exp[-G \alpha^2] \qquad \ldots \quad (1.3)$$

where α is the acute angle between the scattering vector and the normal to the crystallite, and G is the PO parameter. Parameter G is a measure of the half width of the assumed distribution of the Gaussian of normals about the PO direction. Uda (1967) had trialled the same PO function (see equation (1.3)) in an XRD study of the crystal structure of synthetic Fe_3S_4 and the nature of the transition to FeS. Uda obtained reasonable agreement between the calculated and observed intensities except for the intense (311) and (101) reflections in Fe_3S_4 and FeS, respectively.

Pesonen *et al.* (1973) proposed a multi-parameter symmetrised harmonic method for correcting integrated XRD intensities for PO. The method is based on the measurement of the intensity variation for a few reflections in a limited range of polar angle. This method was tested experimentally on four magnesium samples with different degrees of PO. Two independent checks were used. Firstly, the relative intensities of six reflections were measured from each sample separately and, secondly, the same reflections were measured one at a time from all samples in equivalent conditions. The consistency of the results showed that the accuracy of the final intensities after correction for PO was about one percent.

Capkova and Valvoda (1974) studied cylindrico-symmetrical needle-type texture in magnesium and magnesium-cadmium alloy powder samples. The ODF was determined with (002) reflections measured on a texture goniometer. The measured ODFs approximated two different terms for the specimens examined,

$$I_{corr} = I_{obs} \exp[- G(1 - \cos^3 \alpha)] \quad \ldots \quad (1.4)$$

and,

$$I_{corr} = I_{obs} \exp[-G \sin^2 \alpha] \quad \ldots \quad (1.5)$$

Sasa and Uda (1976) used a Gaussian function to correct PO in tetragonal uranium disilicide [USi_2] which showed PO parallel to the plane of the sample holder. The derived PO function had the form

$$I_{corr} = I_{obs} [b + (1 - b) \exp(- G \alpha^2)] \quad \ldots \quad (1.6)$$

Cox *et al.* (1980) described an application of the Rietveld refinement technique to NPD and XRPD data for corundum [Al_2O_3]. Comparisons were made with the integrated intensities from x-ray single crystal data. Inspections of the data showed a dependence which could be approximated by an expression of type :

$$I_{corr} = I_{obs} \exp[-G(\pi/2 - \alpha)^2] \quad \ldots \quad (1.7)$$

Parrish and Huang (1983) and Will *et al.* (1983) obtained optimum XRPD results for National Bureau of Standards (NBS) silicon XRPD structure refinements using the same PO function.

Toraya and Marumo (1981) experimented with various mathematical forms for PO corrections and concluded that the expression of Sasa and Uda (equation (1.6)) gave the best agreement for the various functions which had been proposed. Several samples of taeniolite [$KLiMg_2Si_4O_{10}F_2$] with different particle size distributions were collected by x-ray powder diffractometry. PO corrections were estimated by comparing measured and calculated XRPD patterns.

Dollase (1986) made a major advance by proposing use of the March (1932) model for modelling PO in XRPD pattern analysis. The model is appropriate for samples comprising disk- or rod-shaped crystallites with axial symmetry. Sample rotation ensures that axial symmetry is achieved. The Bragg peak intensity is biased by factor,

$$P_j = (r^2 \cos^2 \alpha_j + r^{-1} \sin^2 \alpha_j)^{-3/2} \quad \ldots \quad (1.8)$$

where r is a fractional measure of crystallite random orientation, and α_j is the angle between the PO direction and the reciprocal lattice vector (RLV) direction for Bragg

peak j. The value r = 1.00 corresponds to random orientation and r = 0.00 to complete PO (for more details - see Section 2.1).

The model has an important advantage over others reviewed above, *viz.* the function P_j is normalised over the full angular range of α_j whereas the other functions are unnormalised. The normalisation property is important in that changes in the ODF shape conserve the total intensity within the diffraction pattern.

Evaluation of the March Expression for PO Characterisation in XRPD

Dollase (1986) experimented with the March expression in Rietveld calculations using calcite [$CaCO_3$] and huntite [$CaMg_3(CO_3)_4$] data sets. The results were compared with those obtained for various mathematical forms of pole-figure profiles proposed by other workers (equations (1.3), (1.4), (1.5), (1.6), and (1.7) - this Chapter). The degree of PO for the calcite was too weak (March r-parameter = 0.89(5)) to demonstrate any superiority of the March formula over the other expressions. However refinements conducted with two huntite specimens, corresponding to low and high orientation, showed the superiority of the March formula. The huntite sample of low orientation (r = 0.79(1)) gave a substantially better match between calculated and observed patterns when the March model was employed; the Bragg R-factor index-of-fit (R_B - refer Section 2.2) with the March model being 5.3% compared with 7.6% for the Gaussian profile employed by Rietveld (equation (1.3)). In the case of the more highly oriented specimen (r = 0.57(1)), the corresponding Bragg R-factor also showed substantially better agreement for the March model with the March being 6% compared with 10% for the Gaussian profiles.

Studies conducted with gibbsite [$Al(OH)_3$] specimens by Li and O'Connor (1989) and Li *et al.* (1990) using Rietveld XRPD pattern-fitting for quantitating PO showed that the agreement between calculated and measured patterns for highly-oriented specimens improves dramatically when the March model is employed in the

Rietveld refinement. Figure 1.3, reproduced from Li *et al.* (1990), shows the agreement between calculated and measured XRPD patterns for a highly-oriented sample for which the Rietveld r-parameter was 0.61. The two papers are discussed in greater detail in Section 2.2 of the thesis.

In assessing the effectiveness of the Rietveld refinements with the March model, Li *et al.* proposed an alternative method for PO corrections in which the r-parameter is derived analytically from the intensity ratio of a pair of lines with different angles, α_j. Use of intensity ratios for PO characterisation had been proposed by Roach and Cornell (1988) for gibbsite in terms of the ratio of integrated intensities for the (002) line and the (110, 200) doublet,

$$M_R = I(002)/I(110, 200) \quad \ldots \quad (1.9)$$

which was designated the 'morphological ratio'.

Li and O'Connor (1989) subsequently derived a theoretical relationship between morphology ratio, M_R, for gibbsite and the March r-parameter :

$$r = 1.15\, M_R^{-0.222} \quad \ldots \quad (1.10)$$

Figures 1.4(a) and (b) from Li and O'Connor (1989) show the plots of r-versus-M_R and log r-versus-log M_R for the gibbsite samples. The theoretical relation of equation (1.10) is shown as unbroken lines in both Figures 1.4(a) and (b). It is seen from Figure 1.4(b) that:

(i) equation (1.10) is a suitable formula to determine March r-parameter of gibbsites according to morphology ratio, M_R, regardless of sample preparation and mounting procedure;

(ii) the March r-parameter results obtained by line ratio method for three mounting procedures (side-drifting, light front-pressing and briquetting) lie close to the linear regression forms.

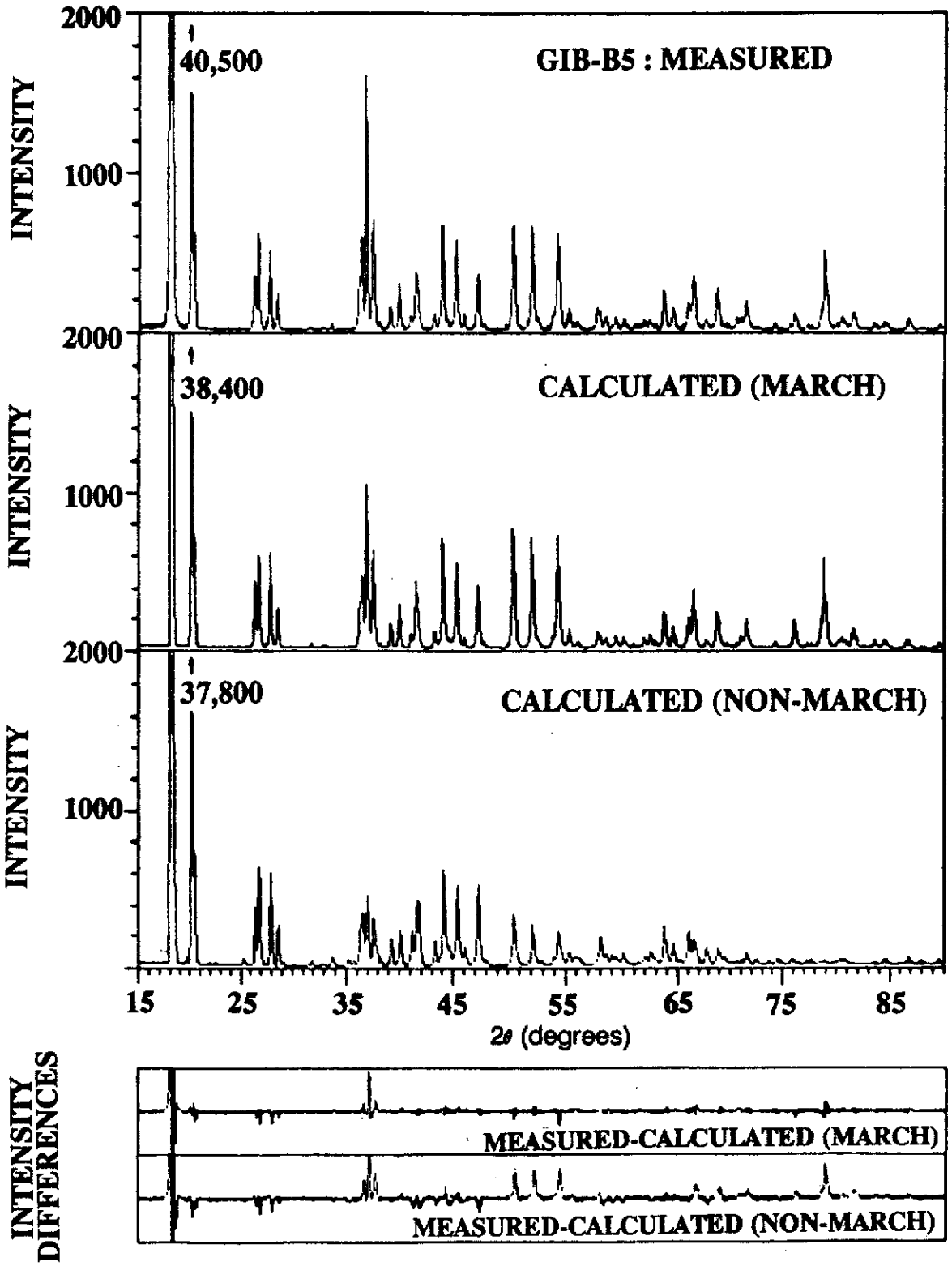

Fig. 1.3. Measured XRPD pattern for a highly-oriented gibbsite (March parameter r = 0.61) and corresponding calculated patterns following Rietveld refinement. (Li *et al.*, 1990).

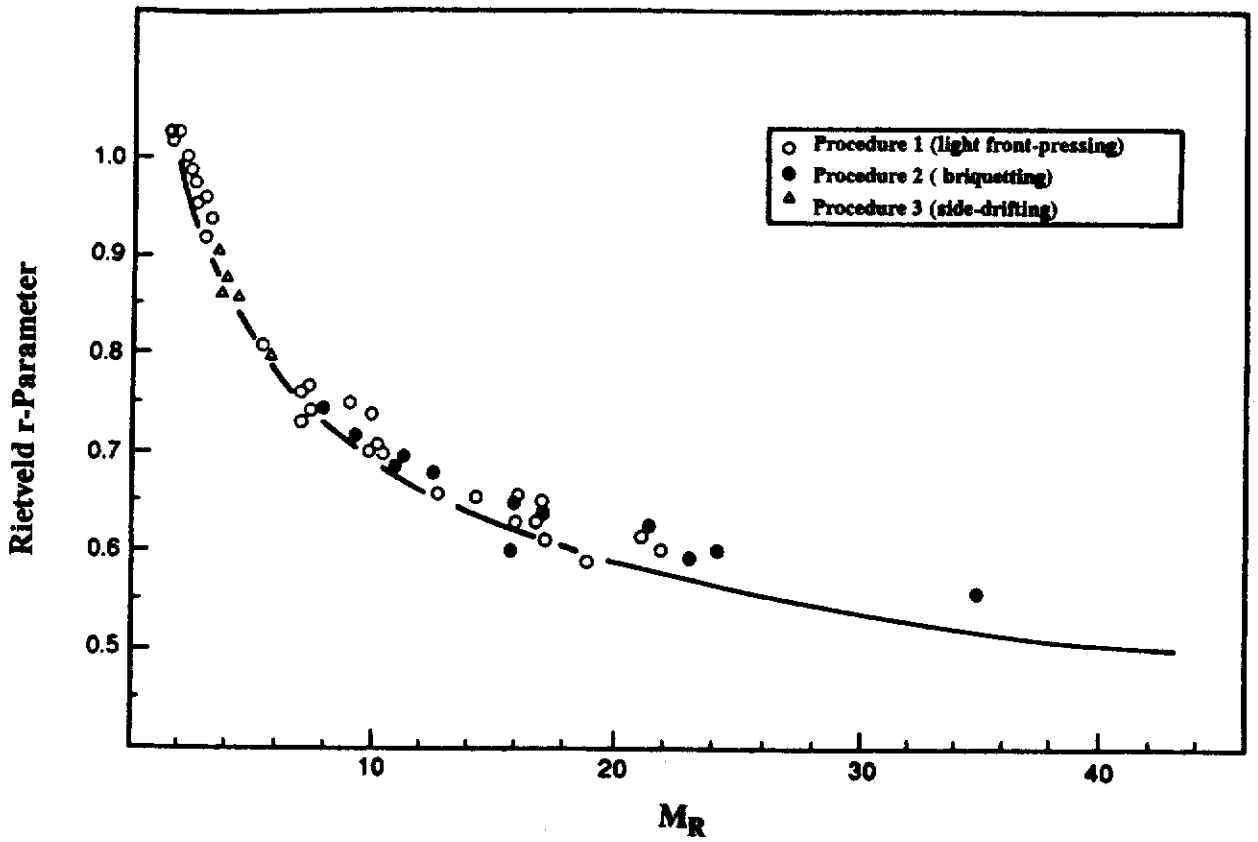

Fig. 1.4(a). Plot of PO parameter r versus line ratio M_R for gibbsite samples. The continuous line represents the theoretical relation, equation (1.10). (Li and O'Connor, 1989).

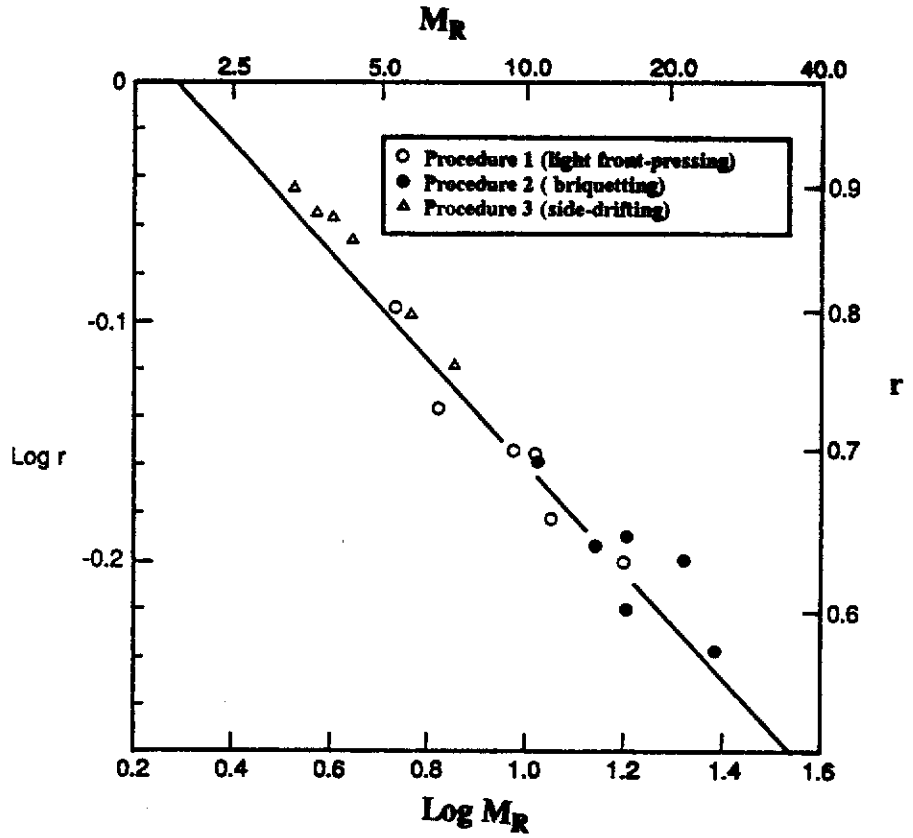

Fig. 1.4(b). Plot of log r-versus-log M_R for gibbsite samples corresponding to figure 1.4(a). The continuous line represents the theoretical relation, equation (1.10). (Li and O'Connor, 1989).

Li and O'Connor reported sound agreement between the r-parameters derived with equation (1.10) using experimental M_R data, and by Rietveld refinement, thus indicating the excellent potential of the March model for describing PO in gibbsites. Extinction was not considered in the gibbsite work. However in view of the excellent results, extinction effects were probably minimal for the specimens examined.

1.2 Study Objectives

The general objective of the thesis study was to evaluate the validity of the March (1932) model, as employed by Li and O'Connor (1989) and by Li *et al.* (1990) for characterising PO in gibbsites, for general assessment of PO in materials analysis, with reference to :

(i) texture characterisation,

(ii) correction of XRPD intensities for PO bias.

The specific objective was to extend the work on gibbsites to other materials using both the Rietveld and line ratio methods to test the general applicability of the March model for PO assessment.

1.3 Research Plan

Materials Selection and Analysis

Materials were to be selected for the study using the selection criteria :

- Conformity of the common crystallite shapes in the selected materials with the rod- or disk-shaped crystallites assumed in the March theory,
- availability of single crystal structural data for the calculation of diffracted intensities for a powdered specimen without PO,

- occurrence in the powder diffraction pattern of reflections with sufficient intensity for the determination of reliable line ratios.

XRPD data were then to be collected for each material using three sample mounting procedures designed to give a range of PO conditions :

(i) side-drifting,

(ii) front-loading in which the sample was lightly pressed,

(iii) briquetting in which the sample was front-loaded with considerable pressure.

Data Analysis and Evaluation

Each data set was to be analysed by Rietveld analysis, with and without the March model included. A second determination of the March parameter was to be determined using line ratio data. The two sets of results were then to be used to test for each material the validity of the March model, and of the Rietveld and line ratio formalisms.

1.4 Thesis Structure

Chapter 1 summarises the literature on PO characterisation with powder diffraction data. The March model of PO is introduced in Chapter 1 and then described in greater detail in Chapter 2 together with experimental methods for determining the single-parameter of the March formula, *viz.* the Rietveld and line ratio methods.

Chapter 3 describes the experimental procedures - in particular specimen selection and handling, XRPD data measurement, Rietveld calculation procedures, line ratio methods and correction of intensities for preferred orientation. The chapter pays particular attention to the rationale adopted in selecting line pairs.

Chapter 4 considers the PO results, for each material in turn, with particular reference to the validity of the March model. Chapter 5 then gives an overview of the results with reference to the objectives of the thesis study.

CHAPTER 2

ASSESSMENT OF PREFERRED ORIENTATION WITH THE MARCH MODEL

2.1 March Model

Table 2.1 lists the mathematical forms of pole-figure profiles which have been used for modelling PO in Rietveld calculations - see discussion in Chapter 1 on the rationale given in the literature for the use of each form. The deficiencies of forms 1-5 were highlighted by Dollase (1986) in proposing use of the March (1932) model. The single-parameter function used in the March model (form 6 in Table 2.1) describes the pole-density distribution produced by rigid body rotation of inequant crystallites upon axially-symmetric, volume-conserving compression or expansion. The value of the pole density ranges from r^3 to $r^{-3/2}$ according to the amount of sample deformation. The March function applies equally well to distributions of either platy or acicular (*i.e.* elongated) crystallites. The physical significance of the March parameter differs in the two cases. In the case of platy crystallites $r = d/d_o$ where d is the sample thickness after axial extension or compaction from its original (hypothetical) thickness. The value of $r = d_o/d$ applies to acicular crystallites.

The model is applicable to crystals of any symmetry and does not require use of data acquired with a multi-axis diffractometer. The two assumptions made concerning the samples in the Dollase method, *viz.*

(i) the sample has cylindrical (axial) symmetry,

(ii) the sample crystallites are effectively rod- or disk-shaped,

are often satisfied by methods used commonly to prepare and mount powder samples, and can be achieved by spinning the sample about its cylindrical axis during data measurement. The second assumption requires caution to ensure that the crystallite types are likely to satisfy the March model for PO.

Table 2.1

Mathematical Forms of the PO Function for Single and Dual Parameter Pole-Figure Profiles (Dollase, 1986)

The functions are stated in the form with PO = maximum at angle $\alpha = 0$.

Form	Expression	Reference
1	$\exp[-G\,\alpha^2]$	(1), (2)
2	$\exp[G(\pi/2 - \alpha)^2]$	(3), (4)
3	$\exp[-G\,\sin^2\alpha]$	(5)
4	$\exp[-G(1 - \cos^3\alpha)]$	(5)
5	$b + (1 - b)\exp[-G\,\alpha^2]$	(6), (7)
6	$(r^2\cos^2\alpha + r^{-1}\sin^2\alpha)^{-3/2}$	(8)

References : *(1) Uda (1967); (2) Rietveld (1969); (3) Parrish & Huang (1983); (4) Will, Parrish & Huang (1983); (5) Capkova & Valdova (1974); (6) Sasa & Uda (1976); (7) Toraya & Marumo (1981); (8) March (1932).*

Definitions : α = the angle in radians between the PO direction and given RLV in radians,

G, b and r = adjustable PO parameters.

Three features of the March model are noted. First, the March model has a physical basis. The second feature is that the March model can be normalised to unit integral which means that a change in PO parameter, r, should not produce a change in the Rietveld scale factor (see Section 2.2). Third, the March model has a single refineable parameter. Even when samples develop PO due to mechanisms other than compaction and grain settling, fitting a March model allows estimation of an intuitively simple equivalent specimen compaction which is useful for quantitative comparison of samples (Dollase, 1986).

The value of r can be determined by Rietveld analysis if the crystal structure of the material is available in the literature. However the computational facilities required for Rietveld calculations are beyond the reach of some analysts. An alternative, a simpler method based on diffraction line ratios, has been proposed by Li and O'Connor (1989). The Rietveld and the line ratio methods are outlined in Sections 2.2 and 2.3 below.

2.2 Rietveld Procedure

Mathematical Basis

The Rietveld (1969) method for crystal structure refinement was developed initially for use with NPD data. The technique, as used in studies of crystal structure, involves mathematical modelling of powder diffraction profile data with fundamental crystallographic parameters, which include atom positions, thermal vibration and site occupancy values. Recently the technique has been extended to facilitate structure refinements with XRPD data. Applications of the technique reported to date have been mainly restricted to the determination of fundamental crystallographic parameters, namely, atom positions, thermal vibration parameters and site occupancy values. Various research groups, including the Curtin X-ray Analytical Science Group, have

considered the Rietveld method for the determination of macroscopic physical descriptors of materials - notably phase composition, residual strain, crystallite size and shape, and PO.

The basis of the Rietveld procedure is to minimise the residual, R, for the measured and calculated XRPD patterns,

$$R = \Sigma_i w_i | Y_i - Y_{ci} |^2 \quad \ldots \quad (2.1)$$

using iterative least squares refinement. Here Y_i is the measured intensity for profile point i, Y_{ci} is the corresponding Rietveld-calculated intensity after refinement and w_i is the weighting factor for point i in the pattern. The weight of reflection i is calculated from the expression,

$$w_i = 1/Y_{ci} \quad \ldots \quad (2.2)$$

The calculations usually require a mainframe computer, for example, the X-ray Analytical Science Group at Curtin University of Technology employs a VAX1185 machine.

The general mathematical form of Y_{ci} employed in the various refinement programs was described by Rietveld (1969). The specific expressions in the software used in this study (Hill and Howard, 1986) have been described by Wiles and Young (1981). The intensity, Y_{ci}, at profile point i for opaque, flat, single-phase specimens is given by summing the contribution from neighboring Bragg reflections and from the background according to :

$$Y_{ci} = s \Sigma_j p_j L_j | F_j |^2 \Phi(2\theta_i - 2\theta_j) P_j + Y_{bi} \quad \ldots \quad (2.3)$$

where $2\theta_i$ and $2\theta_j$ are the detector angles corresponding to point i and Bragg peak j, respectively.

Term s is the Rietveld scale factor which, for the correct model, should give

$$\Sigma_i Y_i = \Sigma_i Y_{ci} \qquad \ldots \quad (2.4)$$

Term p_j is the Bragg peak multiplicity factor. The space group of the material has to be nominated in order to generate correct p_j's. The space group of the material must be available in the literature.

Term L_j is the combined Lorentz and polarization factor for the jth Bragg reflection given by

$$L_j = \frac{1 + \cos^2 2\theta_j}{\sin^2 \theta_j \,.\, \cos \theta_j} \qquad \ldots \quad (2.5)$$

for Bragg angle θ_j.

Factor $|F_j|$ is the modulus of structure factor F_j for Bragg peak j, produced by summing over the k atoms in the unit cell :

$$F_j(hkl) = \Sigma_k f_k \exp[2\pi i\{(hx_k)+(ky_k)+(lz_k)\}] T_k \qquad \ldots \quad (2.6)$$

where f_k is the scattering factor; h, k and l are the Miller indices for line j; a, b and c are the cell parameters; x_k, y_k and z_k are the atom fractional position co-ordinates and T_k is a temperature factor given by :

$$T_k = \exp(- B_k \sin^2 \theta / \lambda^2) \qquad \ldots \quad (2.7)$$

where B_k is the isotropic thermal vibration parameter.

Various mathematical forms of the *peak profile function*, $\Phi(2\theta_i - 2\theta_j)$ are available in the Hill and Howard (1986) Rietveld software employed in the present study. The pseudo-Voigt type of profile function selected for the present study is given by,

$$\Phi(2\theta_i - 2\theta_j) = \tau \frac{\sqrt{C_o}}{H_k \pi} \left[1 + C_o \frac{(2\theta_i - 2\theta_j)^2}{(H_j)^2} \right]^{-1} + (1 - \tau) \frac{\sqrt{C_1}}{H_j \sqrt{\pi}} \exp \left[- C_1 \frac{(2\theta_i - 2\theta_j)^2}{(H_j)^2} \right] \quad \ldots \quad (2.8)$$

where $C_o = 4$, $C_1 = 4 \ln 2$, τ is a refineable mixing parameter and H_j is the full-width at half-maximum (FWHM).

FWHM H_j may be varied in the Hill-Howard software with Bragg angle, θ_j, as

$$(H_j)^2 = U \tan^2 \theta_j + V \tan \theta_j + W \quad \ldots \quad (2.9)$$

where U, V and W are half-width parameters independent of θ_j.

Term Y_{bi} is the background component of the pattern which may be modelled in the Hill-Howard software with the polynomial expression :

$$Y_{bi} = \sum_{m=-1}^{4} B_m (2\theta_i)^m \quad \ldots \quad (2.10)$$

where B_m is one of six refineable parameters.

Term P_j is the PO function. The Rietveld software used in the study employs the March model of PO for uniaxially-oriented disk- or rod-shaped crystallite as discussed in Section 2.1.

Figures of merit, known as the R-factors, can be used to judge the level of disagreement between calculated and measured intensities for a given model. Two R-factor types, described as 'profile' and 'Bragg', are employed. The profile types,

$$R_p = \frac{\Sigma_i \, | Y_i - Y_{ci} |}{\Sigma_i \, Y_i} \qquad \ldots (2.11a)$$

and the corresponding weighted form,

$$R_{wp} = \left[\frac{\Sigma_i \, w_i \quad (y_i - y_{ci})^2}{\Sigma_i \, w_i \quad (y_i)^2} \right]^{1/2} \qquad \ldots (2.11b)$$

are formed by summing across the i profile points in the measured and calculated patterns.

Ideally R_p should have the value,

$$R_{exp} = \left[\frac{N - P}{\Sigma_i \, w_i \, (y_i)^2} \right]^{1/2} \qquad \ldots (2.11c)$$

where N is the number of observations (profile points) and P is the number of least squares parameters.

The Bragg R-factor,

$$R_B = \frac{\Sigma_j \, | I_{jo} - I_{jc} |}{\Sigma_j \, I_{jo}} \qquad \ldots (2.12)$$

is formed by summing I_{jo} and I_{jc} the respective observed and calculated integrated intensities for Bragg reflection j, over the set of Bragg data. Factor Ijo is formed, as described by Rietveld (1969), with expression,

$$I_{jo} = \Sigma_i \left[w_i(F_j)^2 \frac{y_i}{y_{ci}} \right] \quad \ldots \quad (2.13)$$

where Σ_i is the sum over all observed profile intensities, y_i which can theoretically contribute to the observed integrated intensities, I_{jo}.

Example of PO Assessment Using Rietveld Refinement with the March Model

Li and O'Connor (1989) and Li *et al.* (1990) reported that the agreement between the measured XRPD and the Rietveld-calculated patterns for gibbsites with different degrees of PO improves dramatically when the March model is employed in the Rietveld refinement. The effectiveness of the correction can be seen from Figure 1.3 in Chapter 1 and Table 2.2 which compare the measured and calculated intensities (profile and Bragg peak types) when the March model is employed.

2.3 Line Ratio Method

Mathematical Basis

Roach and Cornell (1988) described an empirical procedure for characterising morphology in gibbsite samples according to variations in the relative intensities of their XRPD patterns. They suggested that these differences are caused by PO. An index of morphology, designated the morphology ratio, was defined as

Table 2.2

Correction of Gibbsite Integrated Intensities for PO in Three Samples Using the March Model (Li *et al.*, 1990)

h k l	Intensities		
	Gib-B (r=1.00)	P-1(5) (r=0.76)	Gib-B5 (r=0.61)
0 0 2	41,400	41,400*	46,200*
		91,800	191,100
1 1 0	16,000	14,800*	16,200*
		10,000	8,000
2 0 0	7,800	5,600*	6,700*
		3,800	3,300
3 1 1	8,100	9,200*	8,000*
		6,700	4,400
-3 1 3	6,800	6,200*	6,100*
		5,700	4,700

* March-corrected intensities

$$M_R = I(002)/\{I(110) + I(200)\} \quad \ldots \quad (2.14)$$

for the integrated intensity of Bragg peak (002) and for the intensity doublet of the (110) and (200) line pair. The ratio was found to be highly sensitive to particle morphology. While the M_R data proved to be useful as a qualitative measure of morphology, the M_R values were not used to quantify PO or to correct XRPD data for PO. Li and O'Connor (1989) subsequently derived a relationship between ratio M_R and the March parameter in equation (1.10) which was proposed as a simple alternative to the Rietveld method for determining parameter r and, therefore, for applying PO corrections to XRPD data. Following the approach proposed by Li and O'Connor (1989), the morphology ratio (designated the line ratio in this thesis), M_R, for a phase in a powder sample can be defined in general terms as

$$M_R(\text{oriented}) = \frac{I_r(h_1k_1l_1)\, P(h_1k_1l_1)}{I_r(h_2k_2l_2)\, P(h_2k_2l_2)} \quad \ldots \quad (2.15)$$

where $I_r(h_1k_1l_1)$ and $I_r(h_2k_2l_2)$ are the integrated intensities for any two lines with indices $(h_1k_1l_1)$ and $(h_2k_2l_2)$ in the corresponding randomly-oriented pattern, and $P(h_1k_1l_1)$ and $P(h_2k_2l_2)$ are the factors by which the randomly-oriented intensities are biased in the oriented pattern.

Factors $P(h_1k_1l_1)$ and $P(h_2k_2l_2)$ for the March model are given by :

$$P(h_ik_il_i) = \{r^2 \cos^2 \alpha(h_ik_il_i) + r^{-1} \sin^2 \alpha(h_ik_il_i)\}^{-3/2} \quad \ldots \quad (2.16)$$

where $\alpha(h_ik_il_i)$ is the angle between the direction of PO and the relevant RLV. The variation of $P(h_ik_il_i)$ with angle $\alpha(h_ik_il_i)$ for various values of r is shown in Figure 2.1. Factor $P(h_ik_il_i)$ increases rapidly above 1.0 as $\alpha(h_ik_il_i)$ reduces below 45^o; whereas for $\alpha(h_ik_il_i)$ greater than 45^o $P(h_ik_il_i)$ is less than 1.0 and falls more slowly with change in $\alpha(h_ik_il_i)$.

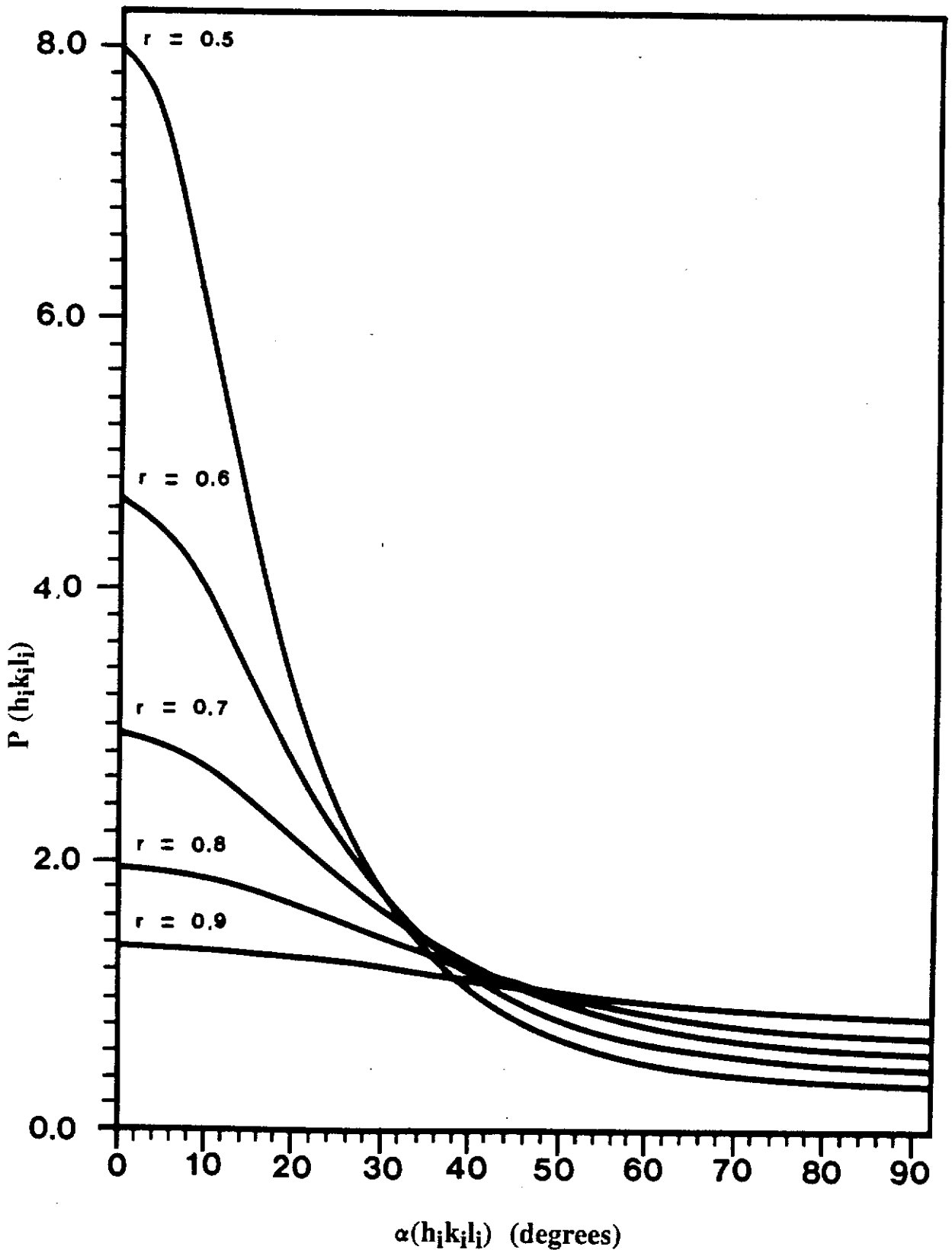

Fig. 2.1. The variation of PO factor P with orientation angle α for different values of March r-parameter.

The value of M_R may be computed for a given value of r using intensity values $I_r(h_1k_1l_1)$ and $I_r(h_2k_2l_2)$ measured with a suitable randomly-oriented sample or taken from the JCPDS-ICDD (Joint Committee for Powder Diffraction Standards - International Centre for Diffraction Data) collection of measured patterns if acceptable data are available. However, in view of the difficulty of obtaining reliable XRPD data for randomly-oriented specimens, it is generally preferable to use theoretically-derived intensity values computed with structure factors. Theoretical intensity values may be derived *a priori* from the atom positions or may be acquired for some materials from the theoretical patterns in the JCPDS collection.

Selection of $(h_1k_1l_1)$ and $(h_2k_2l_2)$ requires careful consideration. First, the intensities of the two lines must be sufficiently strong to give acceptable counting statistics - this judgement is best made with theoretical data. Second, choice of angles $\alpha(h_1k_1l_1)$ and $\alpha(h_2k_2l_2)$ must give a line ratio M_R(oriented) which is sufficiently sensitive to r. Clearly if $\alpha(h_1k_1l_1) = \alpha(h_2k_2l_2)$ then $P(h_1k_1l_1)/P(h_2k_2l_2) = 1.00$ (see equation (2.16)) which conveys no information about r. Figure 2.2 shows the variation of ratio $P(h_1k_1l_1)/P(h_2k_2l_2)$ with $\alpha(h_1k_1l_1)$ and $\alpha(h_2k_2l_2)$ for various values of r. Ideally we need to select intense line pairs for which $\alpha(h_1k_1l_1) = 0^o$ and $\alpha(h_2k_2l_2) = 90^o$.

Gibbsite Example

The direction of PO in gibbsite is <001>. In the studies by *Li et al.* (1990), lines were selected which gave $\alpha(h_1k_1l_1)$ values close to the ideal values. A typical pattern for a highly oriented gibbsite is shown in Figure 1.3 in Chapter 1. The intense (002) line at $2\theta = 18.3^o$ is an obvious choice since $\alpha(h_1k_1l_1) = 0^o$. The intense doublet (110, 200) at $2\theta = 20.3^o$ and 20.5^o, which is a composite of the (110) line ($\alpha(h_2k_2l_2) = 87.7^o$) and the (200) line ($\alpha(h_2k_2l_2) = 85.4^o$), is an excellent choice for the second line in view of the intensity of the doublet and the proximity of the angles to 90^o for the doublet line.

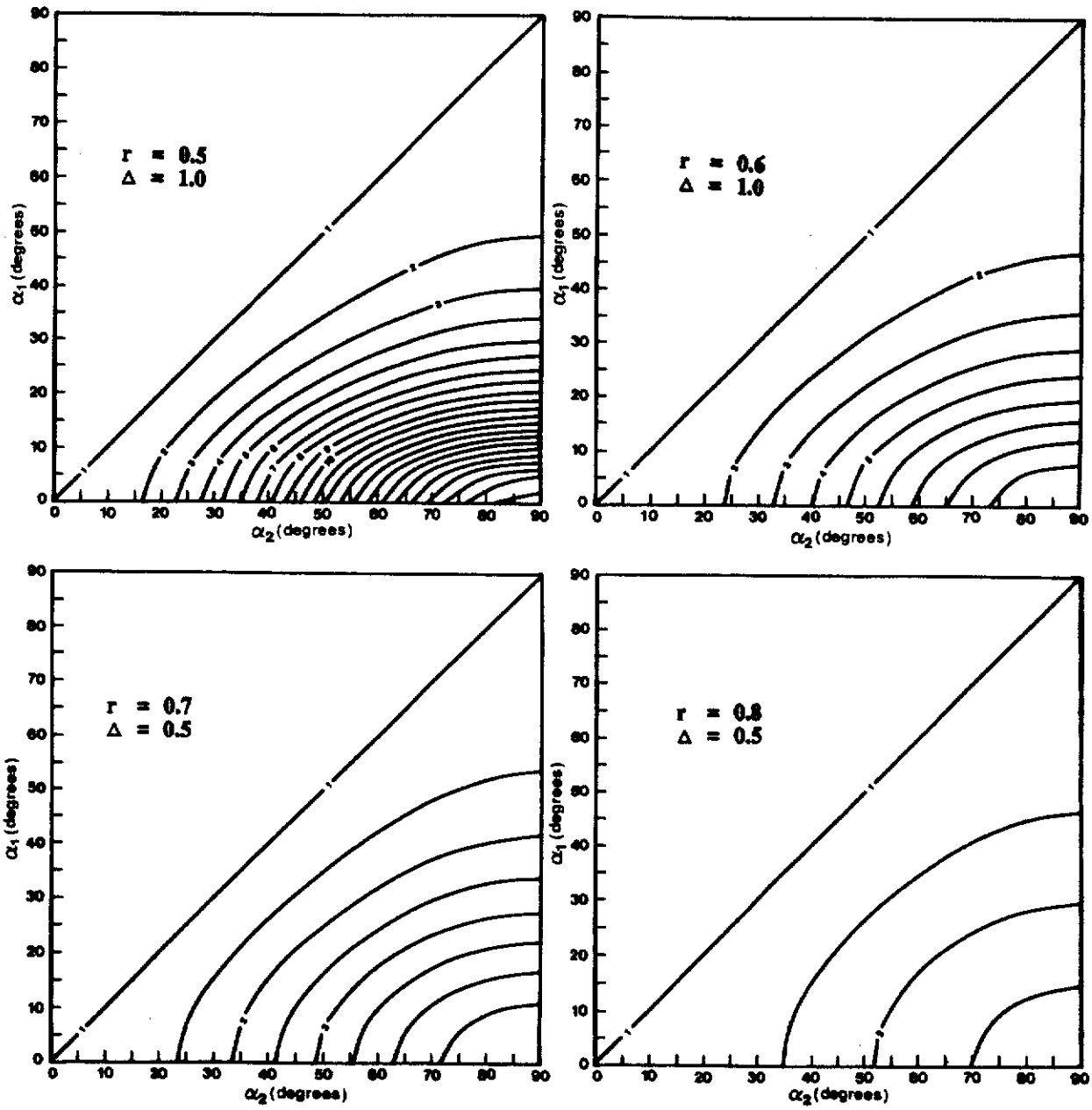

Fig. 2.2. Contours of ratio $P(h_1k_1l_1)/P(h_2k_2l_2)$ for PO factors of the March model for combinations of $\alpha(h_1k_1l_1)$ and $\alpha(h_2k_2l_2)$.

Use of a doublet for gibbsite required modification of equation (2.15) as follows:

$$M_R(\text{oriented}) = \frac{I_r(002)\, P(002)}{I_r(110)\, P(110) + I_r(200)\, P(200)} \quad \ldots \quad (2.17)$$

The relative values of $I_r(002)$, $I_r(110)$ and $I_r(200)$ may be set at 100, 36 and 18, respectively, (JCPDS calculated pattern 29-41). Then the precise form of equation (2.17) becomes :

$$M_R(\text{oriented}) = \frac{(r^2)^{-3/2}}{0.36(0.00161r^2+0.9984r^{-1})^{-3/2} + 0.18(0.0064r^2+0.9936r^{-1})^{-3/2}} \quad \ldots \quad (2.18)$$

This exact form may be reduced to the approximation if the two terms involving r^2 are neglected. Then equation (2.18) reduces to:

$$r = 1.15\, M_R^{-0.222} \quad \ldots \quad (2.19)$$

since $\alpha(h_1k_1l_1)$ approximates to 0^o and the two $\alpha(h_2k_2l_2)$ values are close to 90^o. The exact and approximation forms (equations (2.18) and (2.19)) are shown in Figure 2.3 which also gives experimental data from the study by Li and O'Connor (1989).

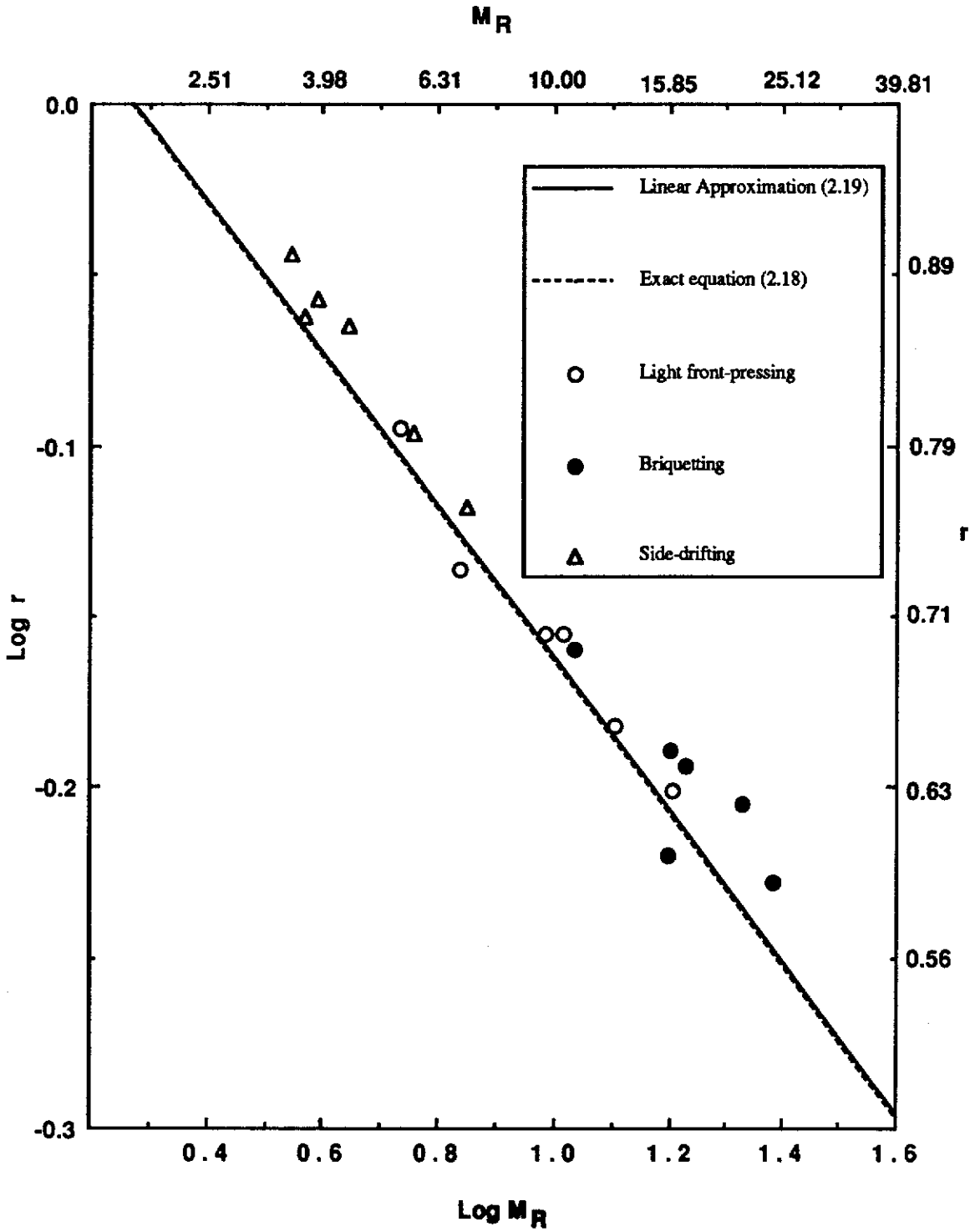

Fig. 2.3. Plot for gibbsite of log r (Rietveld)-versus-log M_R from line ratio data compared with equations (2.18) and (2.19). It can be seen that the results for all three mounting procedures (side-drifting, light front-pressing and briquetting) lie close to the linear regression form shown in this figure, indicating that the expression is a universal relation for gibbsites which is independent of the procedure of sample preparation. (Li *et al.* 1990).

CHAPTER 3

EXPERIMENTAL PROGRAM

3.1 Facilities

The present study made use of facilities in two laboratories - at Curtin University and the Research and Development Department of Alcoa of Australia Ltd., Kwinana. The facilities employed are summarised in Table 3.1.

Initially the principal reason for employing the Alcoa facilities in addition to those at Curtin was to make use of a Hertzog type-HDIF press which is employed routinely at Alcoa for preparing briquette samples. The Hertzog press therefore extended the range of PO conditions beyond those employed at Curtin for sample preparation. Some use was also made of the side-drifting mounting facility at Alcoa as well as that available at Curtin. Due to operational problems with the Curtin x-ray powder diffractometer, the Alcoa instrument was used for all XRPD measurements. The Alcoa instrument is a Siemens D500 type - see Section 3.4 for details.

3.2 Specimen Selection

The specimens selected for the study were chosen to satisfy the objectives stated in Section 1.3 - specifically to provide a wide range of PO conditions in different materials. These were :

- molybdite [MoO_3],
- calcite [$CaCO_3$],
- kaolinite [$Al_2O_3.2SiO_2.2H_2O$].

Table 3.1

Techniques Used in the Study

	Laboratories	
	Curtin	Alcoa
Sample Treatment		
Powder milling	√	√
XRPD Mounting		
Side-drifting	√	√
Light front-pressing	√	-
Briquetting	-	√
Characterisation		
PSD	√	-
XRPD	-	√

PO is likely to be substantial in molybdite powders due to the blade-like needle shape. Calvert *et al.* (1983) demonstrated the considerable sensitivity of molybdite diffraction patterns to sample preparation and mounting by examining data for samples prepared by pressing, side-drifting and spray drying. However, Calvert *et al.* did not make use of the March model in interpreting their data. Calculation by the thesis author of M_R values for the data in Table 1 of Calvert *et al.* showed that the r-values for the three procedures were 0.664, 0.921, 0.963, respectively. In view of the substantial variation in r which can therefore be obtained with molybdite, the material was an excellent choice for the present study. Further attractions were :

(i) the consistency of the platy crystallite shapes with the theoretical requirement for the March model that crystallites should be either disk- or rod-like,

(ii) the availability of a detailed description of the crystal structure in the literature (Kihlborg, 1963).

Calcite was selected in view of the results reported by Dollase (1986) which indicated that PO was moderate for the samples examined in that study, *ca.* $r \simeq 0.9$. The material was thought to merit inclusion in the present study as a means of testing the reliability of the correction procedures for values of r close to 1.0. Also the flat-plate particle shape commonly observed in calcite appears to satisfy the requirement for rod- or disk-shaped crystallites when using the March model. Additionally the crystal structure of calcite is well known (Megaw, 1970 and 1973).

Kaolinite was included in the study because the material has attributes similar to molybdite. In particular the well known sensitivity of the diffraction pattern to variations in the pressure applied to the sample, indicated that a wide range of March r-values should be obtained. Also the crystal structure is reasonably well defined for March calculations (Brindley and Robinson, 1946; Zvyagin, 1960) even though there are some minor differences between the proposed models. A further attribute of the material is the similarity between the platy shape of kaolinite particles and the disk-shaped crystallites considered in the March model. Raven (1989) investigated the extent

of PO in kaolinite samples from six sources using Rietveld refinement with the March model. The March r-parameters for the sample suite ranged from 0.679(2) to 0.950(4) using side-drifted sample mounts.

The molybdite and calcite specimens were obtained from BDM Chemicals Ltd., Poole, England and AJAX Chemical Pty. Ltd., Auburn, Australia, respectively, as Analytical Reagent (ANALAR). The kaolinite specimen selected for the study was kindly provided by Mr. M. Pryce, Chemistry Centre, Western Australia - the specimen was described as a Georgia WP-SD type by the donor.

3.3. Specimen Handling Procedures For X-Ray Diffraction

Rationale

Various sample milling/mounting procedure combinations used commonly in XRPD work were employed in an attempt to produce a wide range of r-values for each specimen. These had been used also by Li and O'Connor (1989) and Li *et al.* (1990) in the study of gibbsite which preceded the thesis investigation.

The principles proposed by Alexander *et al.* (1948) for predicting acceptable PSDs in terms of intensity reproducibility were followed in selecting the milling procedure for each material. Table 3.2 summarises the analysis performed in this planning exercise. The table includes, for comparison, measured PSD data for the materials employed - see 'milling procedures' following.

The size distributions for the as-received materials were modified by 'micronising' with a McCrone rod mill (O'Connor and Chang, 1986).

Three mounting procedures were employed :

- side drifting,
- "light" front-pressing using normal packing of diffraction mount,
- briquetting under substantial pressure.

Table 3.2

Optimum Particle Size From Klug and Alexander (1974) and PSDs for the As-received and Micronised Samples in the Study

Samples	Density (g/cm^3)	MAC (cm^2/g)	LAC (cm^{-1})	Optimum particle size from Klug and Alexander		Measured D[v,0.5] in μm (Figure 3)		
				1%(μm)	2%(μm)	As-received	Micronised (minutes) 10	30
Molybdite	4.71	106.4	501.0	2.5	4.0	10.8	8.6	3.6
Calcite	2.72	69.8	190.0	4.0	7.0	13.4	2.1	-
Kaolinite	2.60	29.5	76.7	7.0	9.0	3.4	3.2	-

Notes :

MAC = mass attenuation coefficient

LAC = linear attenuation coefficient

1%(μm), 2%(μm) = intensity reproducibility for stated particle size

D[v,0.5] = median value for the volumetric PSD.

The sequence above may be expected to give a progressive increase in PO for a particular material.

Milling Procedures

The PSDs of the materials were measured at the Curtin Particle Analysis Facility using a Malvern Master Sizer which is a laser scattering type instrument. The results obtained for the as-received materials are shown in Figures 3.1(a), 3.2(a) and 3.3(a). It was evident from these results that the PSDs for molybdite and calcite as-received were unsatisfactory, whereas that for kaolinite readily met the criteria given in Table 3.2.

The micronising procedures used for molybdite and calcite were based on the procedure described by O'Connor and Chang (1986) to achieve a suitable PSD in α-quartz, for which approximately 3 g of ground sample was fed into the McCrone micronising mill (McCrone Research Associates Ltd., 2 McCrone Mews, Belsize Lane, London NW3 5BG) with 10 ml of acetone, wet-ground for 10 minutes, then transferred into an evaporating dish and dried using infrared radiation.

In this study, milling times were varied to obtain satisfactory PSDs. Milling trials for molybdite involving 10 minutes and 30 minutes gave the PSDs shown in Figure 3.1(b) and (c) from which it was concluded (see Table 3.2) that the molybdite should be milled for 30 minutes. By contrast, a 10 minutes milling period was adequate for calcite - see Figures 3.2 (a) and (b) and Table 3.2.

Micronising performed at Alcoa was carried out with the method used routinely there *viz.* 4 g of sample in 15 ml ethanol. Therefore the micronising procedures employed in the two laboratories differed slightly.

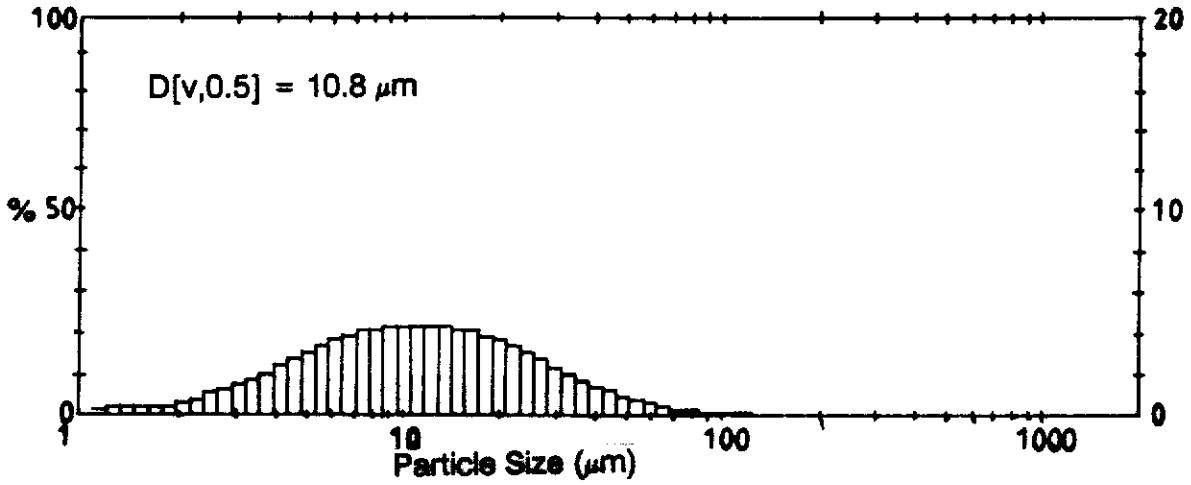

(a) As-received

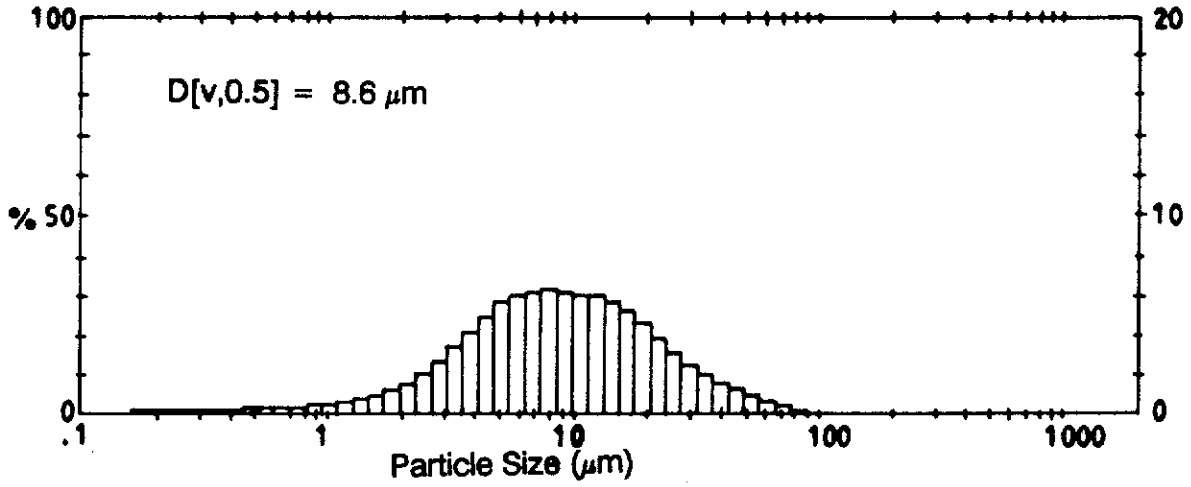

(b) Micronised for 10 minutes

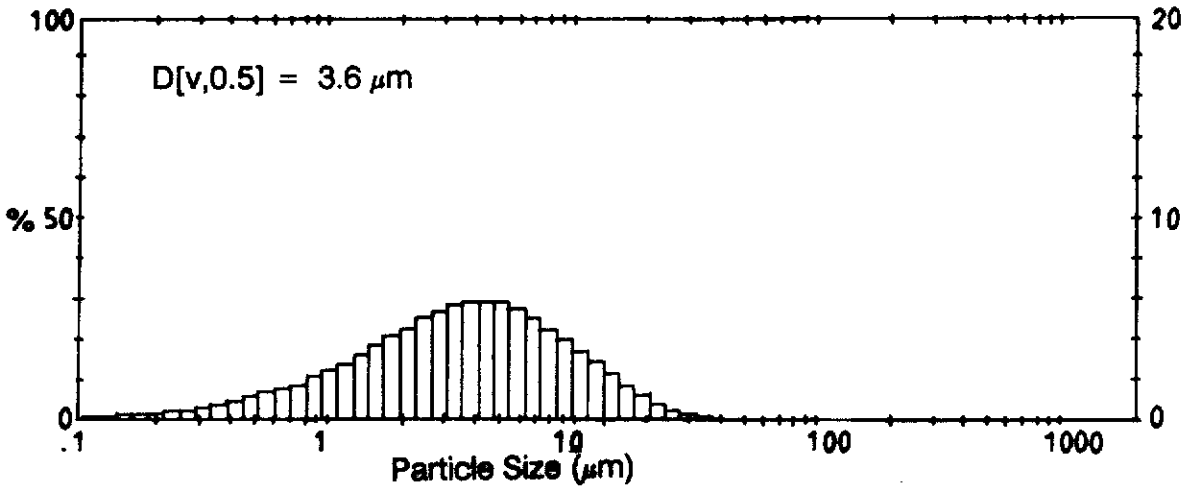

(c) Micronised for 30 minutes

Fig. 3.1. PSDs for molybdite samples. Median volumetric particle size D(v,0.5) is given in each case.

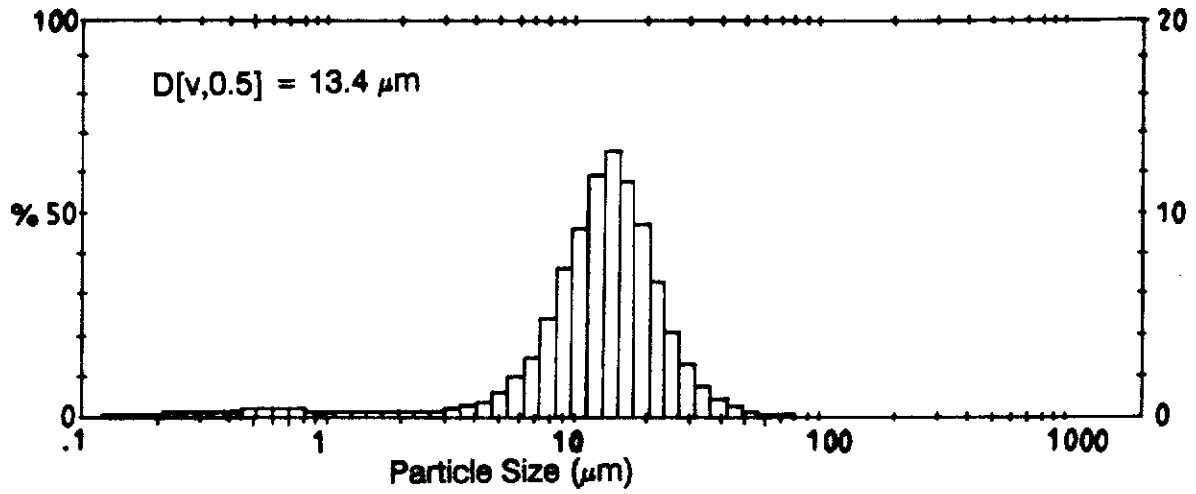

(a) As-received

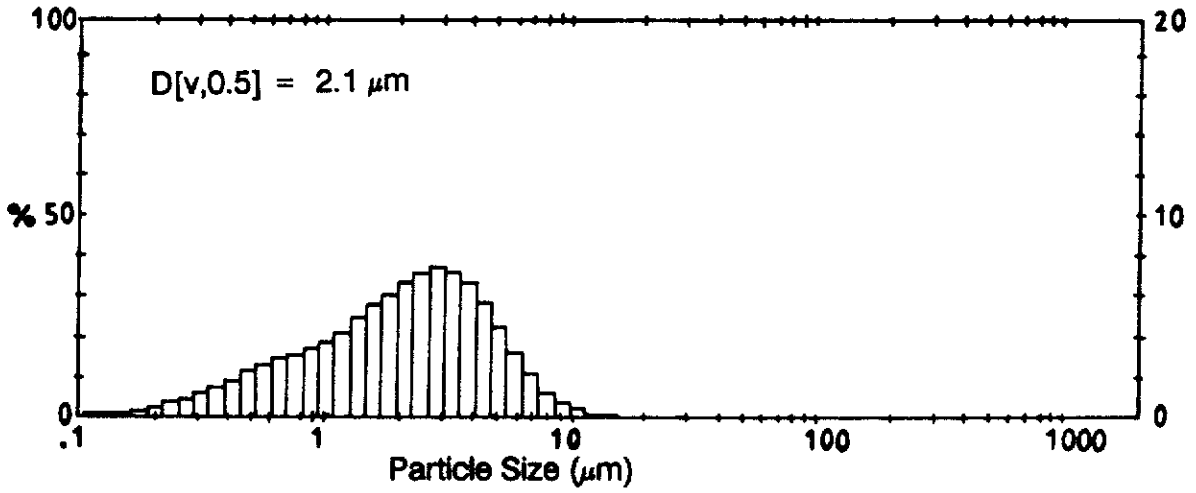

(b) Micronised for 10 minutes

Fig. 3.2. PSDs for calcite samples. Median volumetric particle size D(v,0.5) is given in each case.

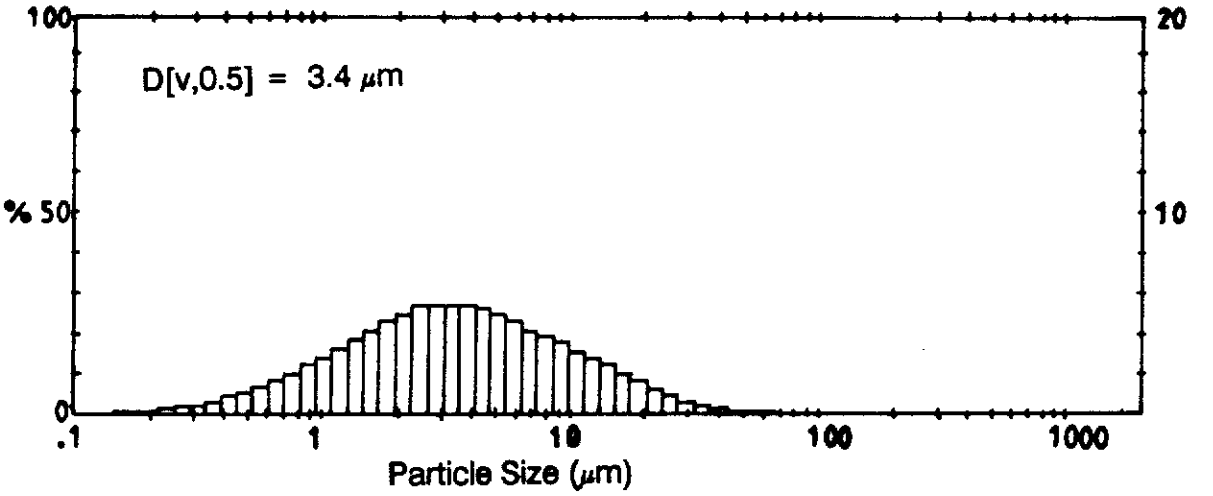

(a) As-received

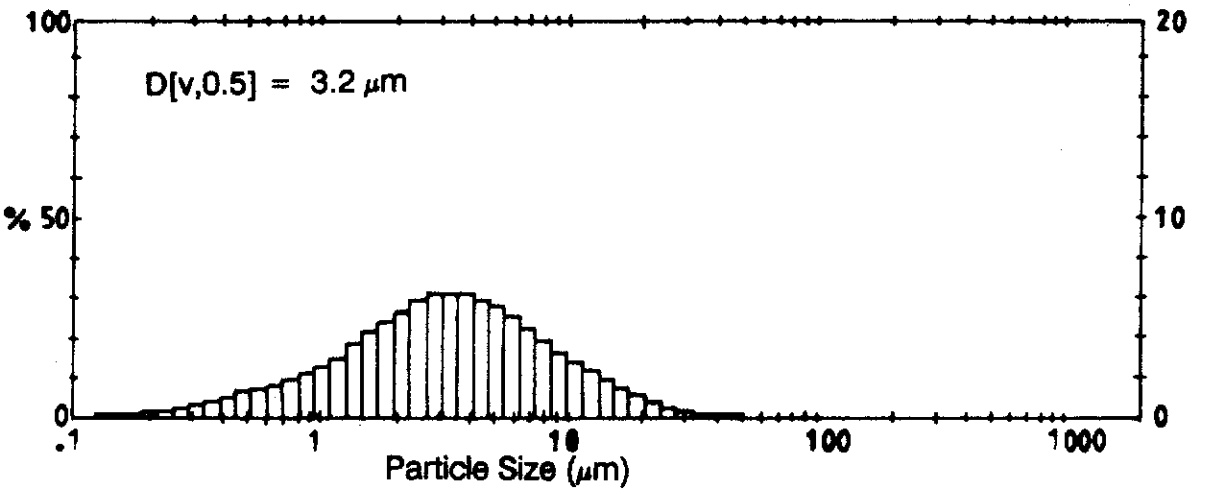

(b) Micronised for 10 minutes

Fig. 3.3. PSDs for kaolinite samples. Median volumetric particle size D(v,0.5) is given in each case.

Mounting Procedures

Side-Drifting

Side-drifting mounting procedures were employed with the aim of producing XRPD mounts with minimal PO for each of the materials investigated. Additional side drifted samples with even less PO were prepared for molybdite by mixing 50% by weight silica gel with the material, as proposed by Calvert *et al.* (1983).

The side-drifting was performed by fixing a glass slide to the front surface of the D500 holder and then loading the material through the gap between the slide and holder by tapping with a spatula. The glass slide was then carefully removed leaving the sample securely packed in the holder when the holder had sufficient material in place.

Light Front-Pressing

This mounting procedure was employed to enhance the level of PO obtained by side-drifting. The powder samples were gently pressed by manual means into standard Siemens D500 plastic specimen holders by lightly pressing with a glass slide. Excess sample was removed by drawing a razor blade across the surface.

Briquetting Under Substantial Pressure

The briquetting procedures were expected to give the highest PO for the methods considered. The samples were back-pressed into aluminium holders at a pressure of 6 bar for 7 seconds with a Hertzog HDIF machine. This procedure is routinely employed by Alcoa of Australia Ltd., Kwinana, Western Australia.

Milling-Mounting Combinations Used for the Three Materials

The combinations selected are indicated in Table 3.3.

Table 3.3

Sample Codes With Treatment and Mounting Combinations

Sample Code	Milling	Mounting procedures	Laboratory
Molybdite			
MDC	Micronised for 30 minutes	Side-drifting	Curtin
MLC	"	Light front-pressing	"
MBA	"	Briquetting	Alcoa
Molybdite mixed with silica gel (50% by weight)			
MDA(S)	Micronised for 30 minutes	Side drifting	Alcoa
MLC(S)	"	Light front-pressing	Curtin
MBA(S)	"	Briquetting	Alcoa
Calcite			
CDA	Micronised for 10 minutes	Side-drifting	Alcoa
CLC	"	Light front-pressing	Curtin
CBA	"	Briquetting	Alcoa
Kaolinite			
KDC	As-received	Side-drifting	Curtin
KLC	"	Light front-pressing	"
KBA	"	Briquetting	Alcoa

Sample Codes :

First letter	=	material : M, C, and K for molybdite, calcite, and kaolinite, respectively.
Second letter	=	mounting procedure : D, L and B for side-drifting, light front-pressing and briquetting, respectively.
Third letter	=	preparation of samples employed in the study, C and A for Curtin and Alcoa laboratories, respectively.
(S)	=	silica gel dilution used.

3.4 X-Ray Diffraction Measurements

Measurement Parameters

The step-scanned patterns were measured at Alcoa with a Siemens D500 Bragg-Brentano x-ray powder diffractometer fitted with a graphite diffracted-beam curved monochromator. The operating conditions were : Cu-anode tube at 40kV and 30 mA, unfiltered radiation, 1° divergence for incident beam and 0.05° receiving slit, goniometer range (2θ) = 10° to 130° in step size of 0.04°, counting time one second per step, and NaI scintillator with PHA.

Angles below 10° in 2θ were not measured because these do not contain diffraction peaks for the materials employed in the present study, and also because the background rises sharply, due to direct beam detection, making background modelling difficult. The counting times and scan step sizes were consistent with the guidelines described by Hill and Madsen (1984, 1986) who showed that increasing counting times beyond one second per step, and reducing the step size below 0.04° 2θ made negligible improvement to Rietveld parameter standard deviations and R-factors.

A complete set of diffraction patterns of the sample set described in Table 3.3 was acquired initially during a single measurement session on 21 December 1989. Following a review of the procedures which had been employed, most of the data sets (*i.e.* for all samples other then CDA and CBA) were re-measured in a single measurement session - on 30 April 1990. Due to a change in instrument sensitivity which occurred between the two sessions, the counting statistics for samples CDA and CBA are inferior to the values for the other samples. In retrospect, all data sets should have been measured under the one set of conditions. However the data used in the study are acceptable given the stated objectives.

Initial Search/Match Analysis of Samples

The XRPD patterns were reduced to peak integrated intensities using the EVA program marketed by SOCABIM, *9 bis.* Villa du Bell-Air, Paris. Background and α_2 components were removed before the determination of integrated intensities. The measured intensities for each of the samples were then matched against the calculated theoretical intensity (*i.e.* random orientation, r = 1.00), for molybdite, calcite and kaolinite, respectively, (see following discussion). The matching of line positions was satisfactory. No extraneous lines were observed.

Estimation of Integrated Intensities

The calculated (*i.e.* theoretical) intensities for randomly-oriented specimens (see equation (2.16)) were computed with the structural models of Kihlborg (1963), Megaw (1970, 1973) and Brindley and Robinson (1946) for molybdite, calcite and kaolinite, respectively, - see Tables 3.4, 3.5 and 3.6 for model details. Version LHPM4 of the Hill and Howard (1986) Rietveld program (see following Section) was used to calculate the intensities for these models.

3.5 Rietveld Calculations

Rietveld refinements were performed with a VAX1185 mainframe computer using the LHPM4 version of the Rietveld software described by Hill and Howard (1986).

Table 3.4

Crystal Structure Model for Molybdite, MoO_3

The structure was taken from Kihlborg (1963). Space group : Pbnm (No. 62 of International Tables for X-ray Crystallography, Vol. I). Unit cell parameters : a = 3.9628 Å, b = 13.855 Å, c = 3.6964 Å and $\alpha = \beta = \gamma = 90^{o}$.

Atom co-ordinates :

Atom Position	Wyckoff	x	y	z	B $(Å)^2$	Occupancy
Mo	4(c)*	0.08669	0.10164	0.250	0.230	0.500
O(1)	4(c)*	0.49940	0.43513	0.250	0.561	0.500
O(2)	4(c)*	0.52120	0.08657	0.250	0.628	0.500
O(3)	4(c)*	0.03730	0.22140	0.250	0.951	0.500

* Co-ordinates, 4(c) = x,y,1/4; 1/2-x,1/2+y,1/4; 1/2+x,1/2-y,3/4; x,y,3/4.

The direction of preferred orientation was taken to be <010> (Wooster, 1931; Brakken, 1931; Anderson and Magneli, 1950 and Kihlborg, 1963).

Table 3.5

Crystal Structure Model for Calcite, $CaCO_3$

The structure was taken from Megaw (1970 and 1973). Space group : $R\bar{3}c$ (No. 167 of International Tables for X-ray Crystallography, Vol. I). Unit cell parameters :

a = 4.990 Å, b = 4.990 Å, c = 17.002 Å, $\alpha = \beta = 90^{o}$ and $\gamma = 120^{o}$.

Atom co-ordinates :

Atom	Wyckoff Position	x	y	z	B $(Å)^2$	Occupancy
Ca	6(b)*	0.000	0.000	0.000	**	0.16667
C	6(a)*	0.000	0.000	0.250		0.16667
O	18(e)*	0.257	0.000	0.250		0.50000

* Co-ordinates 6(b) = 0,0,0; 0,0,1/2.
6(a) = 0,0,1/4; 0,0,3/4.
18(e) = x,0,1/4; 0,x,1/4; -x,-x,1/4; -x,0,3/4; 0,-x,3/4; x,x,3/4.

** Thermal parameters not stated - subsequently determined in Rietveld refinements.

The direction of preferred orientation was taken to be <104> (Dollase, 1986).

Table 3.6

Crystal Structure Model for Kaolinite, $Al_2O_3.2SiO_2.2H_2O$

The structure was taken from Brindley and Robinson (1946). Space group : P1 (No. 1 of International Tables for X-ray Crystallography, Vol. I); calculations performed using group C1. Unit cell parameters : a = 5.14 Å, b = 8.93 Å, C = 7.37 Å, α = 91.8°, β = 104.5° and γ = 90°.

Atom co-ordinates :

Atom Position	Wyckoff	x	y	z	B $(Å)^2$	Occupancy
Al(1)	1(a)*	0.331	0.511	0.456	0.19570	1.0000
Al(2)	1(a)*	0.331	0.844	0.456	0.19570	1.0000
Si(1)	1(a)*	0.031	0.336	0.085	0.00280	1.0000
Si(2)	1(a)*	0.031	0.669	0.085	0.00280	1.0000
O(1)	1(a)*	0.000	0.500	0.000	0.19750	1.0000
O(2)	1(a)*	0.250	0.250	0.000	0.19750	1.0000
O(3)	1(a)*	0.250	0.750	0.000	0.19750	1.0000
O(4)	1(a)*	0.110	0.342	0.307	0.19750	1.0000
O(5)	1(a)*	0.110	0.675	0.307	0.19750	1.0000
OH(1)	1(a)*	0.110	0.008	0.307	0.19750	1.0000
OH(2)	1(a)*	0.050	0.182	0.606	0.19750	1.0000
OH(3)	1(a)*	0.050	0.515	0.606	0.19750	1.0000
OH(4)	1(a)*	0.050	0.849	0.606	0.19750	1.0000

* Co-ordinates, 1(a) = x,y,z.

The direction of preferred orientation was taken to be <001> (Brindley and Robinson, 1946; and Zvyagin, 1960).

The pseudo-Voigt profile function (see Section 2.2) was used in all calculations with the mixing parameter (τ) and half-width parameters (U,V,W) being refined together with the peak asymmetry parameter, A_s, defined by Rietveld (1969). The profile function was calculated for 3.5 half-widths on either side of Bragg position $2\theta_j$. Structure factors (F_j in equation (2.6) Section 2.2) were calculated with neutral atom x-ray scattering (International Tables for X-Ray Crystallography, 1974) corrected for anomalous dispersion. The initial structural parameters and the assumed directions of PO are given in Tables 3.4, 3.5 and 3.6. The background component of the XRPD pattern, Y_{bi}, was modelled with the polynomial expression given in equation (2.10). Other model parameters were the zero point $2\theta_o$ (off-set in the zero degrees position of the 2θ scale on the goniometer) and the unit cell parameters. The weighting factors, w_i, were fixed as in equation (2.2).

Tables 3.7, 3.8 and 3.9 list the parameters refined for molybdite, calcite and kaolinite, respectively. The structural model selected for kaolinite calculations was selected by reviewing papers on kaolinite structure authored by Brindley and Robinson (1946), Zvyagin (1960), Suitch and Young (1983) and Young and Hewat (1988). As the focus of the study was the value of the March r-parameter, it was decided to employ the C1 structure proposed by Brindley and Robinson, rather than the more correct P1 structure, as use of the latter is unlikely to have a marked influence on the r-parameter.

3.6 Line Ratio Calculations

Section 2.3 describes the basis of the line ratio method. This section describes the procedures followed for each of the materials considered in the present study.

Molybdite

The angles, $\alpha(h_ik_il_i)$, required for calculating the $P(h_ik_il_i)$ factors are given by :

Table 3.7

Parameters Refined in Rietveld Pattern-Fitting of Molybdite when March Model was Employed

Parameters	Symbols	Rietveld Parameters Refined
Overall scale factor	s	√
Zero point	$2\theta_o$	√
Unit cell	a	√
	b	√
	c	√
	α	-
	β	-
	γ	-
Background	B_o	√
	B_1	√
	B_2	√
	B_3	√
	B_4	-
	B_{-1}	-
Half-width	U	√
	V	√
	W	√
Atom coordinates	Mo(x)	√
	Mo(y)	√
	Mo(z)	-
	$O_1(x)$	√
	$O_1(y)$	√
	$O_1(z)$	-
	$O_2(x)$	√
	$O_2(y)$	√
	$O_2(z)$	-
	$O_3(x)$	√
	$O_3(y)$	√
	$O_3(z)$	-
Isotropic temperature factors	Mo(B)	√
	$O_1(B)$	√
	$O_2(B)$	√
	$O_3(B)$	√
Site occupation factors	Mo(N)	-
	$O_1(N)$	-
	$O_2(N)$	-
	$O_3(N)$	-

Cont.

Parameters	Symbols	Rietveld Parameters Refined
Asymmetry	A_s	√
Peak shape factor	τ	√
Preferred orientation (March)	r	√

Table 3.8

Parameters Refined in Rietveld Pattern-Fitting of Calcite when March Model was Employed

Parameters	Symbols	Rietveld Parameters Refined
Overall scale factor	s	√
Zero point	$2\theta_o$	√
Unit cell	a	√
	b	√
	c	√
	α	-
	β	-
	γ	-
Background	B_o	√
	B_1	√
	B_2	√
	B_3	√
	B_4	-
	B_{-1}	-
Half-width	U	√
	V	√
	W	√
Atom coordinates	Ca(x)	-
	Ca(y)	-
	Ca(z)	-
	C(x)	-
	C(y)	-
	C(z)	-
	O(x)	√
	O(y)	-
	O(z)	-
Isotropic temperature factors	Ca(B)	√
	C(B)	√
	O(B)	√
Site occupation factors	Ca(N)	-
	C(N)	-
	O(N)	-
Asymmetry	A_s	√
Peak shape factor	τ	√
Preferred orientation (March)	r	√

Table 3.9

Parameters Refined in Rietveld Pattern-Fitting of Kaolinite with March Model.

Parameters	Symbols	Rietveld Parameters Refined
Overall scale factor	s	√
Zero point	$2\theta_o$	√
Unit cell	a	√
	b	√
	c	√
	α	√
	β	√
	γ	√
Background	B_o	√
	B_1	√
	B_2	√
	B_3	√
	B_4	-
	B_{-1}	-
Half-width	U	√
	V	√
	W	√
Atom coordinates	$Al_1(x)$	√
	$Al_1(y)$	√
	$Al_1(z)$	√
	$Al_2(x)$	√
	$Al_2(y)$	√
	$Al_2(z)$	√
	$Si_1(x)$	√
	$Si_1(y)$	√
	$Si_1(z)$	√
	$Si_2(x)$	√
	$Si_2(y)$	√
	$Si_2(z)$	√
	$O_1(x)$	√
	$O_1(y)$	√
	$O_1(z)$	√
	$O_2(x)$	√
	$O_2(y)$	√
	$O_2(z)$	√
	$O_3(x)$	√
	$O_3(y)$	√
	$O_3(z)$	√
	$O_4(x)$*	-
	$O_4(y)$*	-
	$O_4(z)$*	-

* Fixed in refinements - subsequently pointed out by thesis examiner that it is not necessary to constrain an atom position when using group C1.

Cont.

Parameters	Symbols	Rietveld Parameters Refined
	$O_5(x)$	✓
	$O_5(y)$	✓
	$O_5(z)$	✓
	$O_6(x)$	✓
	$O_6(y)$	✓
	$O_6(z)$	✓
	$O_7(x)$	✓
	$O_7(y)$	✓
	$O_7(z)$	✓
	$O_8(x)$	✓
	$O_8(y)$	✓
	$O_8(z)$	✓
	$O_9(x)$	✓
	$O_9(y)$	✓
	$O_9(z)$	✓
Isotropic temperature factors #	$Al_1(B)$	-
	$Al_2(B)$	-
	$Si_1(B)$	-
	$Si_2(B)$	-
	$O_1(B)$	-
	$O_2(B)$	-
	$O_3(B)$	-
	$O_4(B)$	-
	$O_5(B)$	-
	$O_6(B)$	-
	$O_7(B)$	-
	$O_8(B)$	-
	$O_9(B)$	-
Site occupation factors	$Al_1(N)$	-
	$Al_2(N)$	-
	$Si_1(N)$	-
	$Si_2(N)$	-
	$O_1(N)$	-
	$O_2(N)$	-
	$O_3(N)$	-
	$O_4(N)$	-
	$O_5(N)$	-
	$O_6(N)$	-
	$O_7(N)$	-
	$O_8(N)$	-
	$O_9(N)$	-
Asymmetry	A_s	✓
Peak shape factor	τ	✓
Preferred orientation (March)	r	✓

Thesis examiner subsequently advised that the isotropic temperature factors should have been refined.

$$\alpha(h_i k_i l_i) = \cos^{-1}\left[\frac{(h_1h_2/a^2)+(k_1k_2/b^2)+(l_1l_2/c^2)}{[\{(h_1/a)^2+(k_1/b)^2+(l_1/c)^2\}\{(h_2/a)^2+(k_2/b)^2+(l_2/c)^2\}]^{1/2}}\right] \quad \ldots \quad (3.1)$$

for the orthorhombic system adopted by molybdite (Cullity, 1978).

Table 3.10 gives the data used in selecting lines for the $P(h_1k_1l_1)/P(h_2k_2l_2)$ calculation. The values in the table are for a March r-parameter = 0.7. There are three candidate lines with $\alpha(h_1k_1l_1) = 0^o$: (020), (040) and (060) with relative intensities 30, 35 and 22, respectively, from calculated intensities based on the Kihlborg model. For the most intense of these, (020) and (040), the former would be preferable as the tail of (120) overlaps the (040) peak and will not be considered in the following discussion except for the Calvert *et al.* (1983) molybdite data as the intensity I(020) was not quoted by Calvert *et al.* Selection of the second line depends both on the intensity and the value of angle, $\alpha(h_ik_il_i)$. Ratio $P(0k0)/P(h_ik_il_i)$ in Table 3.10 indicated that lines (110), (101) and (111) have the largest values of the ratio - approximately 4.9. Line (110) was selected for M_R calculations in view of its superior intensity.

The line ratio, M_R, for line pair (020)/(110) then becomes,

$$\frac{I(020)}{I(110)} \quad \ldots \quad (3.2)$$

where I(020) and I(110) are the measured intensities of the (020) and (110) lines, respectively, for the oriented material.

The random line ratio can be written as :

$$M_R(\text{random}) = \frac{30}{73} = 0.411 \quad \ldots \quad (3.3)$$

The corresponding expression for the oriented specimen is,

Table 3.10

Molybdite $P(0k0)/P(h_ik_il_i)$ Values for Selecting Line Pairs for Line Ratio Calculations

Calculation for <010> as the direction of PO, *i.e.* $(h_1k_1l_1) = (010)$. All lines with integrated intensity greater than 10 (relative) and d-spacing greater than 2.2 Å are listed.

h k l	Kihlborg (1963) model				
	Integrated intensity (random orientation)	2θ* (degrees)	$\alpha(h_ik_il_i)$ (degrees)	$P(h_ik_il_i)$**	$\frac{P(0k0)^{**}}{P(h_ik_il_i)^{**}}$
0 2 0	30	12.77	0.00	2.915	1.000
1 1 0	73	23.33	74.04	0.632	4.612
0 4 0	35	25.70	0.00	2.915	1.000
1 2 0	25	25.88	60.23	0.763	3.821
0 2 1	100	27.32	61.92	0.742	3.929
1 0 1	16	33.12	90.00	0.586	4.974
1 1 1	28	33.76	78.96	0.607	4.802
0 6 0	22	38.97	0.00	2.915	1.000
1 5 0	14	39.66	34.96	1.402	2.079

Note : * 2θ angle for $CuK\alpha_1$ radiation (λ = 1.5406 Å)

** calculated for March parameter r = 0.7

$$M_R(\text{oriented}) = 0.411 \frac{P(020)}{P(110)} \quad \ldots \quad (3.4)$$

Substituting $\alpha(020)$ and $\alpha(110)$ values into equation (2.16) for $P(h_ik_il_i)$, equation (3.4) then gives :

$$M_R(\text{measured}) = 0.411\,[0.0756 + 0.9244\,r^{-3}]^{3/2} \quad \ldots \quad (3.5)$$

The exact relationship (3.5) may be reduced to approximation,

$$r = 0.80\,M_R(\text{oriented})^{-0.222} \quad \ldots \quad (3.6)$$

if the value 0.0756 in equation (3.5) is neglected.

Figure 3.4 shows the close agreement between the linear approximation and exact formulae - see equations (3.5) and (3.6).

Calcite

The angle $\alpha(h_ik_il_i)$ required for calculating the $P(h_ik_il_i)$ factors is given by :

$$\alpha(h_ik_il_i) = \cos^{-1}\left[\frac{h_1h_2 + k_1k_2 + \tfrac{1}{2}(h_1k_2 + h_2k_1) + (3a^2l_1l_2/4c^2)}{[\{h_1^2+k_1^2+h_1k_1+3a^2l_1^2/4c^2\}\{h_2^2+k_2^2+h_2k_2+3a^2l_2^2/4c^2\}]^{1/2}}\right] \quad \ldots \quad (3.7)$$

for the hexagonal system adopted by calcite (Cullity, 1978).

Table 3.11 summarises the data employed in selecting lines for the $P(h_1k_1l_1)/P(h_2k_2l_2)$ calculation for a value of March r-parameter = 0.7. There is only one intense line with $\alpha(h_ik_il_i) = 0^o$, *i.e.* (104) which has integrated intensity 100 from the calculated intensities based on the Megaw model. Selection of the second line depends both on the intensity and the value of angle, $\alpha(h_ik_il_i)$.

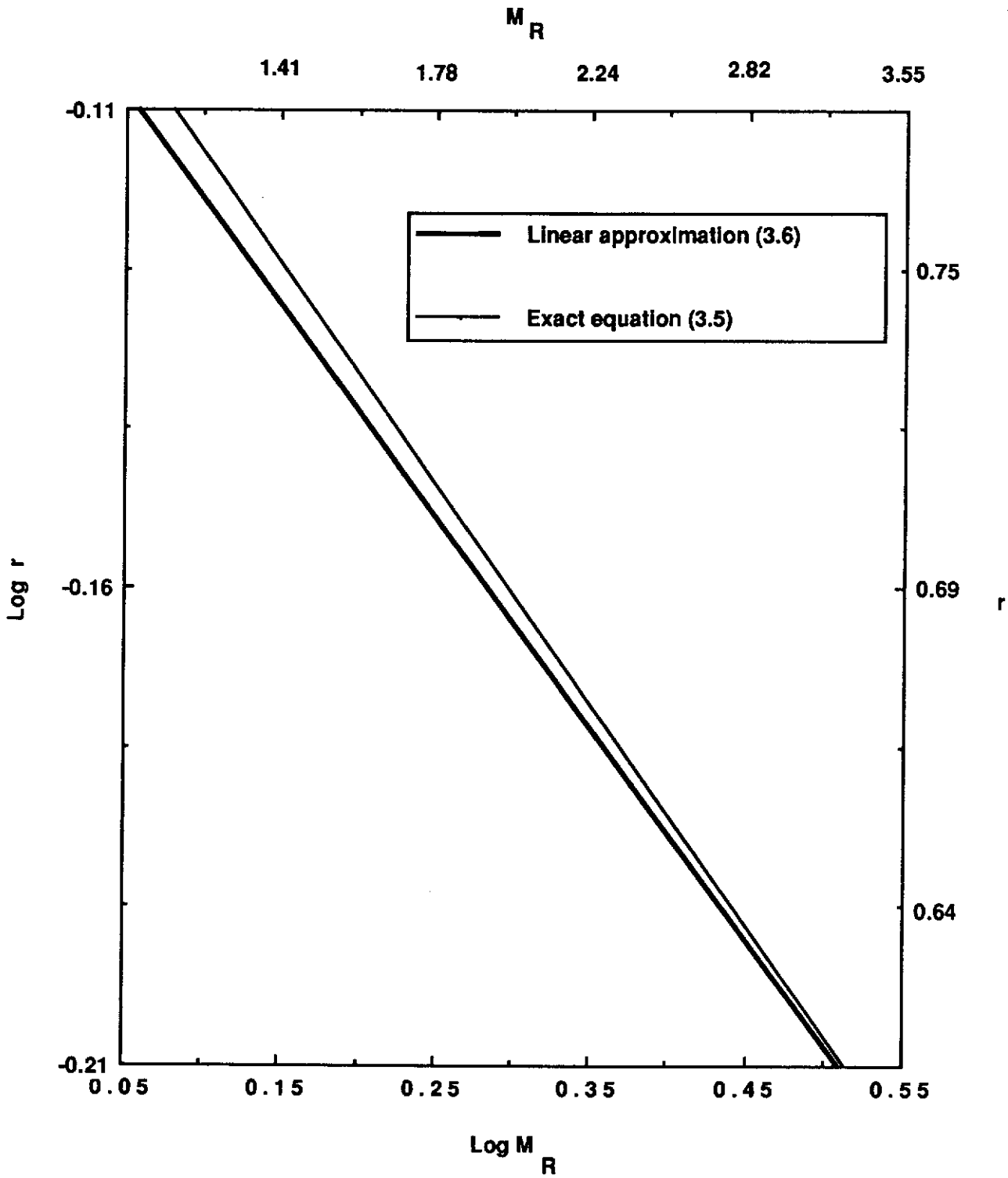

Fig. 3.4. Plots of theoretical values of log r-versus-log M_R for the (020)/(110) line pair of molybdite corresponding to the exact equation (3.5) and approximation equation (3.6).

Table 3.11

Calcite P(104)/P($h_ik_il_i$) Values for Selecting Line Pairs for Line Ratio Calculations

Calculation for <104> as the direction of PO, *i.e.* ($h_1k_1l_1$) = (104). All lines with integrated intensity greater than 10 (relative) and d-spacing greater than 1.6 Å are listed.

h k l	Megaw (1970, 73) model: Integrated intensity (random orientation)	Megaw (1970, 73) model: $2\theta^*$ (degrees)	$\alpha(h_ik_il_i)$ (degrees)	$P(h_ik_il_i)^{**}$	$\frac{P(104)^{**}}{P(h_ik_il_i)^{**}}$
1 0 4	100	29.45	0.00	2.915	1.000
1 1 0	15	35.97	52.61	0.888	3.283
1 1 3	20	39.43	32.54	1.505	1.937
2 0 2	16	43.16	31.21	1.564	0.900
0 1 8	22	47.65	37.39	1.308	2.229
1 1 6	24	48.58	22.04	2.038	1.430
1 2 2	12	57.40	49.07	0.963	3.027

Note : * 2θ angle for CuKα_1 radiation (λ = 1.5460 Å)

** calculated for March parameter r = 0.7

Inspection of ratio $P(104)/P(h_ik_il_i)$ in Table 3.11 indicated that lines (110) and (122) have the largest values for the ratio - approximately 3.0. Lines (104) and (110) were selected as these are clearly resolved from other peaks in the pattern, whereas line (122) suffers from overlap.

The line ratio, M_R, for line pair (104)/(110) then becomes,

$$M_R(\text{measured}) = \frac{I(104)}{I(110)} \qquad \ldots \quad (3.8)$$

The technique employed to calculate the value of PO parameter r was similar to that for molybdite. The random line ratio can be written as :

$$M_R(\text{random}) = \frac{100}{15} = 6.667 \qquad \ldots \quad (3.9)$$

The corresponding expression for the oriented specimen is,

$$M_R(\text{oriented}) = 6.667 \frac{P(104)}{P(110)} \qquad \ldots \quad (3.10)$$

Substituting $\alpha(104)$ and $\alpha(110)$ values into equation (2.16) for $P(h_ik_il_i)$, equation (3.10) then gives :

$$M_R(\text{measured}) = 6.667\,(0.3688 + 0.6312\,r^{-3})^{3/2} \qquad \ldots \quad (3.11)$$

The exact relationship (3.11) cannot be reduced to a linear approximation because value 0.3688 is too large to be neglected.

Figure 3.5 shows the plot between log r-versus-log M_R for equation (3.11).

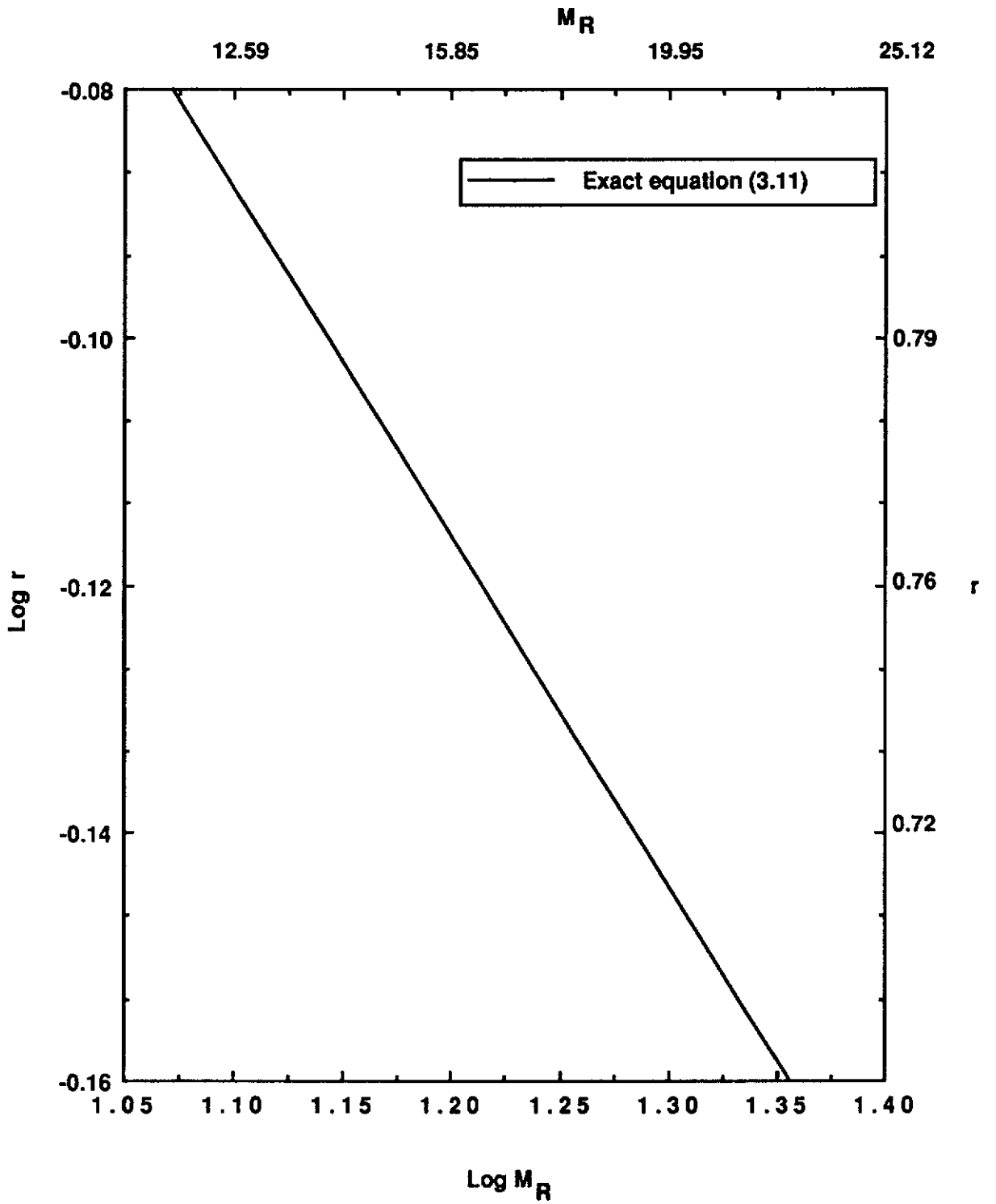

Fig. 3.5. Plot of theoretical values of log r-versus-log M_R for calcite corresponding to equation (3.11).

Kaolinite

The angle $\alpha(h_ik_il_i)$ required for calculating the $P(h_ik_il_i)$ factors is given by :

$$\alpha(h_ik_il_i) = \cos^{-1} \left[(d_1d_2/V^2) \{ S_{11}h_1h_2 + S_{22}k_1k_2 + S_{33}l_1l_2 + S_{23}(k_1l_2 + k_2l_1) + S_{13}(l_1h_2 + l_2h_1) + S_{12}(h_1k_2 + h_2k_1) \} \right] \quad \ldots \quad (3.12)$$

where :

$$V^2 = abc\,(1 - \cos^2\alpha - \cos^2\beta - \cos^2\gamma + 2\cos\alpha\cos\beta\cos\gamma)^{1/2} \quad \ldots \quad (3.13a)$$

$$S_{11} = b^2c^2\sin^2\alpha \quad \ldots \quad (3.13b)$$

$$S_{22} = a^2c^2\sin^2\beta \quad \ldots \quad (3.13c)$$

$$S_{33} = a^2b^2\sin^2\gamma \quad \ldots \quad (3.13d)$$

$$S_{12} = abc^2\,(\cos\alpha\cos\beta - \cos\gamma) \quad \ldots \quad (3.13e)$$

$$S_{23} = a^2bc\,(\cos\beta\cos\gamma - \cos\alpha) \quad \ldots \quad (3.13f)$$

$$S_{13} = ab^2c\,(\cos\gamma\cos\alpha - \cos\beta) \quad \ldots \quad (3.13g)$$

$$d^2 = V^2\,(S_{11}h^2 + S_{22}k^2 + S_{33}l^2 + 2S_{12}hk + 2S_{23}kl + 2S_{13}hk) \quad \ldots \quad (3.13h)$$

for the triclinic system adopted by kaolinite (Cullity 1978).

Table 3.12 summarises the data employed in selecting lines for the $P(h_1k_1l_1)/P(h_2k_2l_2)$ calculation for a value of March r-parameter = 0.7. There are two lines with $\alpha(h_1k_1l_1) = 0^o$; (001) (002) and (003) with relative intensities 100, 53 and 9, respectively, from calculated intensities based on the Brindley and Robinson (1964) model. Line (001) was selected as the first line. The analysis in Table 3.12 for the second line indicated that lines (130) and (060) have similar values for the ratio - approximately 4.9. Line (060) was preferred for M_R calculations as line (130) suffers from overlap.

The technique used to calculate the value of PO parameter r for was similar to that employed for molybdite and calcite.

Table 3.12

Kaolinite P(00l)/P($h_ik_il_i$) Values for Selecting Line Pairs for Line Ratio Calculations

Calculation for <001> as the direction of PO, *i.e.* ($h_1k_1l_1$) = (001). All lines with integrated intensity greater than 10 (relative) and d-spacing greater than 1.49 Å are listed.

h k l	Brindley and Robinson (1964) model		$\alpha(h_ik_il_i)$ (degrees)	$P(h_ik_il_i)^{**}$	$\frac{P(00l)^{**}}{P(h_ik_il_i)^{**}}$
	Integrated intensity (random orientation)	$2\theta^{*}$ (degrees)			
0 0 1	100	12.40	0.00	2.915	1.000
0 0 2	53	24.95	0.00	2.915	1.000
1 3 0	9	35.24	81.04	0.606	4.806
2 0 0	10	36.07	75.49	0.633	4.605
0 0 3	9	37.82	0.00	2.915	1.000
-1 1 3	5	39.26	30.98	3.548	0.821
-2 0 4	10	55.32	40.21	1.970	1.480
0 6 0	10	62.37	88.14	0.586	4.974

Note : * 2θ angle for $CuK\alpha_1$ radiation (λ = 1.5460 Å)

** calculated for March parameter r = 0.7

The line ratio, M_R for a randomly-oriented sample is given by :

$$M_R(\text{random}) = \frac{I_r(001)}{I_r(060)} \qquad \ldots \quad (3.14)$$

where $I_r(001)$ and $I_r(060)$ are the random intensities of the (001) and (060) lines.

If the intensity values $I_r(001)$ and $I_r(060)$ are taken from Table 3.12, then following equation (3.14) the random line ratio can be written as :

$$M_R(\text{random}) = \frac{100}{10} = 10 \qquad \ldots \quad (3.15)$$

The corresponding expression for the oriented specimen is,

$$M_R(\text{oriented}) = 10\,\frac{P(001)}{P(110)} \qquad \ldots \quad (3.16)$$

Substituting $\alpha(001)$ and $\alpha(060)$ values into equation (2.16) for $P(h_i k_i l_i)$, equation (3.16) then gives :

$$M_R(\text{measured}) = 10\,(0.0010 + 0.9989\,r^{-3})^{3/2} \qquad \ldots \quad (3.17)$$

The exact relationship (3.17) may be reduced to approximation,

$$r = 1.667\,M_R(\text{oriented})^{-0.222} \qquad \ldots \quad (3.18)$$

if the value 0.0010 in the equation (3.17) may be neglected.

Figure 3.6 shows the plot between log r-versus-log M_R for equation (3.17) and linear approximation (3.18).

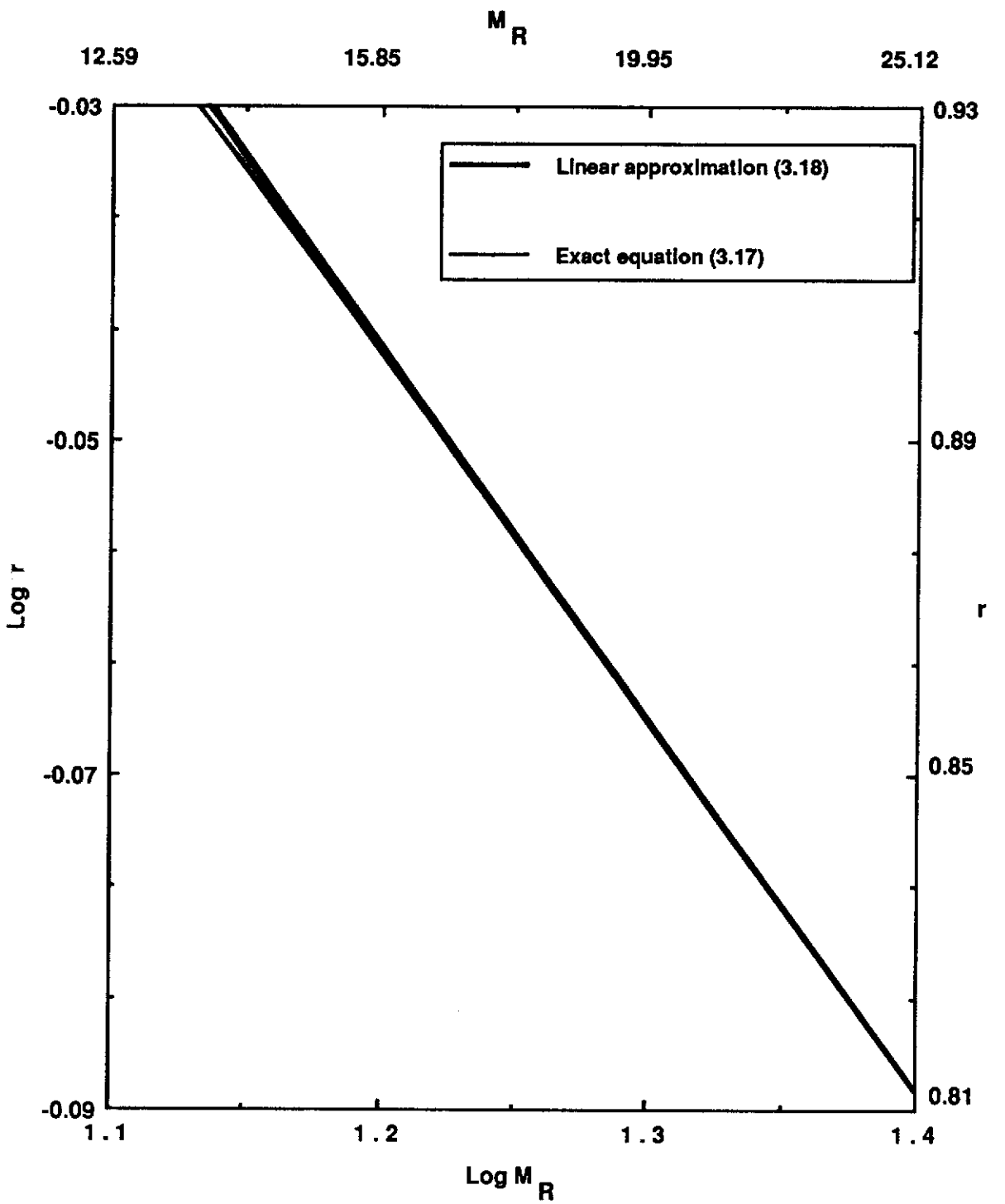

Fig. 3.6. Plots of theoretical values of log r-versus-log M_R for kaolinite corresponding to the exact equation (3.17) and approximation (3.18).

3.7. Correction of Intensities for Preferred Orientation

When the value of r has been obtained then the measured integrated intensities I_{obs} can be corrected for PO according to the relationship :

$$I_{obs} = I_{rnd}\, P(h_i k_i l_i) \qquad \ldots \quad (3.19)$$

where I_{rnd} is the corrected intensity corresponding to random orientation and $P(h_i k_i l_i)$ is the PO factor. The intensities corrected for PO are then

$$I_{rnd} = I_{obs}/P(h_i k_i l_i) \qquad \ldots \quad (3.20)$$

The effectiveness of the corrections may be tested by comparing the measured intensities, corrected for PO, with the theoretical intensities for random orientation. The comparison requires placement of the two intensity sets on the same scale using factor,

$$k = \frac{\Sigma\, I_{th}}{\Sigma\, I_{rnd}} \qquad \ldots \quad (3.21)$$

for which the summation is taken over the integrated intensity set.

The corrected (I_{rnd}) and theoretical (I_{th}) intensities are then placed on the same scale using

$$I_{rnd}^{scaled} = k\, I_{rnd} \qquad \ldots \quad (3.22)$$

The scaled, PO-corrected, measured intensities may be compared with theoretical intensities using an R-factor defined as

$$R_{poc} = \frac{\Sigma \mid I_{rnd}^{scaled} - I_{th} \mid}{\Sigma I_{th}} \quad \ldots \quad (3.23)$$

where the summations are taken over the data set. If the PO has produced a beneficial effect, the value of R_{poc} should be substantially less than the corresponding value for uncorrected data,

$$R_{obs} = \frac{\Sigma \mid I_{obs}^{scaled} - I_{th} \mid}{\Sigma I_{th}} \quad \ldots \quad (3.24)$$

CHAPTER 4

RESULTS

4.1. Molybdite, MoO_3

Rietveld method

The Rietveld refinement results for the PO parameter, r, and the crystallographic R-factors for the molybdite samples are given in Table 4.1. The quality of the refinements may be gauged from the plots in Figures 4.1(a) to (f), which compare the measured and calculated patterns for the various refinements, and the difference plots, which show directly the levels of disagreement between the measured and calculated patterns. The agreement between the measured and calculated patterns was clearly superior when the March model was employed. Further, it is seen from Table 4.1 that the values for the R-factors - R_p, R_{wp} and R_B - all decrease substantially when PO is included in the model. It is noted though that the profile R-factors R_p still substantially exceed the 'expected' results R_{exp} when the March model is applied.

The R_p and R_B values for the three molybdite samples, all of which show substantial PO, ranged between 36.2-61.6% and 35.1-61.9%, respectively, when the March model was not employed; whereas the corresponding factors with the March model, 18.5-19.3%, and 11.2-13.7%, were substantially lower. It is noted in drawing these comparisons that ideally the R_p value should be close to the corresponding 'expected' value - R_{exp} (see equation (2.11c) in Section 2.2). For the three molybdite samples the R_p values are approximately 2.0 times R_{exp}. The magnitude of disagreement between R_p and R_{exp} for the gibbsite refinements of Li *et al.* (1990) with the March model was also substantial, the R_p values exceeding R_{exp} by factors which range from 0.8 to 5.3. The general observation, that R_p exceeds R_{exp} even when the March model is applied, may indicate some shortcoming in the March model.

Table 4.1

Summary of Rietveld Refinement Results for Molybdite

Results for the March r-parameter and the crystallographic R-factors - R_p, R_{wp} and R_B (see Section 2.2).

Sample* Code	R_{exp}	Refinements with zero PO (Non-March model) R_p	R_{wp}	R_B	Refinements with PO (March model) R_p	R_{wp}	R_B	r**
Molybdite - not mixed with silica gel								
MDC	10.91	36.22	44.76	35.08	19.19	23.94	13.74	0.679(2)
MLC	9.02	61.63	69.34	61.88	19.33	27.07	11.38	0.498(2)
MBA	9.33	57.38	65.69	57.00	18.48	25.86	11.18	0.475(2)
Molybdite mixed with 50 % by weight silica gel								
MDA(S)	11.29	24.52	30.61	21.24	19.15	24.04	11.52	0.774(4)
MLC(S)	10.61	30.83	37.71	30.89	18.73	23.35	11.80	0.679(3)
MBA(S)	11.39	32.10	39.21	33.39	18.44	24.23	10.30	0.664(3)

* see Table 3.3.

** number in parentheses is the estimated standard deviation (esd) corresponding to the least significant figure of the corresponding parameter.

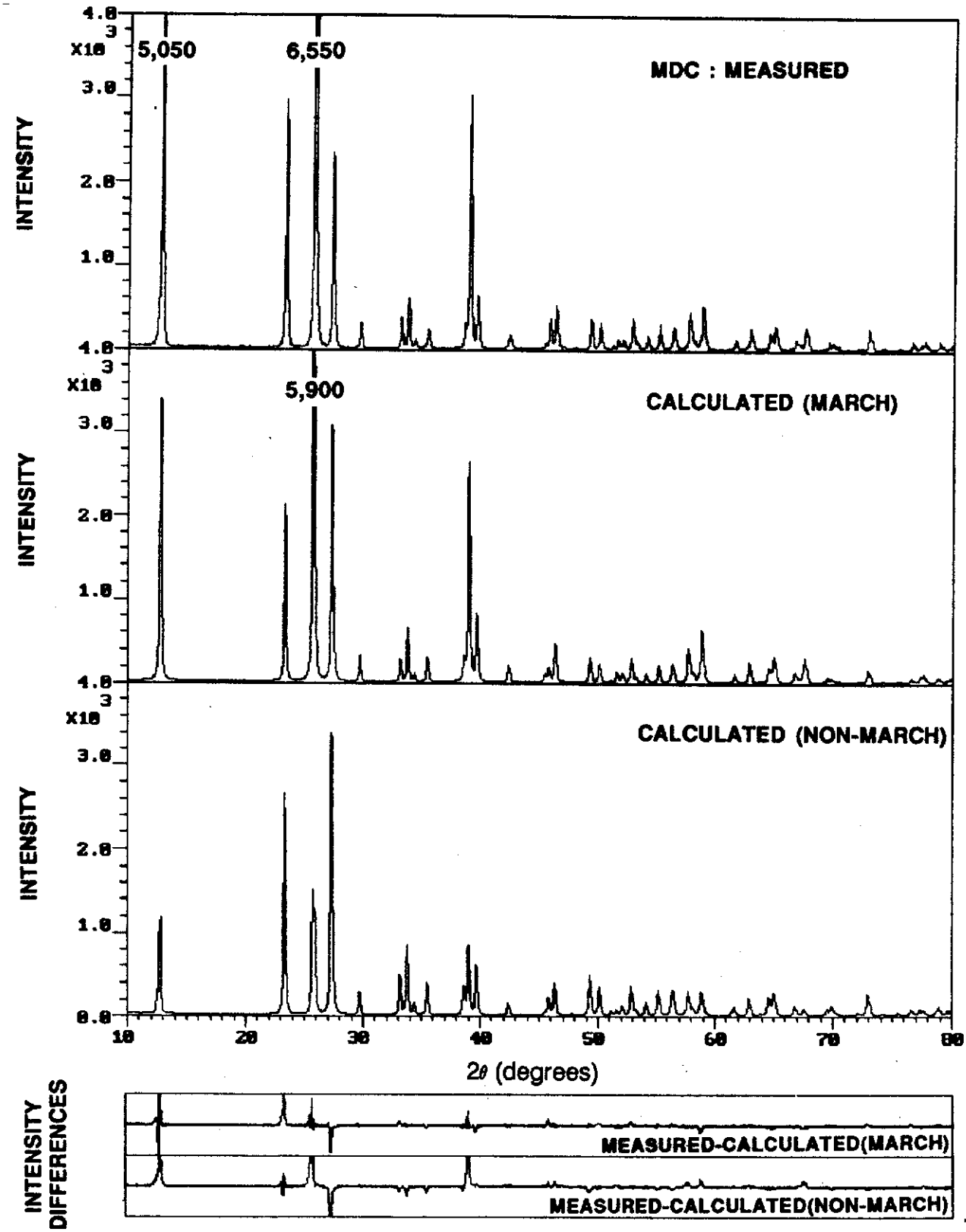

Fig. 4.1(a). Quality of Rietveld pattern-fitting for molybdite - side-drifted sample MDC.

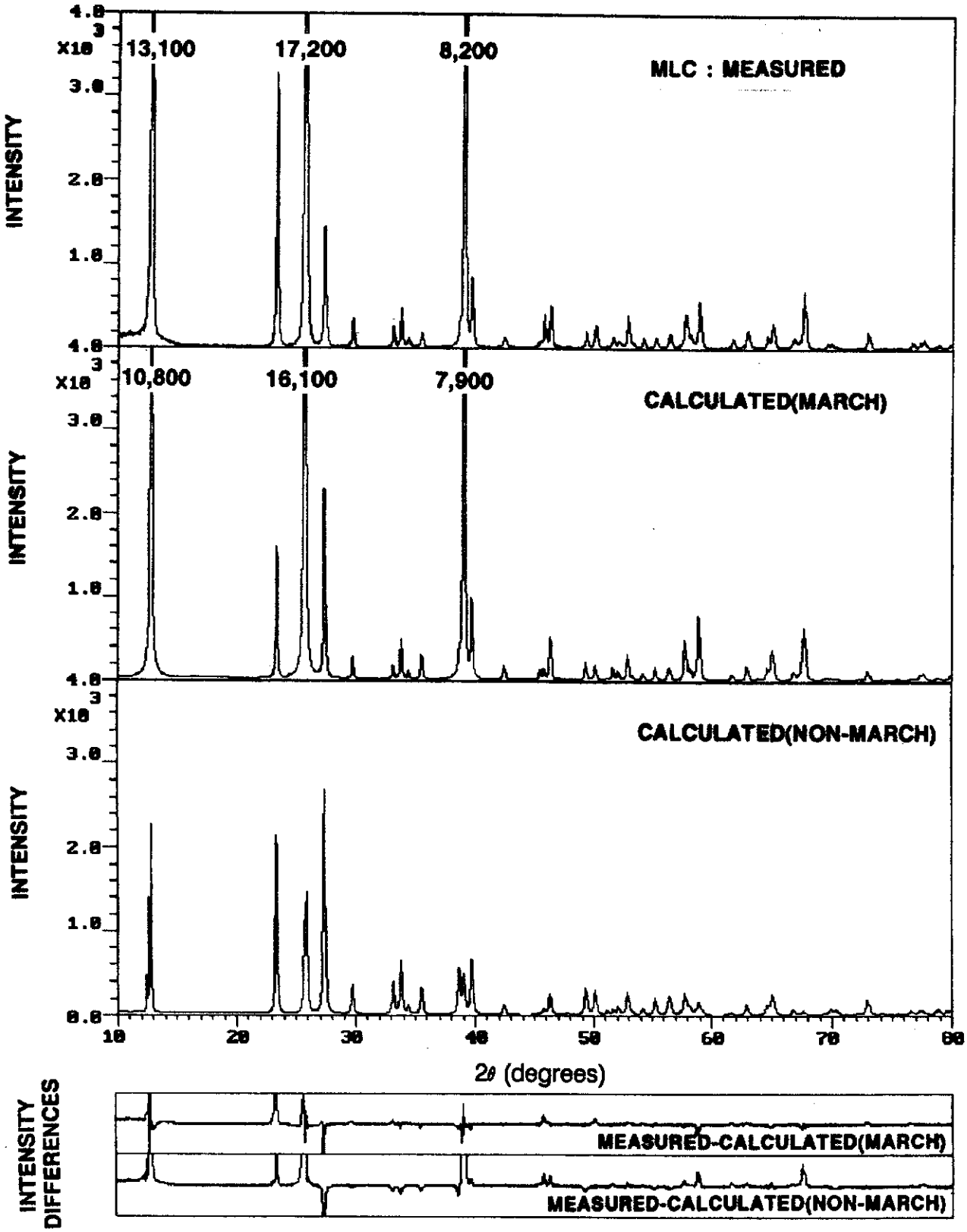

Fig. 4.1(b). Quality of Rietveld pattern-fitting for molybdite - lightly-pressed sample MLC.

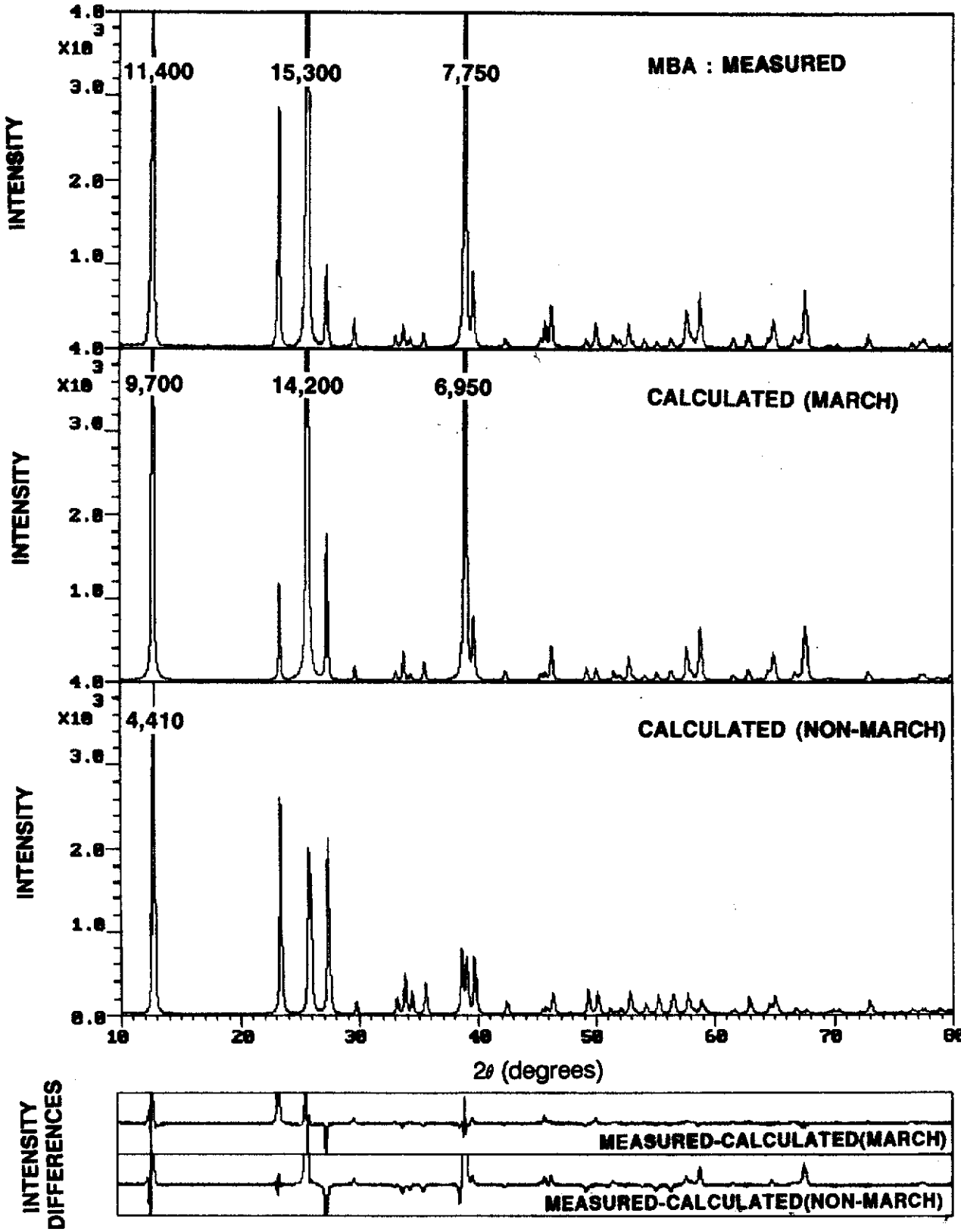

Fig. 4.1(c). Quality of Rietveld pattern-fitting for molybdite - briquetted sample MBA.

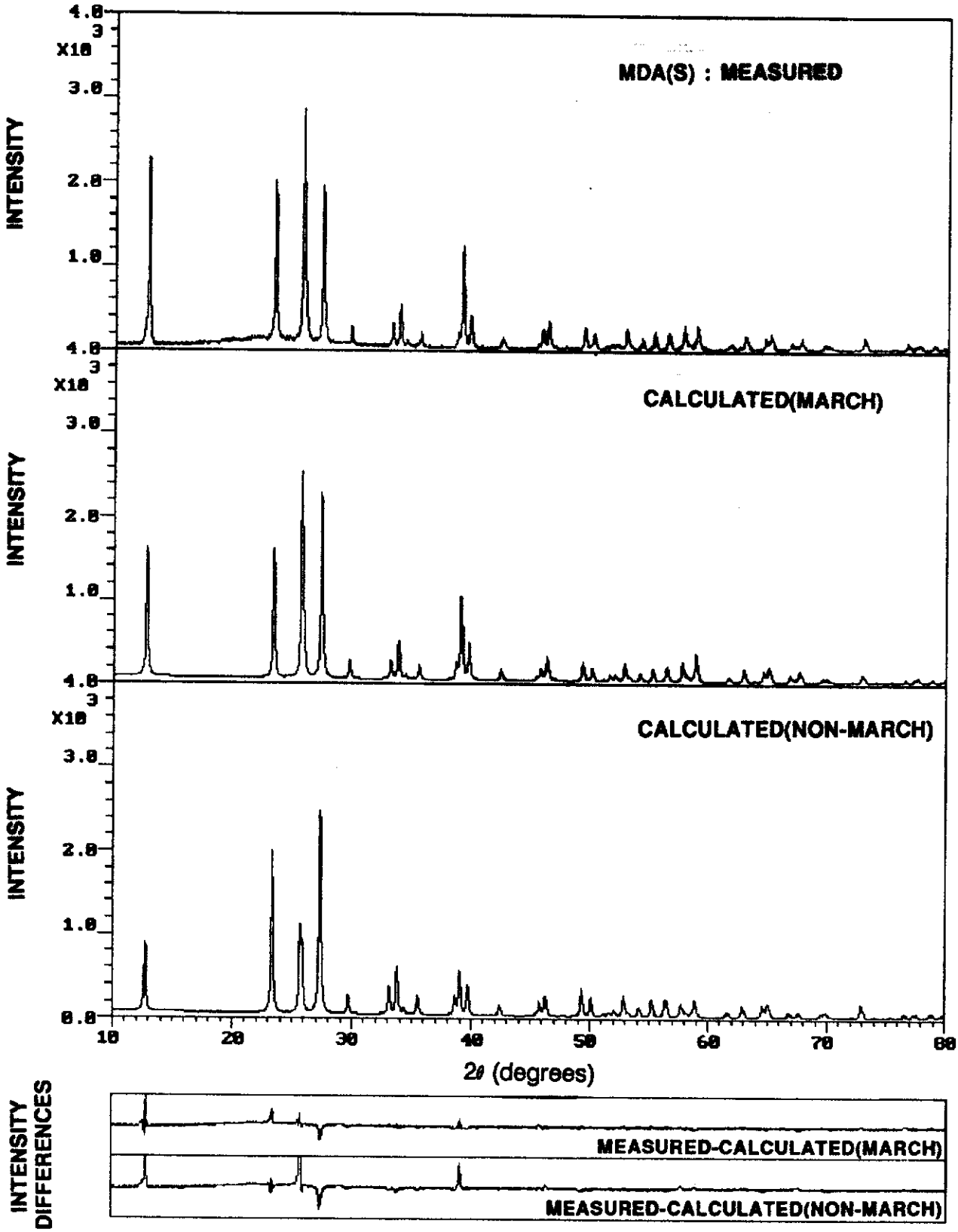

Fig. 4.1(d). Quality of Rietveld pattern-fitting for molybdite mixed with 50% by weight silica gel - side-drifted sample MDA(S).

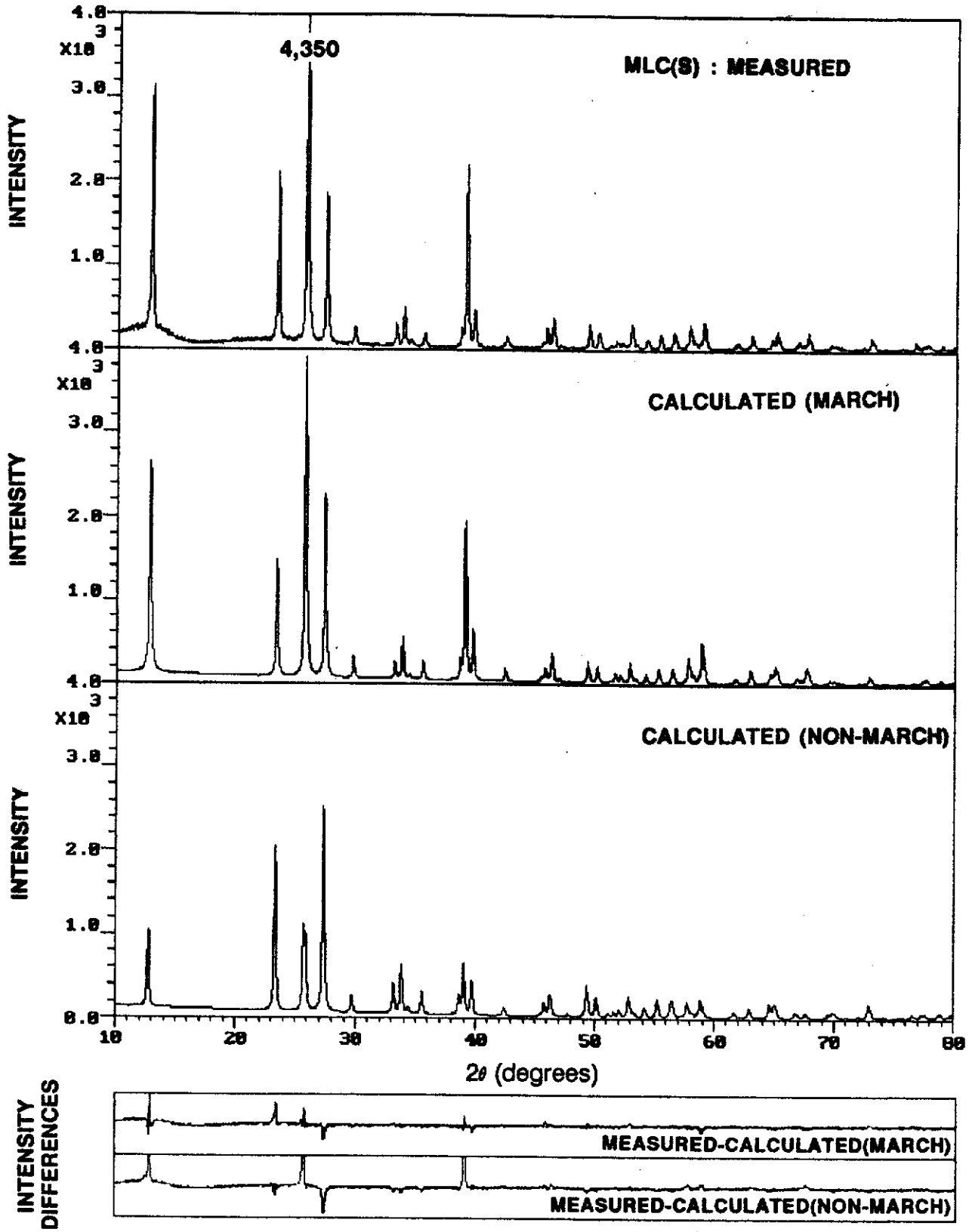

Fig. 4.1(e). Quality of Rietveld pattern-fitting for molybdite mixed with 50% by weight silica gel - lightly-pressed sample MLC(S).

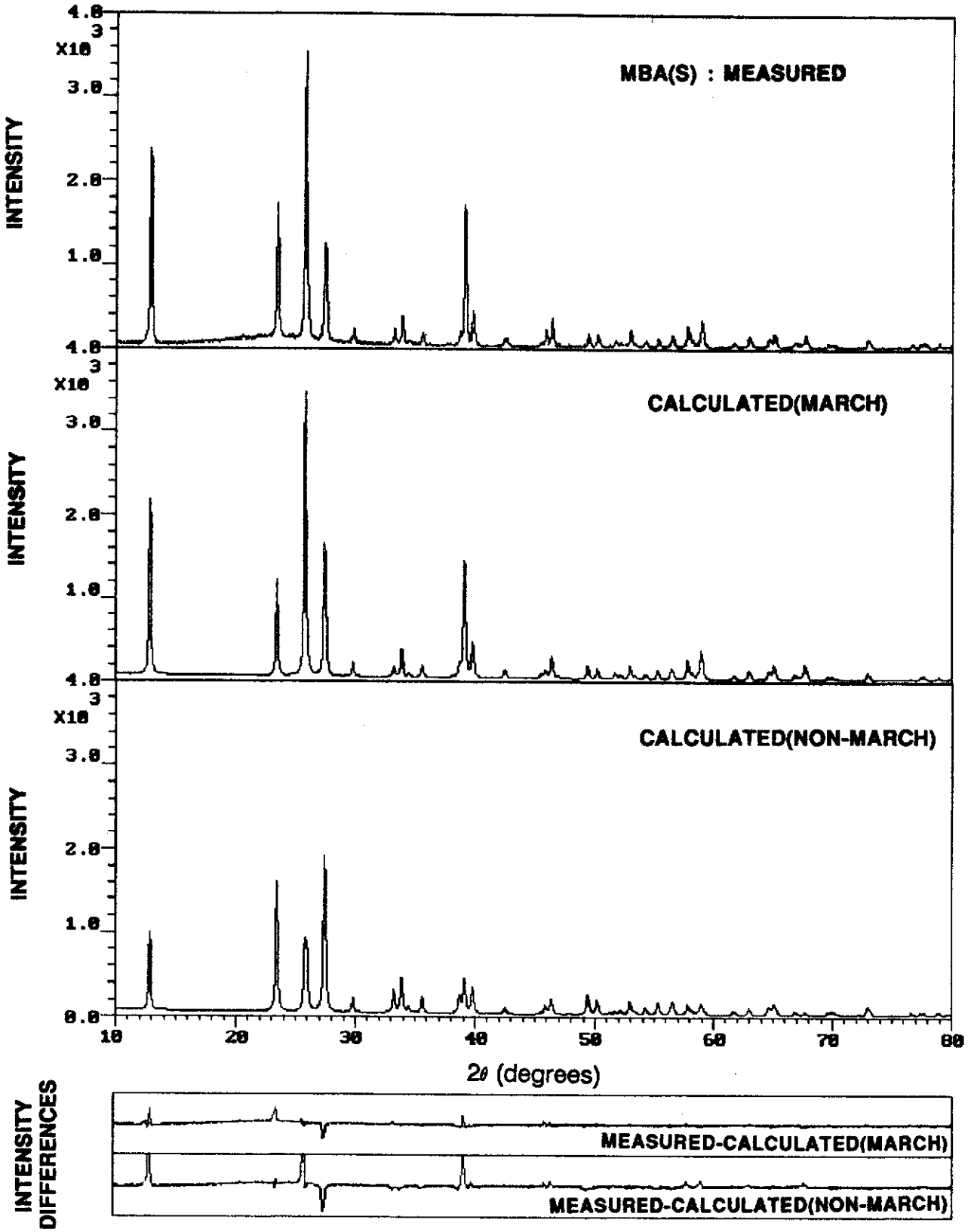

Fig. 4.1(f). Quality of Rietveld pattern-fitting for molybdite mixed with 50% by weight silica gel - briquetted sample MBA(S).

The March r-parameters for the three molybdite samples, corresponding to side-drifting, light front-pressing and briquetting (r = 0.679(2), 0.498(2) and 0.475(2)), clearly show that side-drifting substantially reduces the PO. The difference in the two values for the pressed samples, 0.498(2) and 0.475(2), is negligible.

The R_p and R_B values for the three molybdite samples which were mixed with 50% by weight silica gel to reduce the levels of PO ranged between 24.5-32.1% and 21.2-33.4%, respectively, when the March model was not employed. The corresponding factors with the March model, 18.4-19.2%, and 10.3-11.8%, were substantially lower as was also observed for the molybdite samples not mixed with silica gel. Also the disagreement between R_p and R_{exp} is similar when the March model is applied. The March r-parameters for the three diluted molybdite samples, corresponding to side-drifting, light front-pressing and briquetting (r = 0.774(4), 0.679(3) and 0.664(3)), trend in the manner observed for the undiluted samples. The side-drifted sample again has the highest value, and the two pressed samples give similar r-values. The comparison between the PO parameters obtained by Rietveld refinements with the March model for samples of molybdite (100% by weight) and molybdite mixed with 50% by weight silica gel show that addition of silica gel increases the March r-parameter by 13% (relative) for side-drifting, and by 36-38% for light front-pressing and briquetting. These results occur in the direction expected.

Line ratio method

The results obtained for line ratio M_R using measured line intensities and the corresponding PO parameters, r_M and r_M', for the March model are given in Table 4.2. Here symbols r_M and r_M' are the values calculated from M_R for the exact equation (3.5) and for the approximation expression in equation (3.6), respectively. Agreement between the pairs of r_M and r_M' values is excellent thereby confirming the acceptability of equation (3.6) as an approximation.

Table 4.2

Estimation of PO Parameters from the Molybdite Measured Line Ratios

Results for integrated intensities of (020) and (110) lines with $\alpha(020)=0^{o}$ and $\alpha(110)=74.039^{o}$, respectively. The March parameters r_M and r_M' were derived from the measured line ratios, M_R. The Rietveld results, r_R, from Table 4.1 are included for comparison. Values r_M and r_M' give the results for the exact expression (3.5) and the linear approximation (3.6).

Sample Code	Integrated intensities		Line ratio, M_R			PO parameters		
	I(020)	I(110)	measured	calculated from Rietveld		r_M' (linear approx)	r_M (exact)	r_R
				(linear approx)	(exact)			
Molybdite - not mixed with silica gel								
MDC	990	663	1.49	2.09	2.17	0.738	0.738	0.679
MLC	2246	682	3.29	8.46	8.54	0.614	0.616	0.498
MBA	2129	636	3.35	10.47	10.55	0.612	0.613	0.475
Molybdite mixed with 50 % by weight silica gel								
MDA(S)	464	408	1.14	1.16	1.22	0.777	0.786	0.774
MLC(S)	601	417	1.44	2.09	2.17	0.738	0.744	0.679
MBA(S)	579	345	1.68	2.31	2.39	0.713	0.718	0.664

Comparison of the r_M' and the corresponding Rietveld values r_R from Table 4.1 shows generally systematic discrepancies ranging between 0.003 for MDA(S) and 0.137 for MBA perhaps due to a defect in the March model for the molybdite samples examined and/or other sources of systematic error - see Section 5.1 for discussion.

The results for M_R(measured) and r_R(Rietveld) in Table 4.2 are compared with the theoretical plots for I(020)/I(110) in Figure 4.2. These show that the experimental data :

(i) trend in the manner expected for log r-versus-log M_R;

(ii) do not agree closely with the theoretical plots, whereas similar plots for gibbsite (see Figure 2.3 in Section 2.3) showed excellent agreement.

Reasons for the poor agreement between the experimental and theoretical data are advanced in Section 5.1.

Comparison of Results With Data of Calvert et al. (1983)

Table 4.3 gives the PO parameters (r) derived from the Calvert *et al.* molybdite data using the line ratio method. The results are given for line ratio I(040)/I(110) as the intensity I(020) was not quoted by Calvert *et al.* The March model results for r_M' are physically reasonable. The spray drying value (r_M' = 0.963) is close to ideal (r = 1.00) and the r_M' values for the other two samples trend in the expected manner. The side-drifted result from Calvert *et al.* data (r_M' = 0.921) indicated that the author's side-drifting procedure is less effective than that of Calvert *et al.*

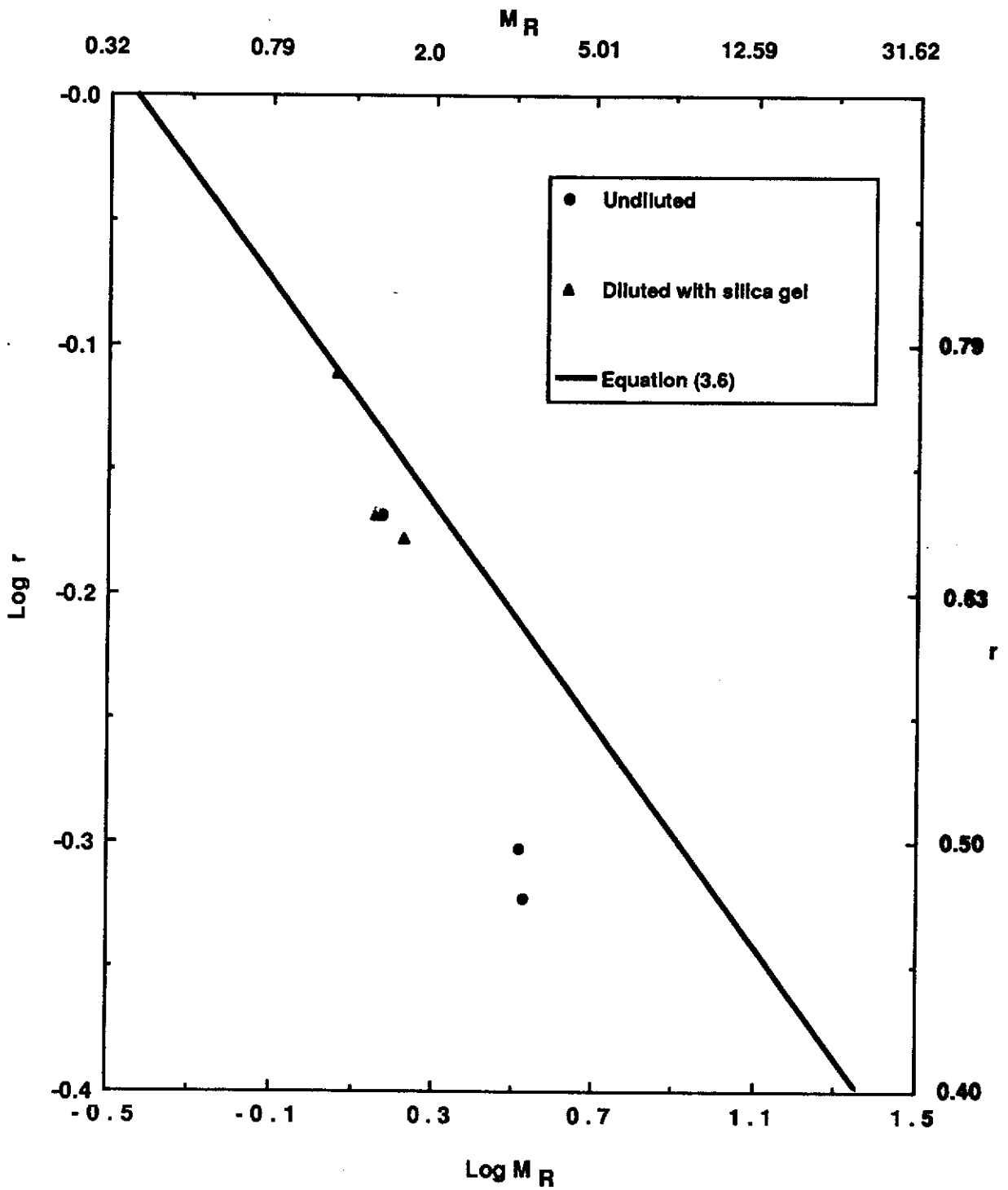

Fig. 4.2. Plots of log r-versus-log M_R for molybdite diffraction data. The line indicates the theoretical relation (linear approximation) described by equation (3.6) for I(020)/I(110). The triangles and circles show the corresponding experimental results involving Rietveld determination of r and line ratio results for M_R - see Table 4.2.

Table 4.3

Estimation of PO Parameters from the Line Ratios for the Molybdite Data Published by Calvert *et al.* (1983)

Results for March parameter r_M' computed with the measured line ratio M_R. The first and the second lines employed were I(040) and I(110), respectively.

Sample	Intensity		Line ratio	PO parameter
0.222	I(040)	I(110)	$M_R = I(040)/I(110)$	$r_M' = 0.84 M_R^{-}$
Spray dried	39	72	0.54	0.963
Side-drifted	52	79	0.66	0.921
Pressed	406	141	2.88	0.664

Note : $r_M' = 0.84\ M_R^{-0.222}$, obtained by substitution of I(040) = 35 into equation (3.2) instead of I(020) = 30.

Table 4.4 summarises the results of the PO correction calculation using the r_R values and the r_M values from Table 4.2. Three corrected intensity values are given for each (hkl) entry as indicated in the table.

The following observations are made on the results :

(i) For each sample, Set 1 (random orientation) produces the highest of the three R-factors, *e.g.* R_1 = 0.550 for MDC. This behaviour is expected as all samples are known to have substantial PO.

(ii) The three procedures used for PO corrections (see Sets 2-3 in Table 4.4) produce R-factors of comparable quality indicating that the line ratio method gives results similar in quality to that from Rietveld refinement.

(iii) The R-factors for each set of results involving the sequence side drifting —> light front-pressing —> briquetting (*i.e.* MDC —> MLC —> MBA) increase progressively indicating that the March model is a far-from-ideal means of correcting for PO. Possible explanations are :

- The March model does not perform PO corrections as well as might be expected.
- Other sources of systematic error may be biasing the intensities.

These possibilities are discussed further in Section 5.1.

Table 4.4

Comparison of Molybdite Measured Integrated Intensities, Corrected for PO, with Calculated Theoretical Intensities for the Random Orientation Model

Three values of measured integrated intensity are given for each of the six samples (MDC, MLC, MBA, MDA(S), MLC(S), MBA(S) - see Table 3.3) as defined below. The scale factor applied to each of the three values is described in Section 3.7.

Value 1 (first line), R_1: measured intensities scaled to theoretical data, no PO correction.

Value 2 (asterisked), R_2: measured intensities corrected for PO using r_R (Rietveld value), then scaled to theoretical data.

Value 3 (parentheses), R_3: measured intensities corrected for PO with r_M (line ratio value) derived from line pair (020)/(110), then scaled to theoretical data.

The R-factors in the Table (R1, R2, R3) are defined in Equations (3.23) and (3.24), Section 3.7.

The lines included in the analysis are those for which there is no discernible peak overlap and for which the theoretical intensity (relative) ≥ 5.

(continued)

Table 4.4 (Continued)

h	k	l	Calculated theoretical intensity (random orientation)	Measured Intensities (Corrected) MDC $r_R=0.679^*$ ($r_M=0.738$)	MLC $r_R=0.498^*$ ($r_M=0.616$)	MBA $r_R=0.475^*$ ($r_M=0.613$)	MDA(S) $r_R=0.774^*$ ($r_M=0.786$)	MLC(S) $r_R=0.679^*$ ($r_M=0.744$)	MBA(S) $r_R=0.664^*$ ($r_M=0.718$)
0	2	0	30	102	169	171	82	87	92
				33*	27*	24*	37*	27*	27*
				(44)	(58)	(61)	(41)	(38)	(36)
1	1	0	73	68	45	47	72	69	69
				114*	144*	161*	100*	112*	120*
				(106)	(121)	(131)	(98)	(104)	(112)
0	2	1	100	54	21	16	73	62	52
				77*	54*	43*	89*	85*	76*
				(73)	(47)	(37)	(88)	(81)	(72)
1	3	0	7	7	5	6	9	7	7
				7*	8*	11*	9*	7*	8*
				(7)	(7)	(10)	(9)	(7)	(8)
1	0	1	16	9	4	2	11	9	8
				17*	13*	8*	16*	15*	16*
				(16)	(11)	(7)	(15)	(14)	(15)
1	1	1	28	14	6	4	20	16	17
				25*	22*	16*	29*	26*	31*
				(23)	(18)	(13)	(28)	(24)	(29)

(continued)

Table 4.4 (Continued)

h	k	l	Calculated theoretical intensity (random orientation)	Measured Intensities (Corrected) MDC $r_R=0.679^*$ ($r_M=0.738$)	MLC $r_R=0.498^*$ ($r_M=0.616$)	MBA $r_R=0.475^*$ ($r_M=0.613$)	MDA(S) $r_R=0.774^*$ ($r_M=0.786$)	MLC(S) $r_R=0.679^*$ ($r_M=0.744$)	MBA(S) $r_R=0.664^*$ ($r_M=0.718$)
0	4	1	8	5	2	2	8	5	7
				5^*	3^*	3^*	7^*	4^*	6^*
				(5)	(3)	(3)	(7)	(4)	(7)
1	3	1	9	6	4	2	7	7	8
				9^*	10^*	6^*	8^*	9^*	11^*
				(8)	(9)	(5)	(8)	(9)	(10)
0	6	0	22	75	140	140	51	82	84
				24^*	22^*	20^*	23^*	25^*	25^*
				(33)	(48)	(50)	(25)	(36)	(33)
1	5	0	14	15	13	16	15	15	19
				11^*	12^*	15^*	12^*	11^*	14^*
				(12)	(13)	(16)	(12)	(12)	(15)
1	4	1	8	3	2	2	4	4	4
				4^*	3^*	4^*	5^*	4^*	5^*
				(4)	(3)	(3)	(5)	(4)	(5)
2	0	0	9	9	6	6	9	9	10
				17^*	23^*	25^*	13^*	15^*	20^*
				(15)	(19)	(20)	(13)	(14)	(18)

(continued)

Table 4.4 (Continued)

h	k	l	Calculated theoretical intensity (random orientation)	Measured Intensities (Corrected) MDC $r_R = 0.679^*$ ($r_M = 0.738$)	MLC $r_R = 0.498^*$ ($r_M = 0.616$)	MBA $r_R = 0.475^*$ ($r_M = 0.613$)	MDA(S) $r_R = 0.774^*$ ($r_M = 0.786$)	MLC(S) $r_R = 0.679^*$ ($r_M = 0.744$)	MBA(S) $r_R = 0.664^*$ ($r_M = 0.718$)
0	6	1	8	13	8	9	13	12	16
				8^*	6^*	7^*	9^*	8^*	10^*
				(9)	(7)	(8)	(9)	(9)	(12)
0	0	2	18	9	3	2	11	11	1
				17^*	10^*	6^*	16^*	18^*	2^*
				(16)	(9)	(5)	(16)	(17)	(2)
2	3	0	11	8	4	5	7	6	8
				12^*	11^*	16^*	9^*	9^*	12^*
				(11)	(10)	(13)	(9)	(9)	(12)
2	1	1	16	10	6	5	10	10	11
				17^*	22^*	18^*	15^*	17^*	20^*
				(16)	(19)	(15)	(15)	(16)	(18)
2	2	1	7	4	2	2	5	4	2
				7^*	6^*	8^*	7^*	6^*	4^*
				(6)	(5)	(6)	(6)	(6)	(3)
1	1	2	13	8	2	1	1	7	4
				14^*	7^*	5^*	2^*	12^*	7^*
				(13)	(6)	(4)	(2)	(11)	(6)

(continued)

Table 4.4 (Continued)

h	k	l	Calculated theoretical intensity (random orientation)	Measured Intensities (Corrected) MDC $r_R=0.679^*$ ($r_M=0.738$)	MLC $r_R=0.498^*$ ($r_M=0.616$)	MBA $r_R=0.475^*$ ($r_M=0.613$)	MDA(S) $r_R=0.774^*$ ($r_M=0.786$)	MLC(S) $r_R=0.679^*$ ($r_M=0.744$)	MBA(S) $r_R=0.664^*$ ($r_M=0.718$)
0	4	2	8	6	3	2	9	7	5
				8^*	7^*	5^*	11^*	9^*	7^*
				(8)	(6)	(4)	(11)	(9)	(7)
1	2	2	6	1	7	8	7	10	7
				1^*	22^*	28^*	10^*	16^*	12^*
				(1)	(18)	(22)	(10)	(15)	(12)
1	7	1	15	11	2	2	12	3	2
				9^*	2^*	3^*	9^*	2^*	1^*
				(9)	(3)	(3)	(10)	(2)	(1)
0	8	1	14	14	10	13	12	12	16
				7^*	5^*	7^*	7^*	6^*	8^*
				(8)	(7)	(9)	(8)	(7)	(9)
2	5	1	13	6	3	3	6	6	6
				8^*	7^*	7^*	7^*	7^*	8^*
				(8)	(7)	(6)	(7)	(7)	(8)
0	6	2	9	5	2	2	6	4	6
				6^*	5^*	4^*	6^*	5^*	7^*
				(6)	(4)	(4)	(6)	(5)	(7)

(continued)

Table 4.4 (Continued)

h	k	l	Calculated theoretical intensity (random orientation)	Measured Intensities (Corrected) MDC $r_R = 0.679^*$ ($r_M = 0.738$)	MLC $r_R = 0.498^*$ ($r_M = 0.616$)	MBA $r_R = 0.475^*$ ($r_M = 0.613$)	MDA(S) $r_R = 0.774^*$ ($r_M = 0.786$)	MLC(S) $r_R = 0.679^*$ ($r_M = 0.744$)	MBA(S) $r_R = 0.664^*$ ($r_M = 0.718$)
1	5	2	7	7	5	6	8	8	8
				10^*	11^*	15^*	9^*	11^*	11^*
				(9)	(10)	(13)	(9)	(10)	(11)
2	3	2	7	6	3	4	7	5	6
				11^*	10^*	12^*	10^*	9^*	10^*
				(10)	(9)	(10)	(10)	(8)	(9)
Scale factors									
				0.145	0.265	0.269	0.104	0.139	0.153
				0.148^*	0.335^*	0.343^*	0.104^*	0.136^*	0.154^*
				(0.155)	(0.384)	(0.403)	(0.105)	(0.144)	(0.162)
Agreement Indices:									
R-factors									
			R_1	0.550	1.080	1.104	0.386	0.537	0.605
			R_2	0.271^*	0.494^*	0.635^*	0.234^*	0.282^*	0.360^*
			R_3	(0.298)	(0.555)	(0.671)	(0.243)	(0.303)	(0.365)

4.2. Calcite, $CaCO_3$

Rietveld method

The calcite Rietveld results for parameter r and for the crystallographic R-factors are given in Table 4.5. The quality of the refinements may be gauged from these results and from the diffraction pattern plots in Figures 4.3(a) to (c).

It was expected from the work of Dollase (1986) on PO in calcite, and from the experience gained by others at Curtin in quantitative phase analysis involving calcite, that PO in calcite would be less severe than that observed in molybdite. The results are consistent with expectation in that the values for r in Table 4.5 are generally higher than the corresponding molybdite results in Table 4.1. The value for calcite side-drifted sample CDA, 0.957(4), is close to the theoretical value for random orientation whereas the corresponding molybdite result was 0.679(2). Use of light-front pressing and the briquetting gave r values of 0.879(8) and 0.814(3), respectively. Therefore the three r-values trend in the expected manner. It is noted that Dollase obtained a value 0.89(5) for a pressed sample which is comparable with the results for this study, although it must be emphasised that Dollase did not give details of the pressing procedure.

Use of the March PO model in refining data from the CDA sample did not change discernibly the corresponding values of R-factors which had been obtained with the random orientation model (*i.e.* neglecting PO), whereas agreement for the CLC and CBA samples improved substantially when the March model was employed. The refinements for sample CLC reduced the R_p and R_{wp} factors only marginally when the March model was employed, but achieved a more obvious reduction in R_B for sample CBA - from 13.5 to 7.1%. The less than expected improvement in R_p and R_{wp} may be due to the relatively poor counting statistics for the CLC data set. The overall improvement in agreement for the CLC and CBA refinements with the March model suggests that the March model has merit, at least in qualitative terms.

Table 4.5

Summary of Rietveld Refinement Results for Calcite

Results for the March r-parameter and the crystallographic R-factors - R_p, R_{wp} and R_B (see Section 2.2).

		Refinements with zero PO (Non-March model)			Refinements with PO (March model)			
Sample* Code	R_{exp}	R_p	R_{wp}	R_B	R_p	R_{wp}	R_B	r**
CDA	10.83	10.94	15.73	5.12	10.68	15.40	3.79	0.957(4)
CLC	15.31	28.59	39.35	13.53	25.88	38.07	7.07	0.879(8)
CBA	10.20	18.51	23.43	16.37	12.25	16.87	6.97	0.814(3)

* see Table 3.3.

** number in parentheses is the estimated standard deviation (esd) corresponding to the least significant figure of the corresponding parameter.

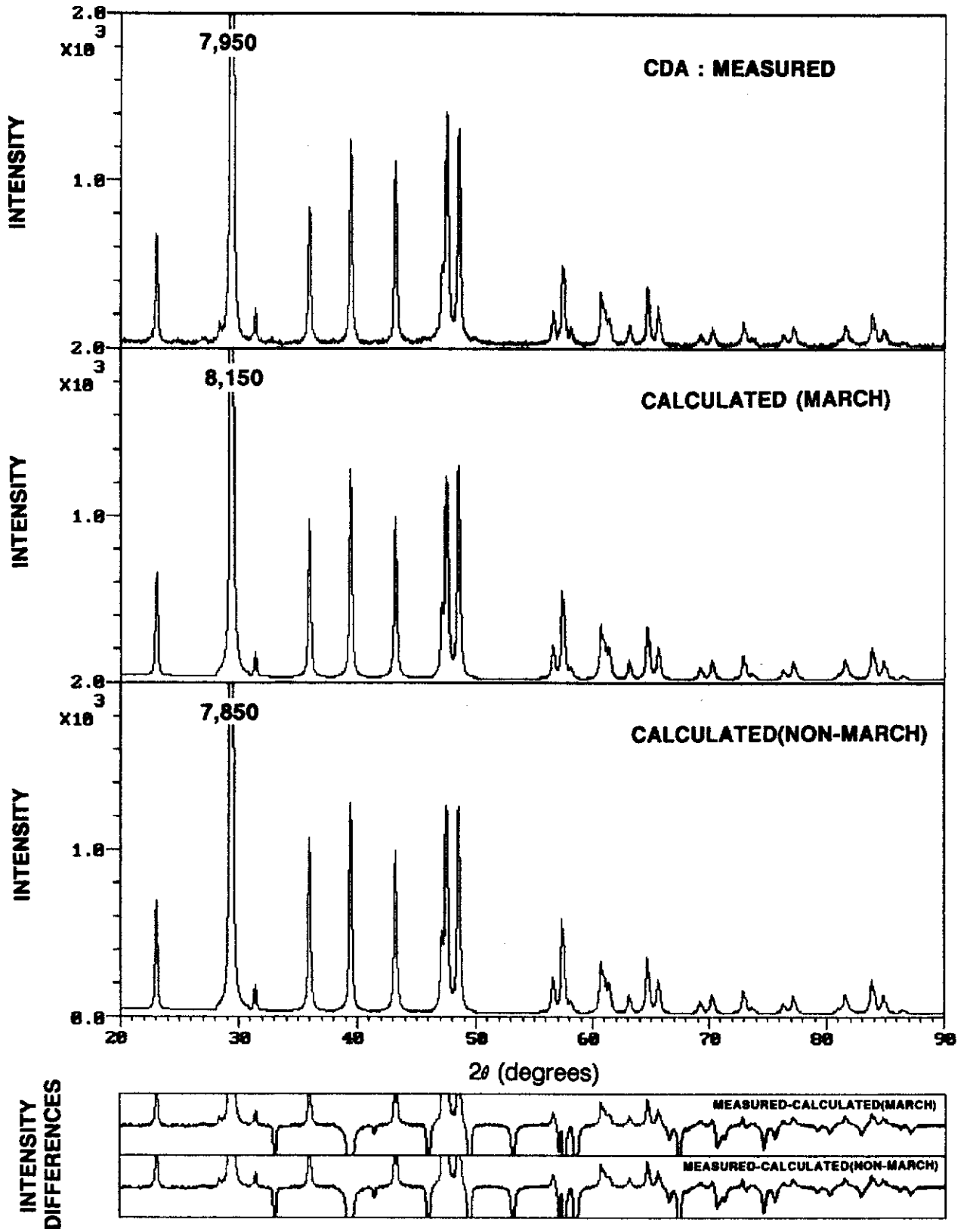

Fig. 4.3(a). Quality of Rietveld pattern-fitting for calcite - side-drifted sample CDA.

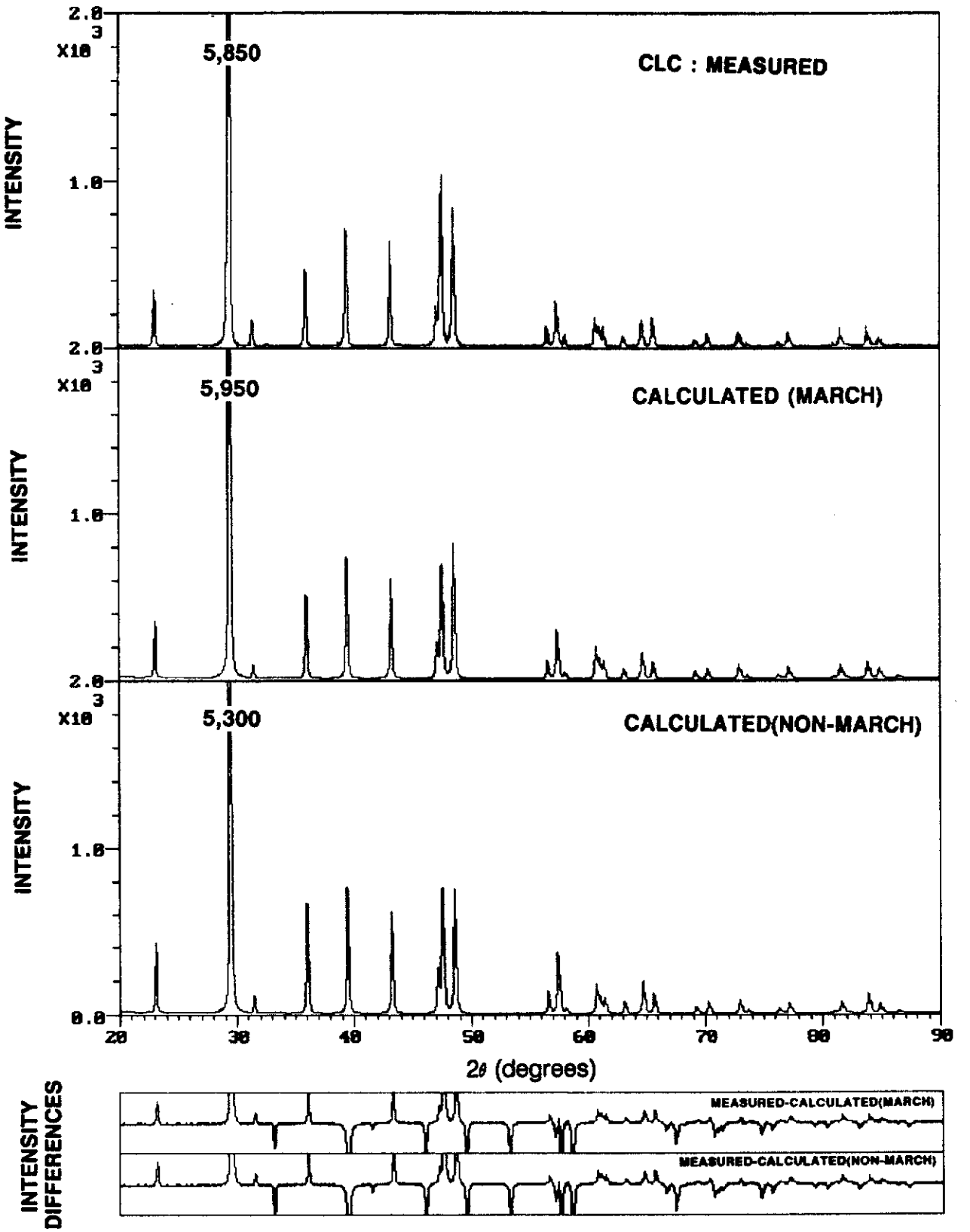

Fig. 4.3(b). Quality of Rietveld pattern-fitting for calcite - lightly-pressed sample CLC.

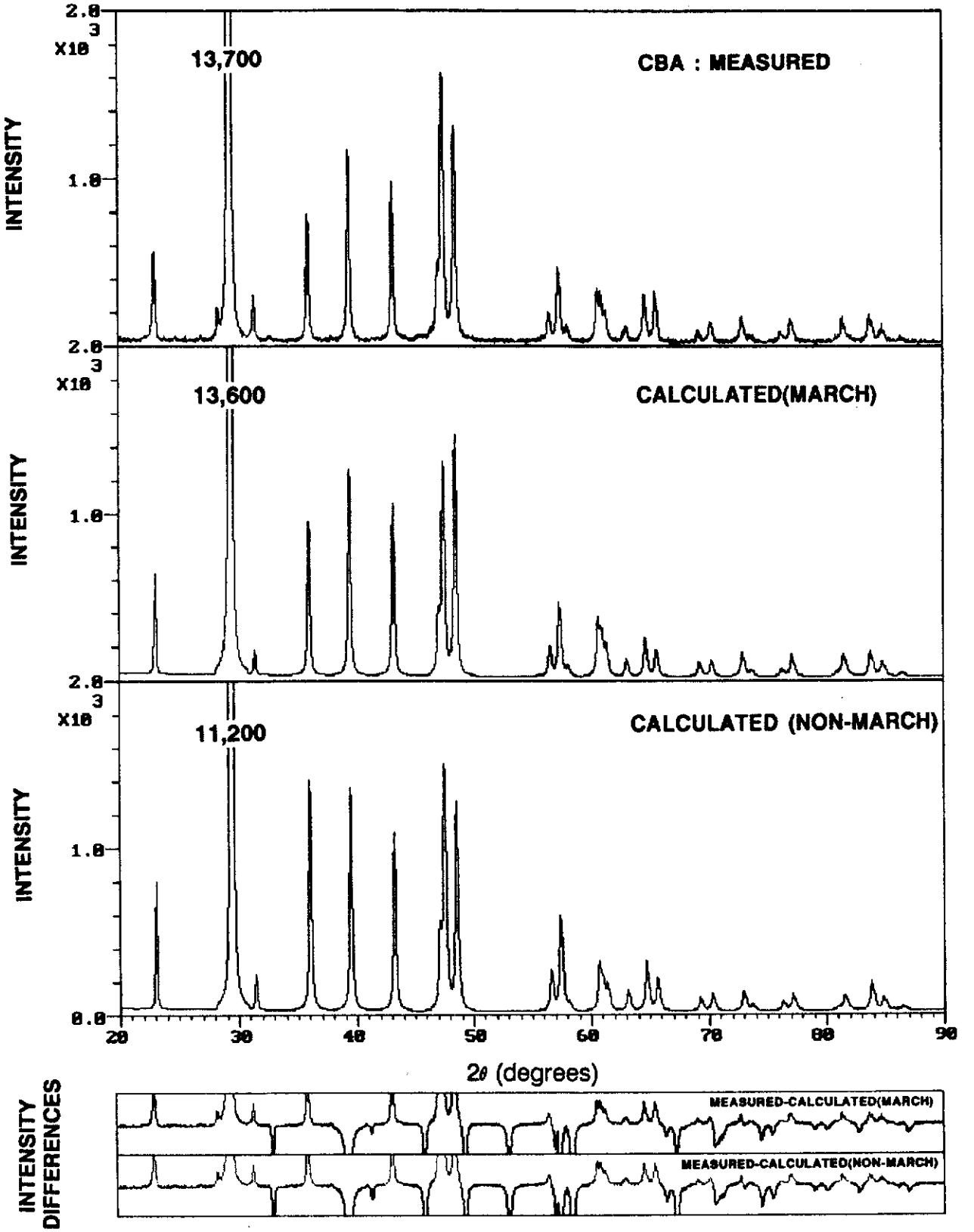

Fig. 4.3(c). Quality of Rietveld pattern-fitting for calcite - briquetted sample CBA.

Inspection of the pattern plots in Figures 4.3(a) to (c) shows essentially no improvement in pattern-matching for the side-drifted sample (CDA) when the March model is used. Again, improvement for sample CLC appears to be marginal in terms of pattern-matching. However the sample with the most pronounced PO (CBA) does appear to give some improvement in pattern matching.

It is noted that the profile R-factors R_p still substantially exceeded the 'expected' results R_{exp}, even when the March model was employed, which may indicate a shortcoming in the March model. The R_p values for the side-drifted and briquetted samples are close to the R_{exp} values, whereas for light front-pressing R_p is approximately 1.5 times R_{exp}. It is noted that the disagreement between R_p and R_{exp} for the gibbsite refinements of Li *et al.* (1990) and for the molybdite refinements in this study were also substantial.

Line ratio method

The results for the line ratio r-parameters and the measured M_R values are given in Table 4.6. Here symbol r_M is the calculated value for the exact expression in equation (3.11). Comparison of the line ratio values r_M and corresponding Rietveld values r_R shows that the r_M values trend in the manner expected, *i.e.* CDA > CLC > CBA. However there are systematic differences between the r_M and r_R sets due to a defect in the March model for the calcite samples examined and/or other sources of systematic error - see Section 5.1 for discussion.

The results for M_R(measured) and r_R(Rietveld) in Table 4.6 are compared with the theoretical plot for I(104)/I(110) in the experimental data :

(i) trend in manner expected for log r-versus-log M_R;

(ii) differ systematically from the theoretical plots as was observed also for the molybdite samples, whereas excellent agreement had been obtained by Li and O'Connor (1989) for a gibbsite (see Figure 2.3 in Section 2.3).

The results are discussed in Section 5.1.

Table 4.6

Estimation of PO Parameters from the Calcite Measured Line Ratios

Results for integrated intensities of lines (104) and (110) with the direction of PO being <104>. The corresponding values of angle $\alpha(104)$ and $\alpha(110)$ are 0^o and 52.6^o, respectively. The March parameter r_M was derived from the measured line ratios, M_R using equation (3.11). The Rietveld results, r_R, from Table 4.5 are included for comparison.

Sample Code	Integrated intensities		Line ratio, M_R		PO parameters	
	I(104)	I(110)	measured	calculated from Rietveld (exact)	r_M (exact)	r_R (Rietveld)
CDA	2093	180	11.6	7.58	0.836	0.957
CLC	1173	76	15.4	9.86	0.770	0.879
CBA	3096	133	23.3	12.73	0.687	0.814

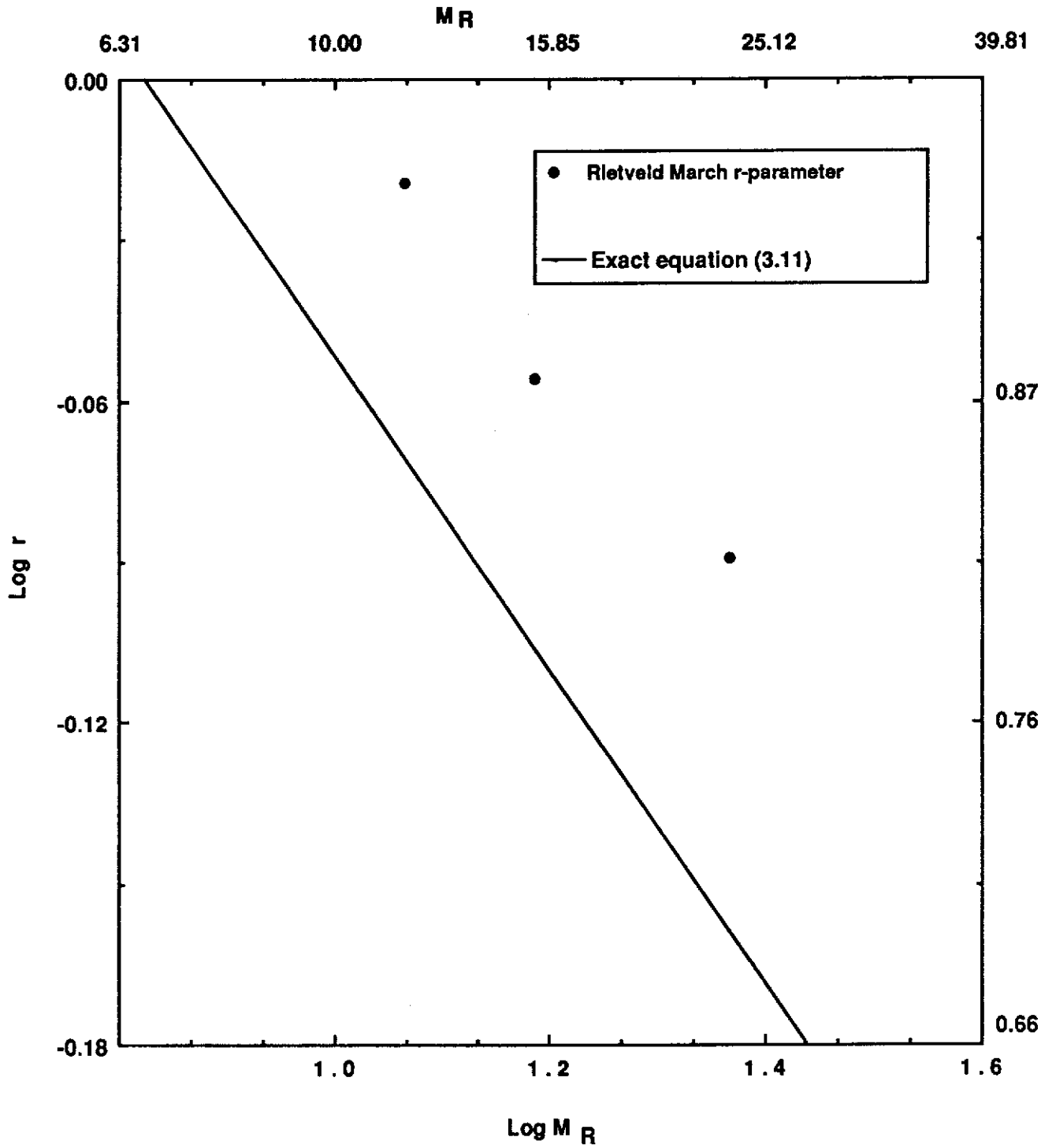

Fig. 4.4. Plot of log r-versus-log M_R for calcite diffraction data - see equation (3.11). The circles show the corresponding experimental results involving Rietveld determination of r and line ratio results for M_R - see Table 4.6.

Table 4.7 summarises the results of the PO correction calculation using the r_R values and the r_M values from table 4.5. Two corrected intensity values are given for each (hkl) entry in the Table 4.7.

It is seen from Table 4.7 that the R-factors increase systematically from CDA —> CLC —> CBA as expected from the Rietveld R-factors. The three R-factors for CDA in Table 4.7 are similar ($\approx$ 0.15) as expected from the Rietveld results which indicates that PO has little effect in the data set. Value R_1 for CLC improves from 0.239 to 0.165 when PO is included in the calculations indicating that the PO intensity correction produces R-factor agreement close to that obtained for the CDA (random) sample. The most oriented sample, CBA, also gives improved intensity agreement after correction for PO. However the two values (R_2 = 0.265 and R_3 = 0.193) obtained with PO are still substantially greater than the three values for CDA.

4.3 Kaolinite, $Al_2O_3.2SiO_2.2H_2O$

Rietveld Method

The kaolinite Rietveld results obtained for the March r-parameter and the corresponding R-factors for the three sample types examined (side-drifting, light front-pressing and briquetting) are given in Table 4.8. The agreement between measured and calculated patterns for random orientation and with the March model is shown in Figures 4.5(a) to (c).

Table 4.7

Comparison of Calcite Measured Integrated Intensities, Corrected for PO, with Calculated Theoretical Intensities for the Random Orientation Model

Three values of measured integrated intensity are given for each of the three samples (CDA, CLC, CBA - see Table 3.3) as defined below. The scale factor applied to each of the three values is described in Section 3.7.

Value 1 (first line), R_1: measured intensities scaled to theoretical data, no PO correction.

Value 2 (asterisked), R_2: measured intensities corrected for PO using r_R (Rietveld value), then scaled to theoretical data.

Value 3 (parentheses), R_3: measured intensities corrected for PO with r_M (line ratio value) derived from line pair (104)/(110), then scaled to theoretical data.

The R-factors in the Table (R1, R2, R3) are defined in Equations (3.23) and (3.24), Section 3.7.

The lines included in the analysis are those for which there is no discernible peak overlap and for which the theoretical intensity (relative) ≥ 5.

(continued)

Table 4.7 (Continued)

h k l	Calculated theoretical intensity (random orientation)	Measured Intensities (Corrected)		
		CDA $r_R = 0.957^*$ ($r_M = 0.836$)	CLC $r_R = 0.879^*$ ($r_M = 0.770$)	CBA $r_R = 0.814^*$ ($r_M = 0.687$)
0 1 2	9	10_* 11^* (14)	6_* 8^* (11)	5_* 9^* (12)
1 0 4	100	116_* 114^* (96)	127_* 114^* (95)	152_* 131^* 2)
1 1 0	15	12_* 13^* (17)	11_* 14^* (19)	8_* 14^* (20)
1 1 3	20	20_* 20^* (21)	17_* 18^* (20)	12_* 15^* (17)
2 0 2	16	17_* 18^* (19)	16_* 17^* (18)	12_* 13^* (15)
0 2 4	7	7_* 7^* (9)	5_* 7^* (9)	5_* 7^* (11)
0 1 8	22	22_* 23^* (26)	24_* 28^* (31)	19_* 24^* (29)
1 1 6	24	21_* 21^* (20)	20_* 20^* (19)	15_* 16^* (15)
2 1 4	7	5_* 5^* (6)	4_* 5^* (5)	4_* 4^* (5)
0 0 12	5	4_* 4^* (5)	4_* 5^* (6)	4_* 5^* (7)
1 3 4	7	3_* 4^* (4)	3_* 4^* (5)	2_* 3^* (4)

(continued)

Table 4.7 (Continued)

h k l	Calculated theoretical intensity (random orientation)	Measured Intensities (Corrected) CDA $r_R = 0.957^*$ ($r_M = 0.836$)	CLC $r_R = 0.879^*$ ($r_M = 0.770$)	CBA $r_R = 0.814^*$ ($r_M = 0.687$)
4 0 4	5	2_* 2^* (2)	2_* 2^* (3)	2_* 2^* (2)
3 1 8	5	3_* 3^* (3)	2_* 2^* (2)	2_* 2^* (2)
Scale factors		0.116_* 0.128^* (0.164)	0.127_* 0.168^* (0.208)	0.152_* 0.283^* (0.312)
Agreement indices :				
R-factors,	R_1 R_2 R_3	0.152_* 0.149^* (0.144)	0.239_* 0.165^* (0.165)	0.426_* 0.265^* (0.193)

Table 4.8

Summary of Rietveld Refinement Results for Kaolinite

Results for the March r-parameter and the crystallographic R-factors - R_p, R_{wp} and R_B (see Section 2.2).

Sample* Code	R_{exp}	Refinements with zero PO (Non-March model)			Refinements with PO (March model)			r**
		R_p	R_{wp}	R_B	R_p	R_{wp}	R_B	
KDC	11.19	21.41	27.02	10.40	20.52	26.18	9.61	0.852(6)
KLC	10.28	23.95	31.18	13.81	18.98	26.10	7.32	0.642(4)
KBA	10.44	25.24	32.58	14.96	17.33	23.78	7.15	0.591(3)

* see Table 3.3.

** number in parentheses is the estimated standard deviation (esd) corresponding to the least significant figure of the corresponding parameter.

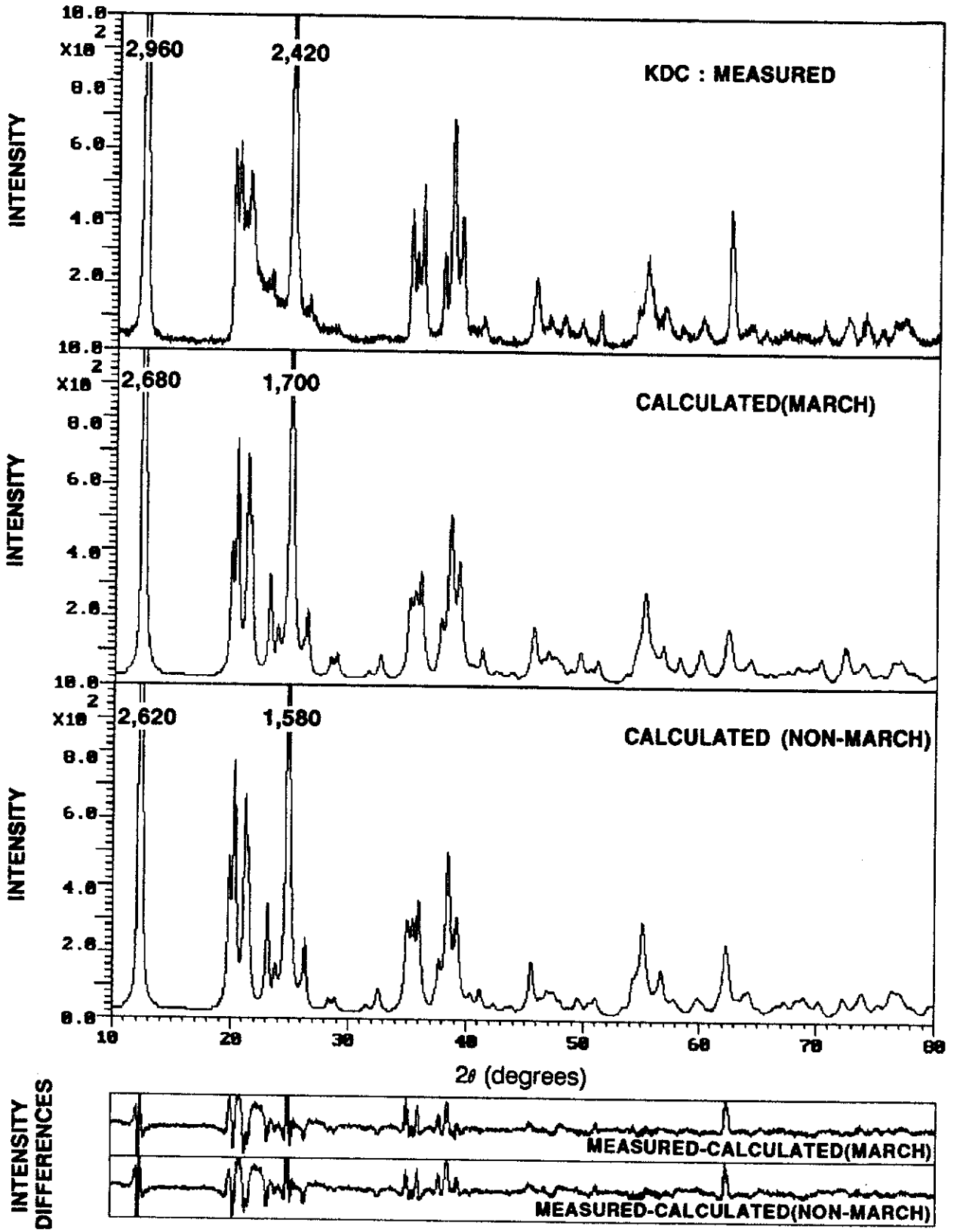

Fig. 4.5(a). Quality of Rietveld pattern-fitting for kaolinite - side-drifted sample KDC.

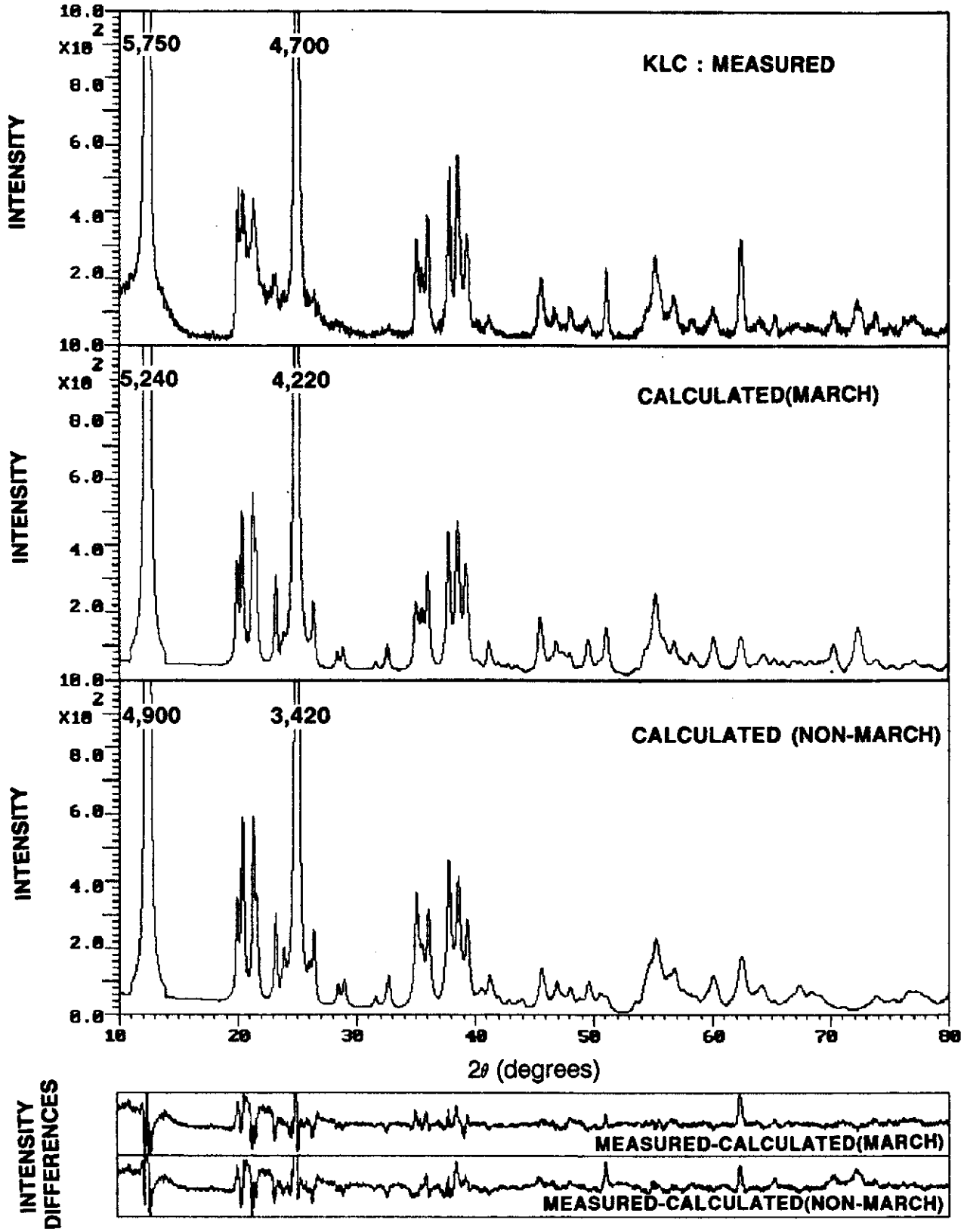

Fig. 4.5(b). Quality of Rietveld pattern-fitting for kaolinite - lightly-pressed sample KLC.

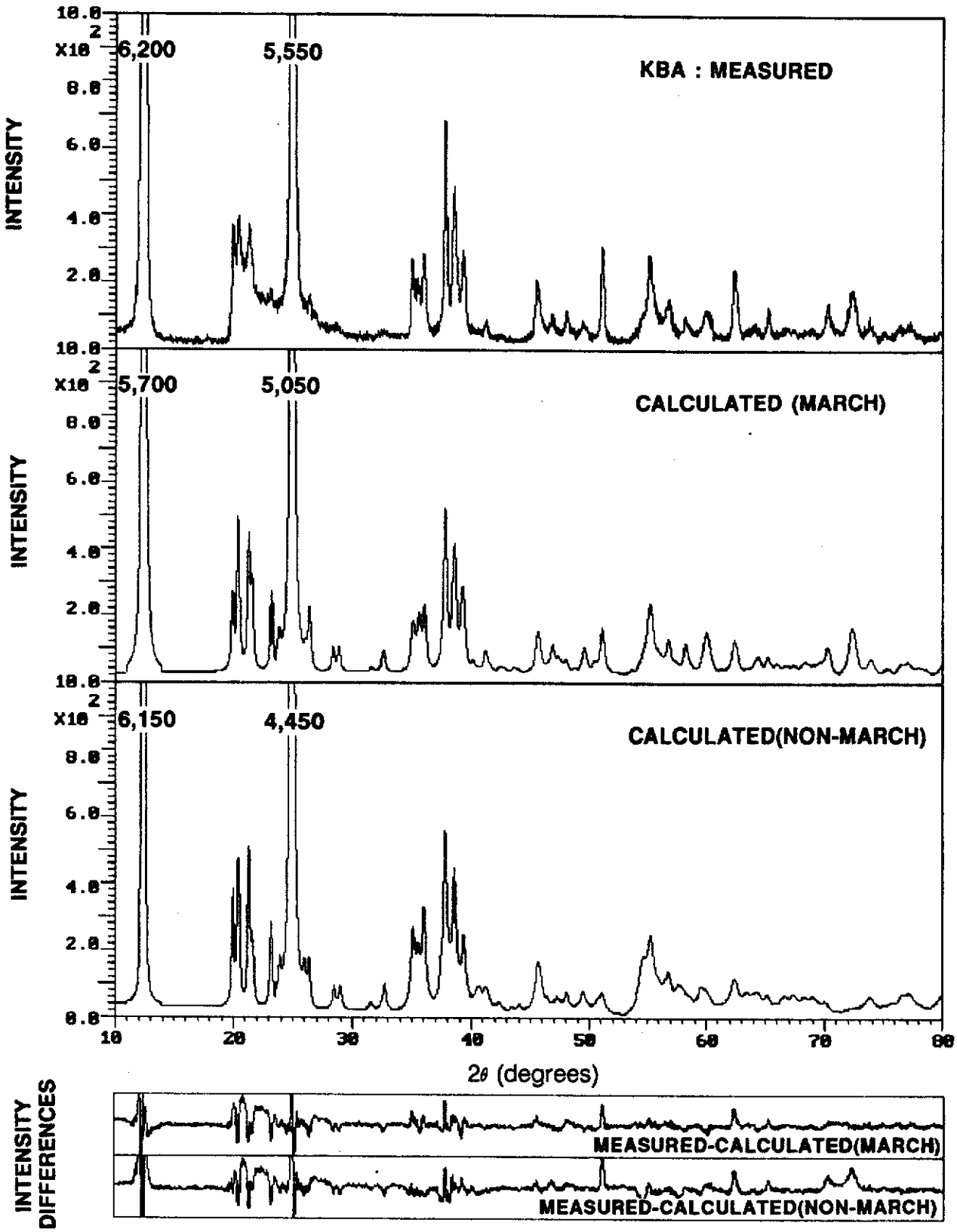

Fig. 4.3(c). Quality of Rietveld pattern-fitting for kaolinite - briquetted sample KBA.

The value of r decreases in the direction expected, *i.e.* side-drifted > light front-pressing > briquetting. The change in R-factors for the side-drifted samples is barely discernible when random orientation is used, which suggests that the side-drifted sample is behaving in the manner expected for random orientation. However the Rietveld r-value for the side-drifted sample, 0.852(6), suggests an upper limit of 0.90 for the parameter which is consistent with there being some PO. Invoking the March model with the two pressed samples does result in some improvement in the R-factors as well as lowering parameter r in the direction expected. While these results are generally consistent with expectation in qualitative terms, observation of $r < 1.0$ for the side-drifted sample is unexplained. Raven (1989), in an independent experiment, obtained a value of $r = 0.791(3)$ for a side-drifted sample of the same material, *i.e.* Georgia WP-SD.

The observations made using the R-factors and r-values are consistent with the appearance of the profile plots in Figures 4.5(a) to (c). The calculated plots for the randomly oriented specimen in Figures 4.5(a) are not appreciably different for the two models. However, the calculated patterns for two pressed samples (light front-pressed and briquetted) show close agreement with the measured patterns when the March model is employed. The improvement is observed for both high- and low-angle data.

Line ratio method

The results obtained for line ratios M_R using measured line intensities and the corresponding PO parameters, r_M', for the March model are given in Table 4.9. Symbol r_M' signifies the value calculated from equation (3.18). Comparison of the r_M' and corresponding Rietveld values r_R shows systematic discrepancies as observed also for the molybdite and calcite data sets. The differences for kaolinite are large, ranging from 0.106 and 0.261 . The results reinforce the speculation made in Section 4.1 and 4.2 on possible defects in the March model for the samples examined and on the possible influences of other sources of systematic error - see Section 5.1 for discussion.

Table 4.9

Estimation of PO Parameters from the Kaolinite Measured Line Ratios

Results for integrated intensities of line (001) and (060) with the direction of PO being <001>. The corresponding values of angle α(001) and α(060) are 0^{o} and 88.141^{o}, respectively. The March parameters r_M and $r_{M'}$ were derived from the measured line ratios, M_R. The Rietveld results, r_R, from Table 4.7 included for comparison.

Sample Code	Integrated intensities		Line ratio, M_R			PO parameters		
	I(001)	I(060)	measured	calculated from Rietveld		$r_{M'}$ (linear approx)	r_M (exact)	r_R
				(linear approx)	(exact)			
KDC	509.2	41.9	12.15	20.56	20.55	0.958	0.957	0.852
KLC	1719.7	108.7	15.82	73.56	73.37	0.903	0.902	0.642
KBA	1862.1	74.2	25.10	106.81	106.48	0.815	0.814	0.591

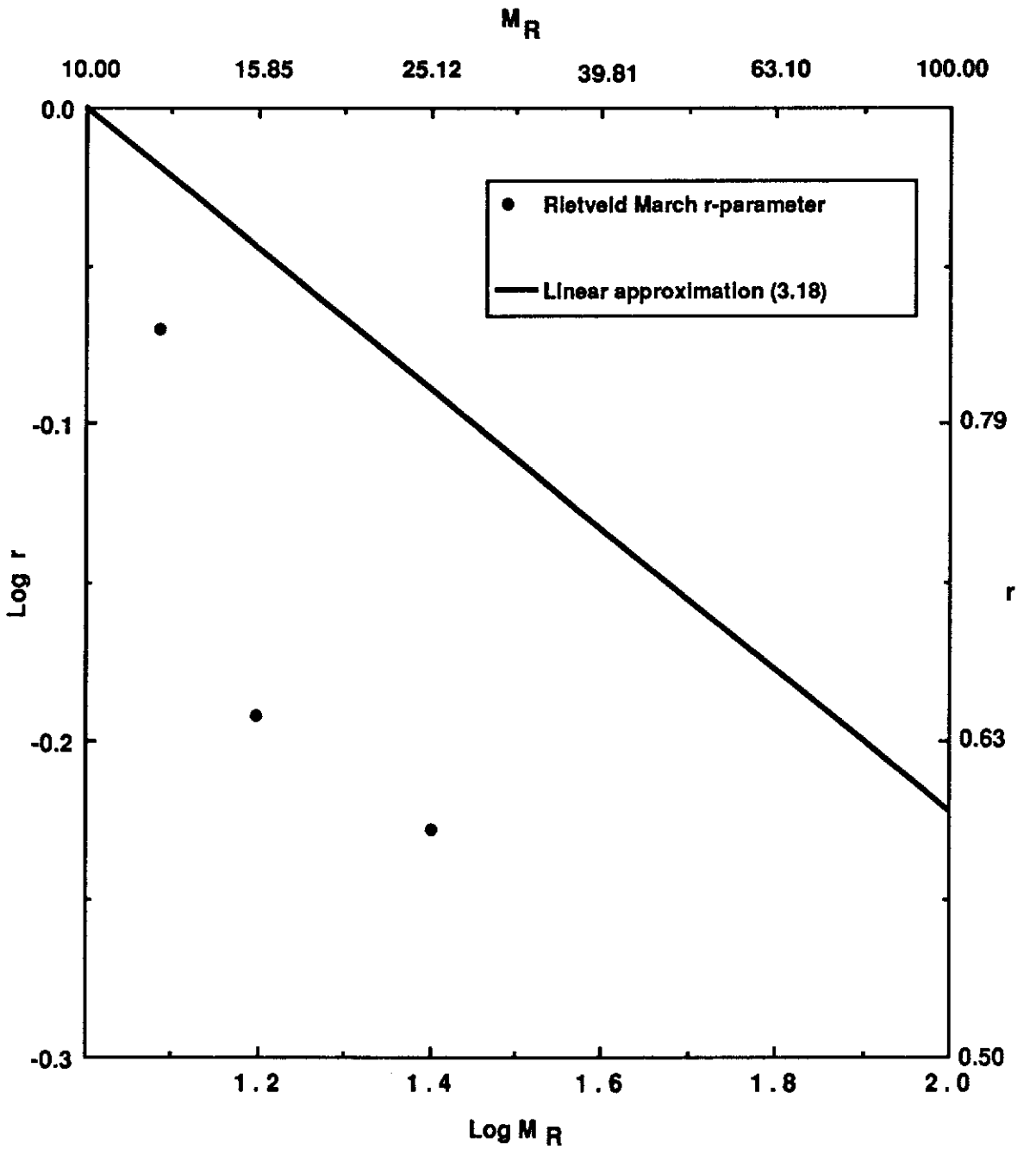

Fig. 4.6. Plots of log r-versus-log M_R for kaolinite diffraction data. The circles show the corresponding experimental results involving Rietveld determination of r and line ratio results for M_R - see Table 4.9.

The results for M_R(measured) and r_R(Rietveld) in Table 4.9 are compared in Figure 4.6 with the theoretical relationship in equation (3.18). As for molybdite and calcite, the measured data are systematically displaced from the theoretical line derived with the March model.

Bragg Intensity Corrections with the March Model

Table 4.10 summarises the results of the PO correction calculations using the r_R values and the r_M values from Table 4.9. Data for three lines only are given in the table as the triclinic symmetry of kaolinite causes substantial peak overlap in contrast to the corresponding results for molybdite and calcite.

The R-factors for the random orientation models, increase systematically from KDC —> KLC —> KBA samples as expected from the March r values. The R-factors obtained with the two March models improve dramatically from the random orientation values when the March model is employed.

Table 4.10

Comparison of Kaolinite Integrated Intensities, Corrected for PO, with Calculated Theoretical Intensities for the Random Orientation Model

Three values of measured integrated intensity are given for each of the three samples (KDC, KLC and KDA - see Table 3.3) as defined below. The scale factor applied to each of the three values is described in Section 3.7.

Value 1 (first line), R_1: measured intensities scaled to theoretical data, no PO correction.

Value 2 (asterisked), R_2: measured intensities corrected for PO using r_R (Rietveld value), then scaled to theoretical data.

Value 3 (parentheses), R_3: measured intensities corrected for PO with r_M (line ratio value) derived from line pair (001)/(060), then scaled to theoretical data.

The R-factors in the Table (R1, R2, R3) are defined in Equations (3.23) and (3.24), Section 3.7.

The lines included in the analysis are those for which there is no discernible peak overlap and for which the theoretical intensity (relative) ≥ 5.

(continued)

Table 4.10 (Continued)

h k l	Calculated theoretical intensity (random orientation)	Measured Intensities (Corrected) KDC $r_R=0.852^*$ ($r_M=0.957$)	KLC $r_R=0.642^*$ ($r_M=0.902$)	KBA $r_R=0.591^*$ ($r_M=0.814$)
0 0 1	100	79	81	79
		73*	68*	66*
		(78)	(80)	(77)
0 0 2	53	69	76	79
		63*	63*	66*
		(67)	(74)	(77)
0 6 0	10	14	5	3
		26*	30*	30*
		(17)	(8)	(8)
Scale factors				
		0.079	0.081	0.079
		0.118*	0.257*	0.319*
		(0.089)	(0.330)	(0.142)
Agreement indices :				
R-factors,	R_1	0.273	0.281	0.324
	R_2	0.336*	0.394*	0.421*
	R_3	(0.255)	(0.265)	(0.294)

CHAPTER 5

DISCUSSION AND CONCLUSION

5.1. Overview of Results

Overview of the Study Objectives

The statement of objectives in Section 1.2 needs to be reviewed in assessing the results reported in Chapter 4, particularly the specific objective :

> *....to extend the work on gibbsites to other materials using both the Rietveld and line ratio methods to test the general applicability of the March model for PO assessment.*

The value of the March formula in modelling PO may be judged in both qualitative and quantitative terms. In the discussion here the results are evaluated qualitatively according to changes in Rietveld R-factors (R_p, R_{wp} and R_B) and in terms of the agreement between measured and calculated XRPD patterns when the March model is applied. It must be emphasised that caution should be exercised in making such qualitative assessments given that the use of any mathematical representation may improve agreement between measured and calculated data even if the representation does not have a physical basis.

The results may also be assessed qualitatively in terms of the trend in March r parameters within a specimen suite in which samples have been prepared by different methods which should systematically change the amount of PO. Specifically, it may be expected that r will reduce progressively within the mounting sequence : side-drifted —> light front-pressed —> briquetted.

Quantitative evaluation may be carried out by testing the validity of equations relating the line ratio to the March r formula - equations (2.15) and (2.16). If the March model is appropriate for the samples examined, and if sources of systematic error other

than PO do not bias the intensity data, it may be concluded that the formula is a valid basis for determining texture and correcting intensity data for PO bias.

Rietveld Results

The Rietveld results for molybdite, calcite and kaolinite (Section 4.1, 4.2 and 4.3, notably Tables 4.1, 4.5 and 4.8, respectively) mainly show substantial improvements in the R-factors (R_p, R_{wp} and R_B) when the March model is introduced. The only exception to this general behaviour is the side-drifted calcite sample (CDA) which gives results consistent with essentially random orientation. In general the index R_p is close to 2.0 times R_{exp} whereas for the gibbsites results of Li and O'Connor (1989) and Li *et al.* (1990) the ratio R_p/R_{exp} was about 1.5 for most oriented samples. Therefore it is evident that the March model produced substantial improvements in the R-indices for the three materials examined in this study, but that the level of disagreement between calculated and measured data sets was more pronounced than had been observed in the gibbsite work. This observation points to two possibilities, *viz.* some deficiency in the March model in representing PO and/or other sources of systematic error in the intensities.

The Rietveld r-values for all three materials trend in the manner expected, *viz.* a reduction in r from side-drifting —> light front-pressing —> briquetting. Moreover, for molybdite the real r-values all increased substantially when the sample was mixed with 50% by weight silica gel. It is disappointing that the side-drifting procedure failed to produce r-values close to 1.0 for molybdite and kaolinite, thus indicating that the technique employed in this study produced samples with substantial PO.

Finally, it is encouraging to note that correction of pattern intensities with the Rietveld r-values substantially proved the agreement between measured and calculated intensities.

Line Ratio Results

The results for molybdite, calcite and kaolinite in Tables 4.2, 4.6 and 4.9, respectively, show systematic differences between the March r parameters from Rietveld refinement and those from line ratio analysis. It is especially interesting to note that the r_M values (determined from line ratios) exceed the corresponding r_R values (from Rietveld calculations) for all molybdite and kaolinite samples whereas the trend is reversed for the calcite results (*i.e.* $r_M < r_R$). The discrepancies may be due to a source or sources of systematic error, in addition to PO, which bias the intensities chosen for line ratio calculations. Primary extinction is, at least in principle, an error source which might heavily bias the intensities of lines chosen for line ratio work, but which would have less influence on the value of r determined by Rietveld analysis.

5.2 Conclusion

- The March model has provided physically sensible results for both the line ratio and Rietveld methods.
- Systematic differences between the sets of March r-parameters from the two methods appear to indicate that the Rietveld method gives superior results. Extinction is suspected as the most likely source of error causing these differences.
- It is evident from these results that the use of line ratios with the March model is likely to be less effective than the Rietveld procedure. Extinction, in particular, is likely to render the line ratio method less effective than the Rietveld technique.

5.3 Further Work

The extinction factor, which can cause bias in the intensity data, should be investigated in future work.

REFERENCES

Alexander, L., Klug, H.P. and Kummer, E. (1948). *Statistical factors affecting the intensity of x-rays diffracted by crystalline powders.* J. Appl. Phys. 19, 742-753.

Anderson, G. and Magneli, A. (1950). *On the crystal structure of molybdenum trioxide.* Acta Chem. Scand. 4, 793-797.

Brakken, H. (1931). *Kurzere originalmitteilungen und notizen. Die kristallstrukturen der trioxyde von chrom, molybdan und wolfram.* Z. Kristallogr. 78, 484-488.

Brindley, G.W. and Robinson, K. (1946). *The structure of kaolinite.* Min. Mag. and J. Min. Soc. 27, 242-253.

Bunge, H.J. (1985). *Representation of preferred orientations.* In Preferred Orientation in Deformed Metals and Rocks, edited by H.-R. Wenk, pp. 73-108. Orlando: Academic Press.

Calvert, L.D., Sirianni, A.F., Gainsford, G.J. and Hubbard, C.R. (1983). *A comparison of methods for reducing preferred orientation.* Adv. X-ray Anal. 26, 105-110.

Capkova, P. and Valvoda, V. (1974). *Preferred orientation in powder samples of magnesium and magnesium-cadmium alloys.* Czech. J. Phys. B24, 891-900.

Cooper, M.J., Rouse, K.D. and Willis, B.T.M. (1968). *Neutron diffraction studies of anharmonic temperature factors in BaF_2.* Acta Cryst. A24, 484-493.

Cooper, M.J. and Rouse, K.D. (1970). *Extinction in x-ray and neutron diffraction.* Acta Cryst. A24, 214-223.

Cox, D.E., Moodenbaugh, A.R., Sleight, A.W. and Chen, H.-Y. (1980). *Structural refinement of neutron and x-ray data by Rietveld method: application to Al_2O_3 and $BiVO_4$.* Nat. Bur. Stands. Special Publ. 567, 189-201.

Cullity, B.D. (1978). *Elements of x-ray diffraction.* 2nd ed. Addison-Wesley, Publ. Co. Inc., Reading, Massachusetts.

Dollase, W.A. (1986). *Correction of intensities for preferred orientation in powder diffractometry : application of the March model.* J. Appl. Cryst. 19, 267-272.

Henry, N.F.M. and Lonsdale, K. (1969). *International tables for x-ray crystallography.* Vol. I. Symmetry Groups. Birmingham: Kynoch Press.

Hill, R.J. and Howard, C.J. (1986). *A computer program for Rietveld analysis of fixed wavelength x-ray and neutron powder diffraction patterns.* Australian Atomic Energy Commission Research Establishment.

Hill, R.J. and Madsen, I.C. (1984). *The effect of profile step counting time on the determination of crystal structure parameters by x-ray Rietveld analysis.* J. Appl. Cryst. 17, 297-306.

Hill, R.J. and Madsen, I.C. (1986). *The effect of profile step width on the determination of crystal structure parameters and estimated standard deviations by x-ray Rietveld analysis.* J. Appl. Cryst. 19, 10-18.

Ibers, J.A. and Hamilton, W.C. (1974). (Editors). *International tables for x-ray crystallography.* Vol. IV. Revised and supplementary tables to Vols. II and III. Birmingham: Kynoch Press. .

Kihlborg, L. (1963). *Least squares refinement of the crystal structure of molybdenum trioxide.* Ark. Kemi. 21, 357-363.

Klug, H.P. and Alexander, L.E. (1974). *X-ray diffraction procedures.* 2nd ed. New York: John Wiley and Sons.

Li, D.Y. and O'Connor, B.H. (1989). *Use of morphological ratio data for applying preferred orientation corrections in x-ray powder diffraction QPA.* Proceedings of AXAA (WA) 5th state conference, Margaret River, 1989, pp. 39-62.

Li, D.Y., O'Connor, B.H., Roach, G.I.D. and Cornell, J.B. (1990). *Use of x-ray powder diffraction Rietveld pattern-fitting for characterising preferred orientation in gibbsites.* Powder Diffraction. 5, 79-85.

March, A. (1932). *Mathematische theorie der regelung nach der korngestalt bei affiner deformation.* Z. Kristallogr. 81, 285-297.

Megaw, H.D. (1970). *Thermal vibrations and a lattice mode in calcite and sodium nitrate.* Acta Cryst. A26, 235-244.

Megaw, H.D. (1973). *Crystal structure: a working approach*. W.B. Saunders Co., Philadelphia, pp. 241-247.

O'Connor, B.H. and Chang, W.J. (1986). *The amorphous character and particle size distributions of powders produced with the micronising mill for quantitative x-ray powder diffractometry*. X-ray spectr. 15, 267-270.

Oertel, G. (1985). *Re-orientation due to grain shape*. In Preferred Orientation in Deformed Metals and Rocks, edited by H.-R Wenk, pp. 259-265. Orlando: Academic Press.

Parrish, W. and Huang, T.C. (1983). *Accuracy and precision of intensities in x-ray polycrystalline diffraction*. Adv. X-ray Anal. 26, 35-44.

Pesonen, A., Jarvinen, M. and Kurki-Suonio, K. (1973). *Correction of integrated x-ray intensities for preferred orientation in hexagonal close-packed powders*. Phys. Fenn. 8, 81-91.

Raven, M.D. (1989). *Characterisation of kaolinite by Rietveld x-ray powder diffraction procedures*. MAppSc. Thesis, Curtin University of Technology.

Rietveld, H.M. (1969). *A profile refinement method for nuclear and magnetic structures*. J. Appl. Cryst. 2, 65-71.

Roach, G.I.D. and Cornell, J.B. (1988). *Morphology analysis by x-ray diffraction*. Proceedings of AXAA88 conference, Perth 1988, 319-328.

Sabine, T.M. (1988). *A reconciliation of extinction theories*. Acta Cryst. A44, 368-373.

Sasa, Y. and Uda, M. (1976). *Structure of stoichiometric USi_2*. J. Solid State Chem. 18, 63-68.

Suitch, P.R. and Young, R.A. (1983). *Atom positions in highly ordered kaolinite*. Clays and Clay Minerals. 31, 357-366.

Toraya, H. and Marumo, F. (1981). *Preferred orientation correction in powder pattern-fitting*. Mineral. J. 10, 211-221.

Uda, M. (1967). *The structure of synthetic Fe_3S_4 and the nature of transition to FeS. Z.* Anorg. Allg. Chem. 350, 105-109.

Weiss, L.E. and Wenk, H.-R. (1985). *An Introduction.* In Preferred Orientation in Deformed Metals and Rocks, edited by H.-R. Wenk, pp. 1-10. Orlando: Academic Press.

Wever, F. (1924). *Uber die wolzstrukture kubisch kristallisierender metalle.* Z. Phys. 28, 69-90.

Wiles, D.B. and Young, R.A. (1981). *A new computer program for Rietveld analysis of x-ray powder diffraction patterns.* J. Appl. Cryst. 14, 149-151.

Will, G., Parrish, W. and Huang, T.C. (1983). *Crystal-structure refinement by profile fitting and least-squares analysis of powder diffraction data.* J. Appl. Cryst. 16, 611-612.

Wooster, N. (1931). *The crystal structure of molybdenum trioxide, MoO_3.* Z. Kristallogr. 80, 504-512.

Young, R.A. and Hewat, A. W. (1988). *Verification of the triclinic crystal structure of kaolinite.* Clays and Clay Minerals. 36, 225 - 232.

Zachariasen, W.H. (1967). *A general theory of x-ray diffraction in crystals.* Acta Cryst. 23, 558-564.

Zachariasen, W.H. (1968). *Extinction and Borrmann effect in mosaic crystals.* Acta Cryst. A24, 421-424.

Zachariasen, W.H. (1969). *Theoretical correction for extinction.* Acta Cryst. A25, 102

Zvyagin, B.B. (1960). *Electron-diffraction determination of the structure of kaolinite.* Soviet Physics-Crystallography. 5, 32-42.